



**Michigan  
Technological  
University**

Michigan Technological University  
**Digital Commons @ Michigan Tech**

---

Michigan Tech Publications

---

2-3-2022

## A review of carbon monitoring in wet carbon systems using remote sensing

Anthony D. Campbell  
*NASA Goddard Space Flight Center*

Temilola Fatoyinbo  
*NASA Goddard Space Flight Center*

Sean P. Charles  
*East Carolina University*

Laura L. Bourgeau-Chavez  
*Michigan Technological University*

Joaquim Goes  
*Lamont-Doherty Earth Observatory*

*See next page for additional authors*

Follow this and additional works at: <https://digitalcommons.mtu.edu/michigantech-p>

---

### Recommended Citation

Campbell, A., Fatoyinbo, T., Charles, S., Bourgeau-Chavez, L., Goes, J., Gomes, H., Halabisky, M., Holmquist, S., Lohrenz, S., Mitchell, C., Moskal, L., Poulter, B., Qiu, H., Resende De Sousa, C., & Sayers, M. (2022). A review of carbon monitoring in wet carbon systems using remote sensing. *Environmental Research Letters*, 17(2). <http://doi.org/10.1088/1748-9326/ac4d4d>  
Retrieved from: <https://digitalcommons.mtu.edu/michigantech-p/15843>

Follow this and additional works at: <https://digitalcommons.mtu.edu/michigantech-p>

---

## Authors

Anthony D. Campbell, Temilola Fatoyinbo, Sean P. Charles, Laura L. Bourgeau-Chavez, Joaquim Goes, Helga Gomes, Meghan Halabisky, Smithsonian Environmental Research Center Holmquist, Steven Lohrenz, Catherine Mitchell, L. Monika Moskal, Benjamin Poulter, Han Qiu, Celio H. Resende De Sousa, and Michael Sayers

TOPICAL REVIEW • **OPEN ACCESS**

## A review of carbon monitoring in wet carbon systems using remote sensing

To cite this article: Anthony D Campbell *et al* 2022 *Environ. Res. Lett.* **17** 025009

View the [article online](#) for updates and enhancements.

You may also like

- [Expansion of EYM amplitudes in gauge invariant vector space](#)  
Bo Feng, , Xiao-Di Li et al.
- [2021 roadmap for sodium-ion batteries](#)  
Nuria Tapia-Ruiz, A Robert Armstrong, Hande Alptekin et al.
- [Suppression of individual peaks in two-colour high harmonic generation](#)  
S Mitra, S Biswas, J Schötz et al.

ENVIRONMENTAL RESEARCH  
LETTERS

## LETTER

## A review of carbon monitoring in wet carbon systems using remote sensing

## OPEN ACCESS

## RECEIVED

18 May 2021

## REVISED

11 November 2021

## ACCEPTED FOR PUBLICATION

20 January 2022

## PUBLISHED

3 February 2022

Original content from this work may be used under the terms of the [Creative Commons Attribution 4.0 licence](#).

Any further distribution of this work must maintain attribution to the author(s) and the title of the work, journal citation and DOI.



Anthony D Campbell<sup>1,2</sup> , Temilola Fatoyinbo<sup>1</sup> , Sean P Charles<sup>3</sup>, Laura L Bourgeau-Chavez<sup>4</sup>, Joaquim Goes<sup>5</sup>, Helga Gomes<sup>5</sup>, Meghan Halabisky<sup>6</sup>, James Holmquist<sup>7</sup> , Steven Lohrenz<sup>8</sup>, Catherine Mitchell<sup>9</sup> , L Monika Moskal<sup>6</sup>, Benjamin Poulter<sup>1</sup>, Han Qiu<sup>10</sup> , Celio H Resende De Sousa<sup>1</sup>, Michael Sayers<sup>4</sup>, Marc Simard<sup>11</sup> , Anthony J Stewart<sup>6</sup>, Debjani Singh<sup>12</sup>, Carl Trettin<sup>13</sup>, Jinghui Wu<sup>5</sup> , Xuesong Zhang<sup>14</sup> and David Lagomasino<sup>3</sup>

- <sup>1</sup> Biospheric Sciences Laboratory, NASA Goddard Space Flight Center, Greenbelt, MD, United States of America
- <sup>2</sup> NASA Postdoctoral Program, Universities Space Research Association, Columbia, MD, United States of America
- <sup>3</sup> Department of Coastal Studies, East Carolina University, Wanchese, NC 27981, United States of America
- <sup>4</sup> Michigan Tech Research Institute, Michigan Technological University, Ann Arbor, MI, United States of America
- <sup>5</sup> Marine Biology, Department of Marine Biology and Paleoenvironment, Lamont–Doherty Earth Observatory, Columbia University, 61 Route 9W, Palisades, NY 10964, United States of America
- <sup>6</sup> School of Environment and Forest Sciences, University of Washington, Seattle, WA 98195, United States of America
- <sup>7</sup> Smithsonian Environmental Research Center, Edgewater, MD 21037-0028, United States of America
- <sup>8</sup> School for Marine Science and Technology, University of Massachusetts Dartmouth, New Bedford, MA 02744, United States of America
- <sup>9</sup> Bigelow Laboratory for Ocean Sciences, East Boothbay, ME 04543, United States of America
- <sup>10</sup> Department of Forest and Wildlife Ecology, University of Wisconsin-Madison, 1630 Linden Drive, Madison, WI, United States of America
- <sup>11</sup> Jet Propulsion Laboratory, California Institute of Technology, Pasadena, CA 91109, United States of America
- <sup>12</sup> Environmental Sciences Division, Oak Ridge National Laboratory, Oak Ridge, TN 37830, United States of America
- <sup>13</sup> USDA-Forest Service, Southern Research Station, Cordesville, SC 29434, United States of America
- <sup>14</sup> USDA-ARS Hydrology and Remote Sensing Laboratory, Beltsville, MD 20705-2350, United States of America

E-mail: [anthony.d.campbell@nasa.gov](mailto:anthony.d.campbell@nasa.gov) and [lola.fatoyinbo@nasa.gov](mailto:lola.fatoyinbo@nasa.gov)

**Keywords:** earth observation, wetlands, ocean, carbon monitoring

Supplementary material for this article is available [online](#)

**Abstract**

Carbon monitoring is critical for the reporting and verification of carbon stocks and change. Remote sensing is a tool increasingly used to estimate the spatial heterogeneity, extent and change of carbon stocks within and across various systems. We designate the use of the term wet carbon system to the interconnected wetlands, ocean, river and streams, lakes and ponds, and permafrost, which are carbon-dense and vital conduits for carbon throughout the terrestrial and aquatic sections of the carbon cycle. We reviewed wet carbon monitoring studies that utilize earth observation to improve our knowledge of data gaps, methods, and future research recommendations. To achieve this, we conducted a systematic review collecting 1622 references and screening them with a combination of text matching and a panel of three experts. The search found 496 references, with an additional 78 references added by experts. Our study found considerable variability of the utilization of remote sensing and global wet carbon monitoring progress across the nine systems analyzed. The review highlighted that remote sensing is routinely used to globally map carbon in mangroves and oceans, whereas seagrass, terrestrial wetlands, tidal marshes, rivers, and permafrost would benefit from more accurate and comprehensive global maps of extent. We identified three critical gaps and twelve recommendations to continue progressing wet carbon systems and increase cross system scientific inquiry.

## 1. Introduction

The Paris Climate Agreement requires net neutral carbon emissions by reducing fossil fuel emissions and balancing sources and sinks by 2100 [1]. Monitoring, reporting, and verification (MRV) are foundational for tracking emission reductions from land-use change and carbon removal attributed to reforestation and afforestation [2, 3]. Oceans, coasts, and wetlands are essential components of the global carbon cycle and are considered critical to achieving emission reductions necessary for fulfilling a variety of Sustainable Development Goals (figure 1) [4–6]. Carbon monitoring of wetlands, water bodies, and oceans pose unique challenges because of their complex ecosystem structure, seasonality, and susceptibility to climate impacts such as sea-level rise, drought, and increased storms [7, 8].

This review focuses on the fluxes and stocks of carbon in wet carbon (WC) systems, a term used hereinafter to include all freshwater, saline, and brackish aquatic and wetland ecosystems, e.g. peatlands, mangroves, and oceans. This term is not a paradigm shift away from ‘blue carbon’ but a broader grouping of carbon cycle systems with shared data needs, restoration and preservation priority, and research direction. ‘Blue carbon’ is a term used to describe carbon-dense coastal wetland ecosystems and has aided significant research progress, with an expansive agenda for monitoring and applications [12]. However, focusing exclusively on ‘blue carbon’ ecosystems emphasizes ~20% of global wetlands (1520–1620 Mha) and excludes terrestrial wetlands, permafrost, lakes, riverine, and marine systems [13, 14]. We primarily consider the oceans a WC system due to the interconnectedness between the oceans and other WC systems, i.e. the land–ocean aquatic continuum (figure 1) [15]. Here, we conducted a synthesis review of these interconnected systems to identify shared data needs, convergent research directions, and carbon monitoring goals.

Carbon monitoring research has rapidly expanded over the last 10–20 years due to international agreements targeted at reducing carbon emissions and establishing the need for accurate MRV of carbon. In 1997, the Kyoto Protocol prioritized the need for agricultural soils and forests to be managed as natural carbon sinks [16], followed by the development of Reduce Emissions from Deforestation and Forest Degradation (REDD) and REDD+ in 2009. The Paris Climate Agreement promotes wetland and coastal ecosystem management and provides a mechanism for developing and implementing their nationally determined contributions (NDCs) [16, 17]. The goal of carbon-neutral land-use change set forth as part of the Paris Climate Agreement has added additional exigency for developing MRV methods to inform carbon offsets and facilitate the inclusion of WC ecosystems within NDCs. To continue the further

expansion of carbon offsets to WC systems requires high-quality remote sensing enabled MRV, a core goal of the NASA Carbon Monitoring System (CMS) Program [18].

Remote sensing data provide spatial and temporal observations that can support carbon monitoring at local, regional, and global scales. WC monitoring of terrestrial and coastal wetlands are concerned with both aboveground and subsurface carbon as most of these systems’ carbon stock is below the surface [19]. Tier 3 Intergovernmental Panel on Climate Change (IPCC) estimates require the inclusion of modeled, local processes that impact emissions and reduce uncertainty [20]. Therefore, spatially resolving subsurface carbon requires modeling of hydrological, biophysical, and topographic indicators [21]. At local scales, carbon MRV can be conducted exclusively with *in situ* data. However, WC monitoring at regional and global scales requires combinations of *in situ* measurements and remote sensing observables. Remote sensing introduces uncertainty but helps resolve spatial variability that *in situ* estimates cannot (figure 2). Enabling our end goal of global continuous monitoring of all WC systems and their interactions.

The NASA CMS program seeks to prototype methods for MRV of the entire carbon cycle, and these WC systems represent an essential component with unique data needs and methodologies. As part of this review, we surveyed nine WC systems to determine earth observation-based WC monitoring status within each. The inclusion of more systems into global carbon budgets can reduce uncertainty, improve modeling outputs, and diversify climate mitigation solutions. WC monitoring is a relatively new field that we explore through a systematic review of the literature identifying gaps in our understanding, including location, ecosystem function, and methodological. We set forth the current state of carbon monitoring science within a subset of WC systems, including mangroves, peatlands and permafrost, tidal marsh and flats, terrestrial wetlands, oceans, coastal and continental shelf seas, lakes and ponds, rivers and streams, and submerged aquatic vegetation (SAV) (including seagrasses, kelp). We focus on natural WC systems due to their connections and shared data needs; it should be noted that anthropogenic WC systems, such as, rice paddies, are also important, but beyond the scope of our review. We discuss the current state of carbon monitoring data, stakeholder engagement, and provide recommendations to inform the future of WC monitoring, the NASA CMS program, and carbon accounting.

## 2. Systematic review

### 2.1. Methodology

The Web of Science was used to conduct this review with the inclusion of the CMS literature archive, and Google Scholar searches. Our search descriptions

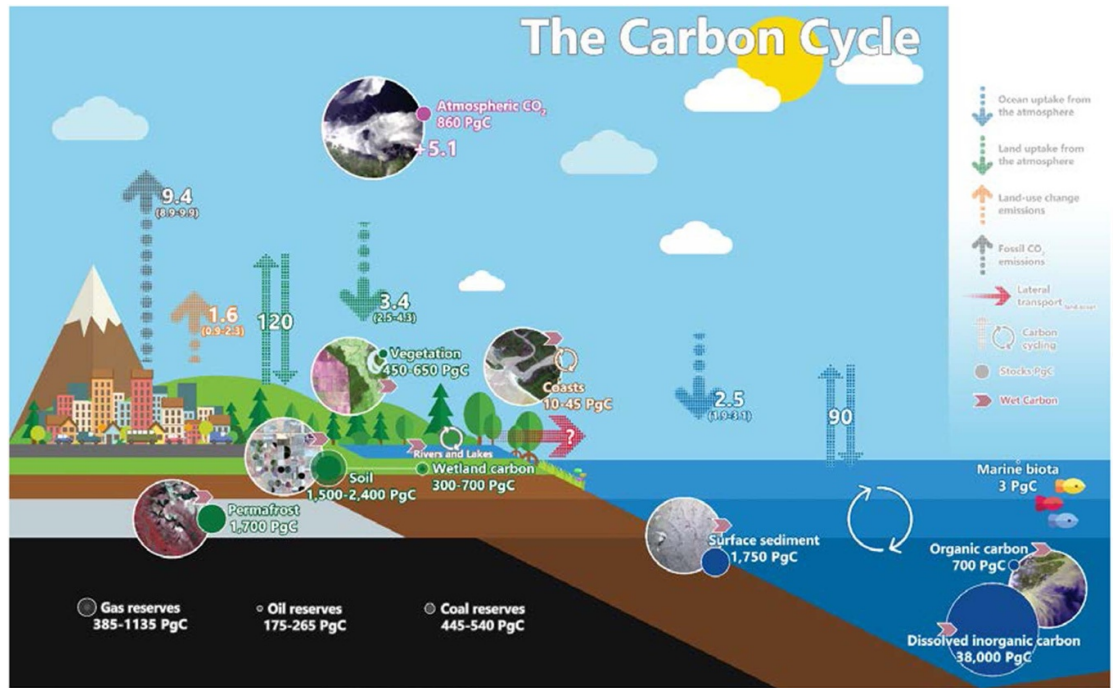


**Figure 1.** The global carbon cycle adapted from [9]. Wet carbon systems are highlighted with the interaction symbol from systems ecology [10]. Vegetation and soil are both denoted as wet carbon systems, but only a portion of these carbon stores are wet carbon. Images are Planetscope (permafrost, soil, vegetation, coasts), Sentinel-3 (atmospheric and organic carbon), and surface sediment camera system (photo credit Kevin Stokesbury). Wetland soil carbon value from Bridgman *et al* [11]. Photo credit: Kevin Stokesbury. Reproduced with permission.

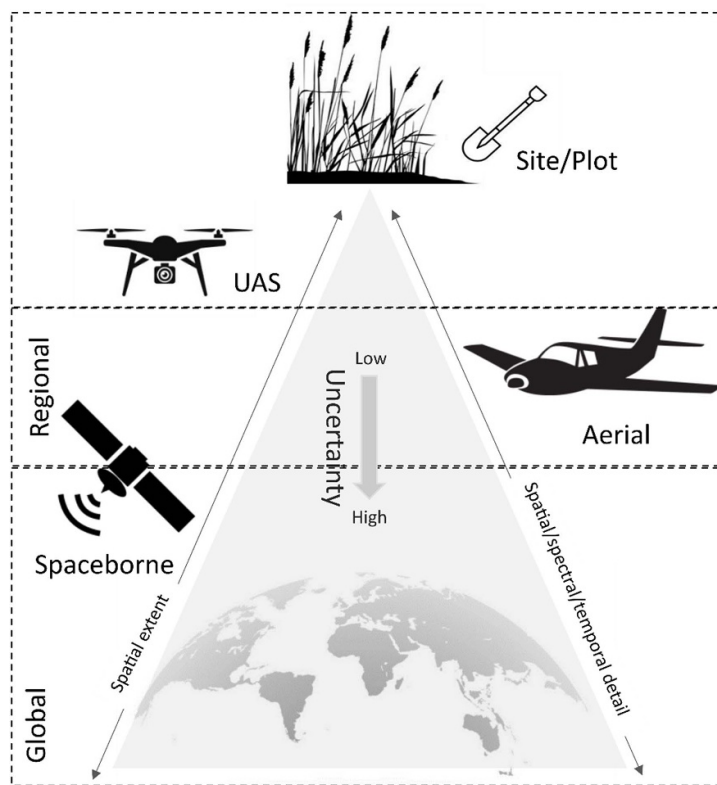


**Figure 2.** Terrestrial carbon monitoring extents, platforms in relation to uncertainty and remote sensing spatial, temporal, and spectral resolution domains.

and strings can be found in supplemental table 1 (available online at [stacks.iop.org/ERL/17/025009/mmedia](https://stacks.iop.org/ERL/17/025009/mmedia)). This example search string resulted in 466 references within the Web of Science and cumulatively all searches amounted to 1622 records. The system terms used included salt marsh, tidal marsh, mangroves, wetland, coral, seagrass, forested wetland, riparian, bog, peat, benthic, ocean, tidal flat, mudflat, marsh, bog, vernal pool, salt flat, submerged aquatic vegetation, beach, kelp, and playa. The Google Scholar results, and CMS program outputs were screened with an automated text selection algorithm, ensuring that all abstracts had a remote sensing and WC system term. The resulting studies were input into Cadima, a webtool for facilitating systematic reviews. All abstracts were screened by at least two reviewers to identify if they fulfilled three requirements.

- (a) The study used remote sensing data
- (b) The study reports carbon monitoring findings (land cover mapping or solely *in situ* finding were excluded)
- (c) The study at least partially focuses on a WC system

If all these questions were answered in the affirmative, we included that paper in the data extraction step of the literature review. If reviewers disagreed on an abstract's relevancy, a three-reviewer panel adjudicated its inclusion with most references being passed to the next step i.e. full review by an expert on that system. This process found 496 relevant references. Additional references were added based on expert knowledge resulting in a total of 574 (supplemental data 1). The references were divided into WC systems including mangroves ( $n = 79$ ), tidal marsh and flats ( $n = 47$ ), (SAV;  $n = 45$ ), mineral wetlands ( $n = 55$ ), peatlands ( $n = 129$ ), permafrost ( $n = 80$ ), lakes ( $n = 64$ ), rivers ( $n = 33$ ), oceans ( $n = 102$ ), and ocean shelf ( $n = 30$ ). References were allowed to have multiple system designations.

### 3. Results

Since 2010, studies of WC monitoring with remote sensing have increased substantially (figure 3). The research growth tracks with major literature milestones, e.g. Nellemann *et al* [22], which first coined the term 'blue carbon,' and Page *et al* [23], which demonstrated the importance of tropical peatland carbon. Interest further developed with a call for the use of remote sensing to identify land-use change, priority areas for protection, and methods for measuring C stocks within sediments [24]. However, growth was not consistent between WC systems, with some having more research interest, including oceans, peatlands, and mangroves.

Disparate levels of research interest across remote sensing monitoring of WC systems are evident in this

result. In the past, 'blue carbon' research and media coverage were highly skewed towards coral [25]. Realignment of research interest, media attention, and funding is critical for understanding understudied WC systems and providing scientific justification and public support for WC mitigation. However, total yearly citations demonstrate that WC research utilization has remained relatively consistent since 2010 (figure 4) despite more studies. Many systems are still developing remote sensing methodologies to enable carbon monitoring (see sections 3.1.2, 3.1.3, 3.2.1 and 3.3.2). A shared language of carbon monitoring was evident across our WC systems. The use of earth observation to capture spatial heterogeneity is apparent in the two most common keywords, i.e. dynamics and variability. These keywords were identified in clusters across the literature and were areas of shared interest (figure 5). Thematic mapping of the literature revealed that climate change, dynamics, and carbon were the most fundamental research themes and that forested WC systems were prominent in multiple clusters. These two forest-related clusters correspond with peatlands and mangroves, two systems with considerable growth in research interest from 2000 to 2019 (figure 3). An emerging cluster associated with coastal remote sensing was evident, likely due to a recent focus on the data requirements for monitoring coastal systems. These keywords were apparent within our detailed reviews of WC systems and framed our discussion of the status of carbon monitoring.

WC systems were separated into three categories for this review: coastal wetlands, inland wetlands, and ocean and shelves. Coastal wetlands included mangroves, SAV, and tidal marshes and flats. Inland wetlands comprised of mineral wetlands, peatlands and permafrost, whereas, inland waterbodies, lakes and ponds, and rivers and streams. Each of these system sections discusses the status of carbon monitoring within the system.

#### 3.1. Coastal wetlands

Coastal wetlands are located along the terrestrial-aquatic interface and influenced by ocean and freshwater processes [28]. 'Blue carbon' ecosystems (seagrass, mangroves, tidal marshes and forests) comprise a portion of coastal wetlands. Coastal wetlands have consistently lost extent across the 19th and 20th century ( $-0.228\% \text{ yr}^{-1}$ ), slightly less than inland wetland loss ( $-0.391\% \text{ yr}^{-1}$ ) [29].

##### 3.1.1. Mangroves

In total, we found 79 papers relevant to carbon monitoring with remote sensing in mangrove ecosystems. Mangroves have some of the highest carbon (C) density ( $401 \pm 48 \text{ Mg C ha}^{-1}$ ), with between 49%–98% of carbon stored in the soils [30]. Mangroves are a small fraction of global forest area (0.3%–0.5%) but a significant global C stock



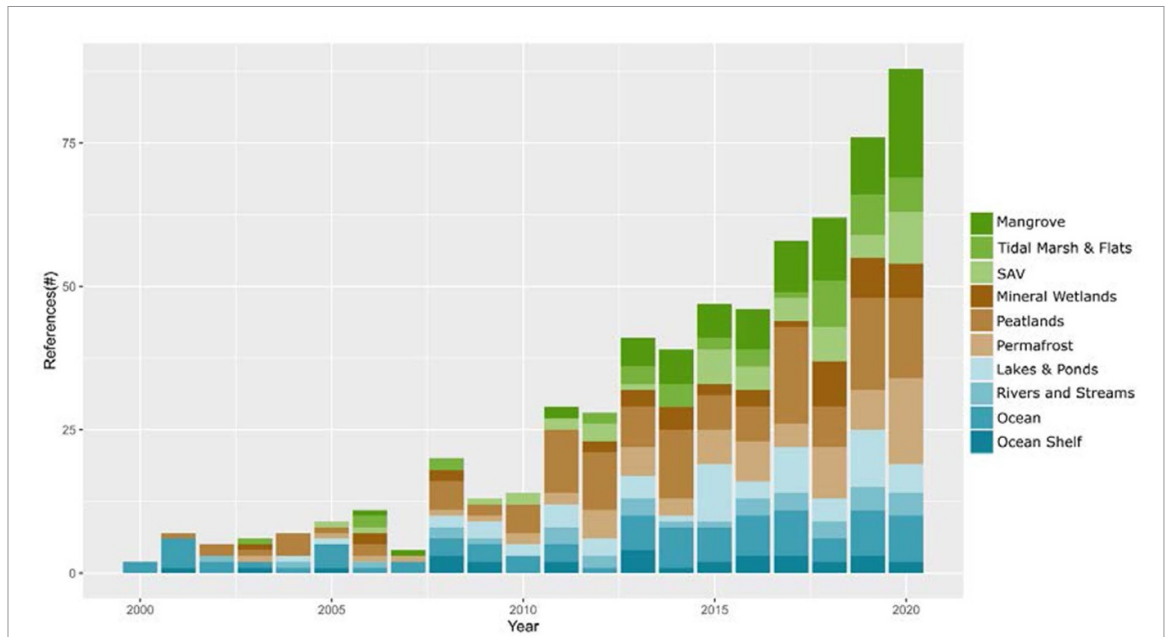


**Figure 3.** The results of the systematic review. References separated by year and WC system. We have separated peatlands and permafrost from terrestrial wetlands to demonstrate the disparity in research interest.

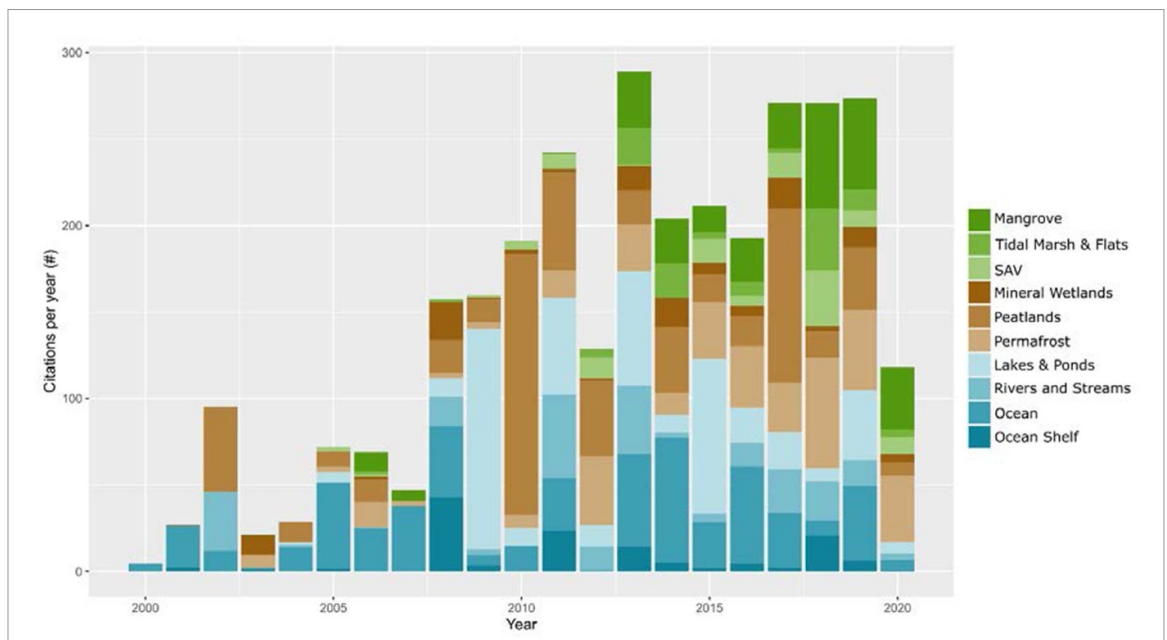


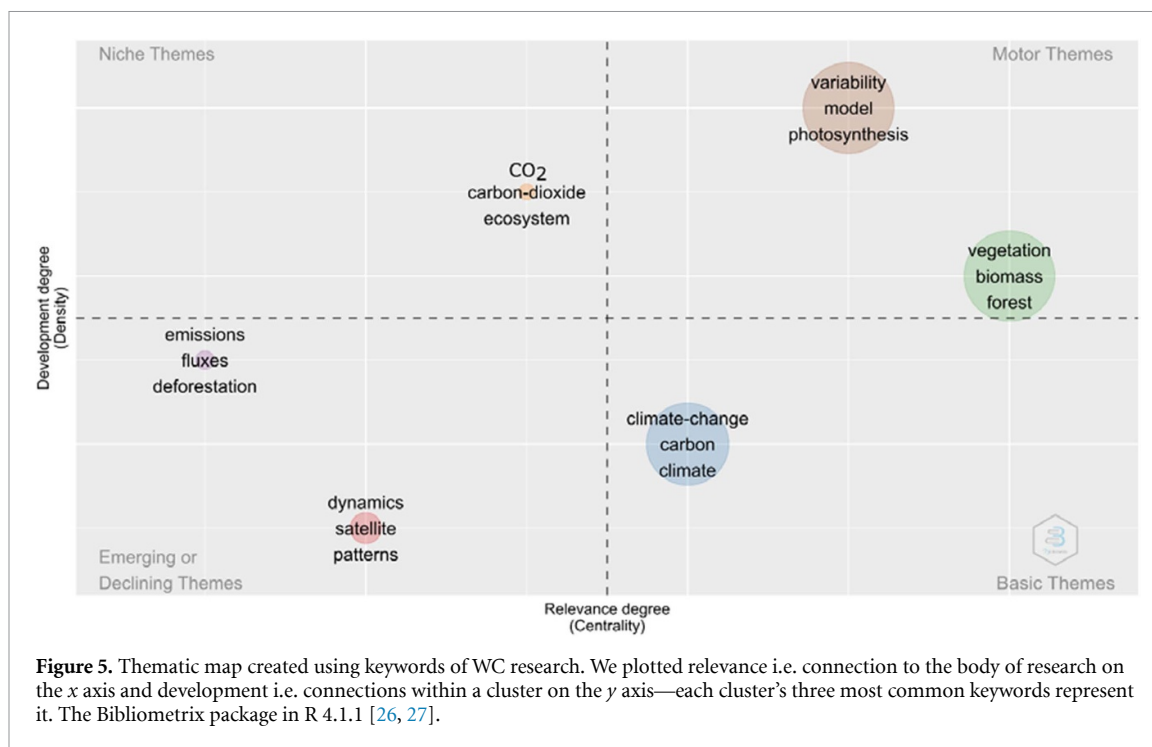
**Figure 4.** Total average citations per year by publication year and WC system category.

(5–10.4 PgC) [21, 31–36]. Recently, Global Mangrove Watch identified 137 600 km<sup>2</sup> of mangrove extent in 2010 and has since measured change from 1996 to 2017 [35, 37]. These forests are under significant threat from anthropogenic activity and sea-level rise [38–40]. In general, mangroves are difficult to survey, but remote sensing has increased our capacity to monitor their extent, C stocks, and change. We have grouped our synthesis of the status of carbon monitoring in mangroves into three sections: (a) carbon monitoring status, (b) data and applications.

**3.1.1.1. Carbon monitoring status**

Not long ago, mangrove biomass and carbon estimates relied upon the extrapolation of field data, environmental conditions, and partial extent maps [e.g. 31, 41–45]. Giri *et al* [46] created the first global mangrove map using Landsat imagery. This map and other advances in remote sensing have enabled regional-to-global-scale analyses of mangrove carbon stocks and carbon stock change [21, 36, 38, 40, 47–49]. Mangrove carbon monitoring combining field-based surveys and remote





sensing occurs across; local [e.g. 50–56], regional [e.g. 49, 57–62] and global [21, 34, 36, 63–67] scales. Continued advancement, including machine learning, have led to recent studies classifying species [68–71], quantifying height distributions and biomass [36, 72–74], change in extent [40, 47, 49, 75] and stand age [60], and productivity [76, 77].

Passive sensors are used to map mangrove extent, change, and extrapolate C storage with field data [8, 59, 60, 78–81]. Active sensors (e.g. light detection and ranging and radar) can measure mangrove structural attributes, such as canopy height. Simard *et al* [56] first derived accurate height estimates in the Everglades with Shuttle Radar Topographic Mission (SRTM). Subsequently, canopy height was estimated using satellite stereo images, Synthetic Aperture Radar (SAR) interferometry, and lidar [56, 60, 82–84]. Canopy height enables estimates of aboveground biomass [e.g. 36, 85–88]. Additional active spaceborne sensors (e.g. SRTM, Sentinel-1, TanDEM-X, ICESat, and GEDI) have improved canopy height models [e.g. 82, 84, 89] enabled the identification of change hotspots [39, 40, 49], and the development of mangrove carbon monitoring initiatives [37, 47, 60, 90]. The Japanese Aerospace Exploration Agency L-band SAR sensors (ALOS and ALOS-2) are an important active sensor for mangrove mapping, including the identification of invasive species [58], prediction of aboveground biomass (AGB) [74, 91], and long-term monitoring [39, 92]. Medium resolution sensors have enabled global-scale analysis but can miss small mangrove patches and edges or small-scale restoration efforts.

The recent increase in the resolution and accessibility of satellite imagery has provided fine-scale

mangrove data products suitable for MRV. The European Space Agency’s (ESAs) Sentinel-1 and Sentinel-2 launched in 2014 and 2015, respectively, increased the spatial resolution of new mangrove maps from 30 m (i.e. Landsat) to 10 and 20 m [53, 93, 94]. Moreover, access to high-resolution satellite, aerial, and unoccupied aerial systems (UAS) imagery has further increased the spatial resolution of mangrove maps (<5 m) [51, 59, 60, 70, 71, 79, 94, 95]. Data fusion with combinations of multispectral, hyperspectral, lidar, radar, and high-resolution data have been applied to increase the spatial and temporal resolution of mangrove carbon storage and flux estimates [60, 88]. The increased temporal resolution also facilitates monitoring of short-term disturbance and recovery [8, 49].

Coarse spatial resolution sensors such as MODIS are also informative and often used with other satellite imagery [96]. The high temporal resolution of MODIS is particularly beneficial when tracking net primary productivity (NPP) [76] or gross primary productivity (GPP) change [55, 77], including due to disturbance events like hurricanes [97] and insect outbreaks [77].

### 3.1.1.2. Data and applications

Field and climate studies provided the first global mangrove carbon models [41, 63] and continue to be essential for monitoring mangrove carbon [30, 66, 98, 99]. Mangrove height and biomass models have increased in accuracy, providing improved estimates of aboveground C stocks and change through restoration [100, 101], afforestation and encroachment [50, 51, 59, 102, 103], natural disturbances [40, 49, 57, 58] and local anthropogenic

**Table 1.** Global carbon monitoring value for mangroves from the literature. Method refers to four categories, modeled, data synthesis, extrapolation (*in situ* combined with extent to upscale estimates), and remote sensing (mapping or predicting spatial heterogeneity for an indicator).

| Carbon indicator         | System                           | Value  | Units                               | Method                        | Source            |
|--------------------------|----------------------------------|--|-------------------------------------|-------------------------------|-------------------|
| System Extent            | Mangroves                        | 0.137–0.16   | 10 <sup>6</sup> km <sup>2</sup>     | Remote Sensing                | [35, 46, 47]      |
| System Extent Change     | Mangroves                        | 0.16%–0.39% (2000–2012), 2.1% (2000–2016)<br>* only losses, does not include gains, 0.214% (1995–2016) | Percent loss yr <sup>-1</sup>       | Remote Sensing                | [35, 40, 47, 119] |
| Carbon stock             | Mangrove (total)                 | 7.29–15.4  | PgC                                 | Remote Sensing, Extrapolation | [21, 67, 120]     |
|                          | Mangrove (aboveground)           | 1.75–2.83  | PgC                                 | Remote Sensing, Extrapolation | [63, 120]         |
|                          | Mangrove (belowground)           | 2.6–6.4 (1 meter), 11.2–12.6 (2 m)   | PgC                                 | Remote Sensing, Extrapolation | [21, 34, 67]      |
| Carbon burial Emissions  | Mangroves                        | 22.5–34.4  | Tg OC yr <sup>-1</sup>              | Extrapolation                 | [24, 108, 121]    |
|                          | Mangrove (total emissions)       | 0.01–0.52  | PgC yr <sup>-1</sup>                | Extrapolation, Remote Sensing | [19, 48, 122]     |
|                          | Mangrove (belowground emissions) | 2–8.1  | TgC yr <sup>-1</sup>                | Remote Sensing, Extrapolation | [21]              |
| CH <sub>4</sub> Flux     | Mangrove                         | 0.191  | Tg CH <sub>4</sub> yr <sup>-1</sup> | Extrapolation                 | [121]             |
| Net Primary Productivity | Mangrove                         | 0.5–1.5  | PgC yr <sup>-1</sup>                | Extrapolation                 | [44, 123–125]     |

impacts [40, 49, 57, 58]. Anne *et al* [104] modeled mangrove soil carbon with hyperspectral data, which improved on Landsat-based models. Global mangrove carbon density has been extrapolated from 250 m to 30 m with a combination of machine learning, earth observation, and ancillary data [e.g. 21, 34].

Remote sensing further complicates the quantification of uncertainty in carbon monitoring (figure 2). Simard *et al* [36, 56] demonstrate that allometric equations can introduce considerable bias (>100%). However, the remote sensing canopy height model error was low with a root mean square error (RMSE) of 2 m). *In situ* carbon monitoring samples are limited globally. If these samples are not representative, uncertainty will be high and unquantified. Extrapolating carbon stocks and fluxes from relatively few *in situ* measurements makes the accurate quantification of spatial uncertainty extremely important. For example, Sanderman *et al* [21] used the existing 250 m SoilGrid data, *in situ* training data, and Landsat imagery to create a 30 m organic carbon stock (OCS) map. The study resulted in an average uncertainty of 40.4% of the mean OCS [21]. Remote sensing methods can quantify the spatial uncertainty improving stakeholder understanding of regional carbon estimates and accuracy.

Despite comprising only 0.3% of global coastal ocean area, mangroves contribute ~55% of air-sea CO<sub>2</sub> exchange from the world's wetlands and estuaries, 60% of dissolved inorganic carbon (DIC) and 27% of dissolved organic carbon (DOC) from tropical rivers to the coastal ocean [105–107]. Over

half of mangrove carbon production was unaccounted for until recently [45, 108], when mangrove carbon export (particularly DOC and DIC) were quantified [106, 107]. Only 14 TgC yr<sup>-1</sup> of mangrove NPP is buried in soils, while export to coastal oceans is approximately an order of magnitude higher (158 TgC yr<sup>-1</sup>) [107]. Mangroves export an estimated 15 Tg particulate organic carbon (POC) yr<sup>-1</sup>, 51 Tg DOC yr<sup>-1</sup>, and 124 Tg DIC yr<sup>-1</sup> to coastal oceans [106, 107]. Models of river and tidal flow through mangroves informed by remote sensing have improved estimates of carbon export [126], identifying relationships between environmental conditions (tidal height, river-flow, precipitation, biogeochemical constituents of water) and carbon export associated with tidal pumping [45, 126], particularly of DIC [127]. Furthermore, ocean color techniques can identify the source of organic matter through absorption coefficients [109, 110], allowing for detection of mangrove derived chromophoric dissolved organic matter (CDOM) and DOC [111]. Carbon export from mangroves is spatially and temporally heterogeneous, and remote sensing can help resolve this variability indirectly through characterizing water flow and directly through the identification of CDOM.

Remote sensing has been essential for carbon monitoring of mangroves due to their unique landscape position, structure, and spectral characteristics. These data have enabled relatively precise quantification of mangrove extent, carbon stocks, and carbon fluxes from local-to-global scales (table 1).

Mangroves are among the most carbon-dense ecosystems (table 1) [107] and are likely to become increasingly impacted by anthropogenic and natural disturbances [112]. Continued remote sensing carbon monitoring is necessary with a particular focus on climate-related range-shifts associated with sea-level rise (coastal contraction and inland expansion [113, 114]) and poleward range expansion [115–118].

### 3.1.2. Tidal marsh and flats

In total, we found 47 papers relevant to carbon monitoring with remote sensing in tidal marsh and flat ecosystems. Tidal marshes and flats share several characteristics, including tidal inundation and a relatively low energy environment; they may be salt, brackish, or fresh water. These ecosystems provide carbon storage and other valuable ecosystem services [128]. Tidal wetlands, like mangroves, are carbon-dense systems providing some of the highest carbon burial rates [24]. Global estimates of salt marsh and tidal flat extents are 54 950 km<sup>2</sup> and 127921 km<sup>2</sup>, respectively [129, 130]. Freshwater tidal wetlands also exist with ~2000 km<sup>2</sup> around the great lakes [131]. Due to the results of our review, this section's primary focus was on salt marshes. However, carbon accounting of freshwater tidal and non-mangrove forested tidal wetlands would benefit from remote sensing integration. Tidal ecosystems are changing due to anthropogenic drivers, including sea-level rise [132], coastal development [133], and reduced sediment input [130, 134–136]. Coastal wetlands can also be a variable source of methane emissions [137]. These emissions can be classified as anthropogenic in cases where built impoundments block tidal flow, leading to artificial freshening and enhanced methane emissions [138]. We have grouped our synthesis of the status of carbon monitoring in tidal marsh and flats into three sections: (a) carbon monitoring status, and (b) data and uncertainty.

#### 3.1.2.1. Carbon monitoring status

Tidal marsh studies utilized earth observation data to constrain and upscale *in situ* data, predict biomass and soil organic carbon (SOC) stocks, and model productivity. Land-use change was a primary theme, including migration, invasion, and long-term monitoring. The most common carbon indicators were GPP and biomass. Other indicators included sedimentation, leaf area index (LAI), vegetation fraction, nitrogen, and gas fluxes [104, 139–141]. Temporal dynamics of spectral indicators of biomass, i.e. normalized difference vegetation index, were explored in tidal flats, too [142, 143]. Most tidal system studies ( $n = 33$ ) pertained to marshes dictating this section's focus.

GPP is a common carbon indicator for tidal systems ( $n = 8$ ). MODIS combined with eddy covariance towers was used to predict GPP in tidal environments [144–146]. Less common were gas flux

chambers and incubation [139, 143]. Feagin *et al* [147, 148] improved on the MOD17 GPP product with an ecosystem-specific model. Tidal inundation is a source of uncertainty within GPP estimation, and studies addressed the tidal stage with spectral index filtering and tidal modeling [143, 145, 149]. These studies primarily rely on MODIS at a minimum spatial scale of 250 m, biomass, derived from Landsat or other high-medium resolution sensors is often used to track finer scale change.

In the 1980s, tidal marsh AGB was first predicted with *in situ* spectral measurement and expanded to Landsat imagery [150–152]. Since those foundational studies, researchers have assessed other sensors' capacity to predict AGB, including Worldview-2, Hyperion, UAS, lidar, MODIS, AVIRIS-NG, Planetscope, and data fusion [141, 153–160]. A major limitation of biomass prediction in tidal marshes is the site and species-specific limitations of the modeling results. Studies have sought to address this limitation with model transfer but resulted in inaccurate predictions [157], though regionally trained models have been successful [161–163]. AGB prediction scope and accuracy have increased since the first modeling approaches, but scale and uncertainty limit their applicability to global carbon monitoring.

Tidal marsh change was a frequent research topic, including tracking invasive species [164], determining marsh migration [165], time-series change analysis [166], and multitemporal regional change [167]. Studies frequently upscaled carbon measurements with land-use maps [167–170]. Braun *et al* [171] determined that geomorphic change can dictate whether and how freshwater coastal wetlands serve as sources or sinks for terrestrial carbon and how carbon stocks can fluctuate on a geologically rapid timescale. A few studies used remote sensing data to constrain *in situ* sampling with land-use maps [165, 172]. The lack of baseline data availability and a focus on local methods limited regional monitoring applications.

#### 3.1.2.2. Data and uncertainty

The lack of a global extent map and change estimates limits the use of remote sensing in tidal marsh carbon estimates (table 2). CMS has supported the development of the US coastal wetland greenhouse gas inventory [173]. In the contiguous US between 2006 and 2011, coastal wetlands emitted 10.3 Tg CO<sub>2</sub>e yr<sup>-1</sup> (1.6–21.3 Tg CO<sub>2</sub>e yr<sup>-1</sup>), and a robust sensitivity analysis demonstrates major sources of uncertainty where remote sensing could improve the model, including coastal salinity classifications—and resulting CH<sub>4</sub> emission categories—and the depth of soil deposits lost to erosion [174, 175]. Improved predictions on the fate of soil carbon following marsh loss events could combine earth observations and additional ocean physical modeling. Carbon stock values are well constrained compared to the uncertainty of methane emissions and loss events [174, 175]. So far,

**Table 2.** Global carbon monitoring values for tidal marsh and tidal flat systems from the literature. Tidal marsh and salt marsh were considered interchangeable. Tidal flat and unvegetated sediments were also considered interchangeable. Method refers to four categories, modeled, data synthesis, extrapolation (*in situ* combined with extent to upscale estimates), and remote sensing (mapping or predicting spatial heterogeneity for an indicator). When available uncertainty is reported 95% confidence intervals in parenthesis and standard error after  $\pm$ .

| Carbon indicator         | System      | Value                  | Units                | Method   | Source     |
|--------------------------|-------------|------------------------|----------------------|--|------------|
| System extent            | Tidal marsh | 0.055                  | $10^6 \text{ km}^2$  | Field and remote sensing   | [129]      |
|                          | Tidal flats | 0.128<br>(0.124–0.132) | $10^6 \text{ km}^2$  | Remote sensing   | [130]      |
| System extent change     | Tidal marsh | Not available          |                      |  |            |
|                          | Tidal flats | 0.5                    | $\% \text{ yr}^{-1}$ | Remote sensing   | [130]      |
| Carbon burial            | Tidal marsh | 0.028–0.070            | $\text{PgC yr}^{-1}$ | Extrapolation  | [180]      |
|                          | Tidal flats | 0.126                  | $\text{PgC y}^{-1}$  | Extrapolation<br>(total coastal burial in unvegetated sediments) | [181, 182] |
| Carbon stock             | Tidal marsh | 1.84                   | PgC                  | Extrapolation  | [107]      |
|                          | Tidal flats | Not available          |                      |  |            |
| Carbon Loss              | Tidal marsh | 0.016<br>(0.005–0.065) | $\text{PgC yr}^{-1}$ | Extrapolation  | [19]       |
|                          | Tidal flats | Not available          |                      |  |            |
| CH <sub>4</sub> Flux     | Tidal marsh | $0.85 \pm 0.32$        | $\text{TgC yr}^{-1}$ | Extrapolation  | [183]      |
|                          | Tidal flats | Not available          |                      |  |            |
| Net Primary Productivity | Tidal marsh | 0.17–0.42              | $\text{PgC yr}^{-1}$ | Extrapolation  | [180]      |
|                          | Tidal flats | $0.01 \pm 0.013$       | $\text{PgC yr}^{-1}$ | Extrapolation<br>(unvegetated sediments)                         | [184]      |

strategies for mapping US coastal wetland soil carbon stocks using nationally available soil and wetland maps have not outperformed simpler strategies of applying a single average value for carbon stocks. Holmquist *et al* [175, 176] utilized an extensive soil core database to predict tidal marsh soil carbon to 1 m depth (0.72 PgC) within the Contiguous United States (CONUS). The study also showed a way to improve future mapping would be to generate maps based on environmental drivers that differentiate between organic and inorganic soils, differentiated by a threshold of 13% organic matter by dry mass. Elevation relative to the tidal amplitude [177, 178], and long-term rates of relative sea-level rise [179] could be potential predictors of carbon stock. These CMS funded studies demonstrate the need for connecting earth observations and models between land, wetland, and open water; further *in situ* data collection of environmental driver data such as salinity and tidal elevation; and the development of tidal marsh class and change products that can be applied globally.

Additionally, global carbon export from tidal marshes to estuaries is uncertain. The connection between tidal marshes and coastal waters is a long-standing consideration. Teal [185] identifies outwelling as an important potential component of the system, and its magnitude and role have been debated since [186]. The magnitude of C export is highly variable, with tidal marshes being both a sink and a carbon source to coastal waters [187]. Salt marshes export an estimated  $3.3 \text{ Tg POC yr}^{-1}$ ,

and  $14 \text{ Tg DOC yr}^{-1}$ , and  $29 \text{ Tg DIC}$  to coastal oceans [107]. Remote sensing of ocean color to estimate DOC and CDOM can discern spatial and temporal patterns of tidal marsh export [188]. Gao *et al* [144] explored the connection between tidal marsh productivity and detritus export using *in situ* sampling of detritus. Monitoring coastal waters is a difficult remote sensing task (see sections 3.1.3 and 3.3.1). The use of ocean color methods and fine-scale satellite imagery could enhance the capacity to monitor C export from tidal marshes.

### 3.1.3. Submerged aquatic vegetation

In total, we found 45 papers relevant to carbon monitoring with remote sensing in SAV with a primary focus on seagrass. Seagrass is found along all continents except Antarctica and refers to seventy-two species, including *Zostera marina*, *Posidonia oceanica*, *Thalassia testudinum*, and *Zostera noltei* [189]. Seagrass is estimated to store 10%–20% of the ocean's carbon within 0.2% of the total ocean area [24, 125, 190]. However, seagrass extent decreased  $\sim 30\%$  in the last century [191]. During deterioration, seagrass beds can release their carbon into the atmosphere [192]. Improvements in mapping seagrass extent, structure, and carbon storage will enable management by valuing and including seagrass beds in REDD+ type programs. We have grouped our synthesis of the status of carbon monitoring in SAV into two sections: (a) carbon monitoring status and (b) data and limitations.

**Table 3.** Global carbon monitoring value for seagrass from the literature. Method refers to the categories, modeled, data synthesis, extrapolation (*in situ* combined with extent to upscale estimates), and remote sensing (mapping or predicting spatial heterogeneity for an indicator).

| Carbon indicator         | System   | Value                                 | Units                           | Method        | Source                |
|--------------------------|----------|---------------------------------------|---------------------------------|---------------|-----------------------|
| System extent            | Seagrass | Confirmed: 0.15–0.35; potential: 1.6* | 10 <sup>6</sup> km <sup>2</sup> | Extrapolation | [190, 202, 204, 215]* |
| System extent change     | Seagrass | 0.9% (1879–1940), 7% (1990–2006)      | Percent loss yr <sup>-1</sup>   | Extrapolation | [216]                 |
| Carbon stock             | Seagrass | 4.2–8.4                               | PgC                             | Extrapolation | [190]                 |
| Carbon burial            | Seagrass | 48–112                                | TgC yr <sup>-1</sup>            | Extrapolation | [125]                 |
| Emissions                | Seagrass | 0.014–0.09                            | PgC yr <sup>-1</sup>            | Extrapolation | [19, 190]             |
| CH <sub>4</sub> Flux     | Seagrass | Not Available                         |                                 |               |                       |
| Net Primary Productivity | Seagrass | 0.06–1.94                             | PgC yr <sup>-1</sup>            | Extrapolation | [180]                 |

### 3.1.3.1. Carbon monitoring status

Seagrass biomass is below the water's surface; therefore, atmospheric and coastal water conditions influence mapping [190]. Similarly, temporal and spatial variability in water quality and depth hinder seagrass identification e.g. [193–197]. These difficulties can result in misclassification between seagrass and algae [197–201]. Due to the remote sensing challenges, seagrass mapped extent is an order of magnitude less than modeled extents [202, 203]. Consequently, scientists lack a global map of seagrass extent, and recent estimates are uncertain (160 387–266 562 km<sup>2</sup>) [204]. Seagrass aboveground carbon stocks are even more uncertain due to mapping error and regional, intraspecies, and interspecies variability in biomass [199, 203, 205, 206]. Globally, two-thirds of seagrass living carbon ( $2.52 \pm 0.48$  Mg C ha<sup>-1</sup>) is belowground, and seagrass SOC is ~65 times greater (165.6 Mg C ha<sup>-1</sup>) [190].

Novel methods for linking remote sensing and *in situ* data have improved our understanding of seagrass cover and carbon storage. For example, seagrass cover estimates from UAS and *in situ* images can bridge the scale differences of AGB samples and remote sensing imagery [194, 196, 197]. Seagrass extent mapped with UAS imagery has been used to scale *in situ* carbon samples to the landscape by percent cover [207]. Zoffoli *et al* [208] used a linear model to predict biomass with *in situ* radiance (RMSE = 5.31 g m<sup>-2</sup>) and applied that to Sentinel-2 imagery, successfully capturing seasonality. Modeling optical properties of seagrass has led to the development of a model to estimate LAI that does not require *in situ* data [209, 210]. In addition to satellite and aerial platforms, ship-based acoustic sensors can identify species [211] and estimate biomass [205]. Data fusion between ship-based sensors, satellites, and UAS has improved seagrass extent maps [212] and benefit biomass mapping.

### 3.1.3.2. Data and limitations

Mapping was the primary seagrass research topic reviewed due to the challenges of modeling seagrass carbon and the need to address data gaps in known

seagrass extent. These challenges have resulted in high uncertainty in seagrass extent estimates (table 3). For example, high-resolution imagery, informed by a species distribution model, was used to manually digitize seagrass beds within a single bay, resulting in a 44% increase in mapped seagrass extent [213]. Poursanidis *et al* [214] map change between submerged vegetation and other benthic substrate following the cyclone season. Both Landsat and Sentinel-2 have the capacity for regional to global mapping of seagrass.

Additionally, higher spatial resolution sensors, such as PlanetScope, have improved classification accuracy compared to Sentinel-2 [197]. UAS imagery (<5 cm) has shown the capability to map local seagrass extent and carbon [207, 217]. Object-based methods help separate areas of similar seagrass cover, water quality, and depth [212] but do not necessarily improve accuracy [217]. Recent advancements in acoustic measurements of photosynthesis-derived oxygen bubbles [218] and tracking seagrass grazing animals [219] have increased seagrass mapped extent. Furthermore, machine learning has improved seagrass bed identification [195, 220, 221]. Remote sensing methods, including object-based image analysis, machine learning, physics-based modeling, and integration of multiple scales of training data, have improved carbon monitoring of seagrass.

Estimating seagrass carbon fluxes with remote sensing is difficult due to varying light, tides, currents, water quality, [e.g. 192, 197, 203] and biogeochemical process (i.e. carbon fixation and CaCO<sub>3</sub> [201, 222–225]), even with *in situ* CO<sub>2</sub> flux measurements [226]. Furthermore, the major drivers of sediment carbon changes within regions from autochthonous to allochthonous based on seagrass canopy complexity, turbidity, and wave environment, further complicating carbon flux monitoring [227]. Water depth is an important factor in estimating seagrass carbon storage [227–229]. Thomas *et al* [230] demonstrate a data fusion approach using ICESat-2 and Sentinel-2 to map bathymetry in shallow, optically clear coastal water addressing a key data gap in most optical seagrass mapping approaches. Carbon fluxes are challenging to



monitor, but modeling and remote sensing have improved our understanding of the biogeochemical processes and site characteristics contributing to flux variability.

The carbon impacts of seagrass loss are hard to quantify due to a lack of precise mapping and carbon storage information. Local estimates of seagrass loss range from highs of  $\sim 2.8\% \text{ yr}^{-1}$  [191, 231] to lows of  $1.2\% \text{ yr}^{-1}$  [206], and globally, since 1990, seagrass loss rate is estimated to be  $\sim 7\% \text{ yr}^{-1}$  [24]. The major drivers of seagrass loss are direct anthropogenic impacts [232–234] from boats, development, dredging, and marine pollution [191, 235], as well as overgrazing due to alterations to the food web [236]. Marine heat waves due to climate change can exacerbate seagrass loss [192, 237], and temperature increases are likely to drive future losses [206]. Seagrass beds experience multiple stressors associated with water quality, temperature increases, and overgrazing which can shift seagrass beds from stable ecosystems to rapid deterioration [192, 206, 217]. However, both improvements in water quality [207, 231, 238] and planting have successfully restored seagrass and increased carbon storage and ecosystem services [239, 240]. High but uncertain loss rates and the success of restoration necessitate improved remotely sensed and *in situ* quantification of seagrass baseline and change in extent to facilitate its inclusion into carbon monitoring and offset programs.

### 3.2. Inland wetlands

In total, we found 55 papers relevant to carbon monitoring with remote sensing in mineral wetlands. We found an additional 129 papers relevant to carbon monitoring with remote sensing in peatlands and 80 in permafrost due to the current status and prevalence of the research themes we have separated these into two sections. Wetlands are defined by vegetation type, hydrology, and soil properties [241] and classified in the US based on hydrogeomorphic position and vegetation [242]. These landscapes are dynamic with highly variable carbon fluxes, changing hydrology, and impacted by anthropogenic disturbance such as draining for agricultural development and deforestation [29, 243]. Palustrine wetlands span organic soil peatlands to mineral soil saline wetlands in arid regions [242]. By this definition, inland wetlands disproportionately contribute to carbon storage, storing 30% (202–754 PgC) of the global SOC stock (1500 PgC) while only occupying 8%–11% of the land surface [11, 244, 245]. Due to the magnitude of carbon storage in inland wetlands, Nahlík and Fennessy [245] referred to this carbon as ‘teal carbon.’ However, there is a distinction within inland wetlands between peatlands and mineral soil wetlands. Peatland is a general term used to describe a wetland with an organic soil; however, the definition of an organic soil varies by country and region. We have grouped

our synthesis of the status of carbon monitoring in inland wetlands into two sections: (a) mineral wetlands and (b) peatlands and permafrost.

#### 3.2.1. Mineral wetlands

As previously mentioned, wetlands are defined by vegetation, soils, and hydrology but remotely mapping wetland extent requires indirectly associating these attributes with remote sensing data and introduces additional uncertainty. The extent of wetlands is a long, sought-after metric and has changed greatly over time [246]. The United States National Wetland Inventory demonstrated that baseline mapping followed by subsequent updated digitization from aerial imagery can be utilized to create robust wetland change estimates [247]. Mineral wetlands are difficult to map due to their high diversity, hydrologically dynamic, and variable size. These factors impact carbon monitoring uncertainty and increase from local to global extent (figure 2). Mineral wetland carbon is challenging to measure, upscale, and monitor over both large spatial extents and at fine scales. Recent research has utilized time-series analysis of satellite imagery to estimate inundation extents and hydroperiods and, therefore, a variable approximation of wetland extent at the site level [248, 249]. Ignoring temporal variability, lidar has been used to map wetland extent via landform delineation. Lidar has been especially effective for mapping wetlands under a forested canopy [250, 251]. SAR has also been increasingly used in wetland extent mapping research, e.g. using the L-Band frequency to detect inundation at various spatial scales [252]. We have grouped our synthesis of the status of carbon monitoring in mineral wetlands into two sections: (a) carbon monitoring status and (b) data and uncertainty.

##### 3.2.1.1. Carbon monitoring status

Wetland belowground carbon is primarily determined with field-intensive surveys to collect soil core samples, e.g. the National Wetland Condition Assessment in the United States [245]. Remote sensing has been increasingly deployed to upscale field observations from sample points to the plot or study area scale. For example, distribution maps of soil carbon stocks have been created from soil core measurements using satellite imagery [253, 254]. Satellite imagery has also aided measurements of carbon accumulation in sediments [255, 256]. Other fine-scale approaches have used UASs and Ground Penetrating Radar [257–259]. Despite these advances, high uncertainty in soil carbon estimates from remote sensing remain due to a lack of consistent depth measurements, including the depth of the upper horizons where most carbon is stored and can differentiate more mineral soil wetlands from peatlands [245].

The prediction of carbon storage in AGB with remote sensing is well studied, particularly in forested ecosystems. For mineral wetlands, studies have used



remote sensing to upscale plot-level data of AGB to wider extents, such as the watershed-scale [260–262] including forested riparian wetlands [263]. Lidar has been used extensively in forest biomass research, and mineral wetland applications are increasing [264]. Studies scale site-level aboveground carbon metrics from estimates of AGB or carbon through land-use maps and spectral indices from Landsat [265], MODIS [266], Hyperion [267], and commercial satellites [268]. Budzynska *et al* [269] predicted other carbon indicators, e.g. LAI and % soil moisture, with SAR and optical data. Riegel *et al* [264] estimated aboveground carbon using aerial lidar and aerial imagery. Productivity rates, including both GPP [270, 271] and NPP [261], have been measured and upscaled to local, regional, and global scales.

Carbon gas fluxes, in particular methane ( $\text{CH}_4$ ) emissions, have been of interest in recent research for mineral wetlands [272]. Most of this research has focused on peatlands in northern latitudes with fewer measurements and less a focus on mineral soil wetlands [241]. In terms of scale,  $\text{CH}_4$  has been evaluated with remote sensing at the regional or country level by combining satellite imagery with process models [273]. Inundation detection has been a key component to broad-scale  $\text{CH}_4$  mapping with many models using the Global Inundation Extent from Multi-Satellites dataset [274, 275]. However, more recent research has used fine-scale, 3 m resolution satellite imagery to map inundation detection at the watershed scale to evaluate  $\text{CH}_4$  fluxes [276]. Lu *et al* [277] used eddy covariance data from flux towers to demonstrate that mineral wetlands are net sinks and identify a need to incorporate remote sensing to predict  $\text{CO}_2$  flux spatially.

### 3.2.1.2. Data and uncertainty

Global assessment of mineral wetland carbon is limited by *in situ* carbon measurements and wetland map coverage. Recent assessments of global wetland coverage have utilized coarse-scale inundation mapping downscaled by topographic metrics [257, 278]. However, inundation approaches do not distinguish wetland types, e.g. these maps often include peatlands (section 3.2.2) and mineral wetlands. Thus, the best-estimated extent comes from Lehner and Döll [279] and the Global Lakes and Wetlands Database, which estimated that non-peatland marshes, swamps, and forested wetlands cover  $3.7 \times 10^6 \text{ km}^2$  or  $\sim 2.5\%$  of the terrestrial land surface [13].

Global scale carbon measurements have yet to account for these changes in areal extent estimates. For example, Bridgham *et al* [11] used an average of two older sources [280, 281] for freshwater mineral soil wetland area ( $2.315 \times 10^6 \text{ km}^2$ ) to upscale carbon burial, carbon soil stock, and  $\text{CH}_4$  flux (table 4). Similarly, Roehm [282] utilized two older sources [283, 284] to combine areal extent estimates of northern and tropical marshes and

swamps ( $3.5 \times 10^6 \text{ km}^2$ ) to upscale NPP and  $\text{CO}_2$  flux (table 4). This latter estimate is closer to the Lehner and Döll [279] estimate than the one used in Bridgham *et al* [11]. Carbon monitoring research interest in  $\text{CH}_4$  is high due to its global warming potential. Thus, the global assessment of a  $\text{CH}_4$  flux has been parsed by wetland type and separated from peatlands [275].

### 3.2.2. Peatlands and permafrost

Peatland extent comprises  $\sim 3\%$  of the globe's terrestrial area [285], and their carbon stock is estimated to be between 528 and 600 Pg [286], representing 30% of the global belowground soil organic C stock [287–289]. Generally, peatland refers to a class of wetlands where the long-term rate of primary production is greater than the decomposition rate and losses from other sources such as wildfire and dissolved carbon export [290]. Thus, peatlands have soils with deep accumulations of organic matter, but the minimum thickness necessary to be considered peat varies significantly ( $\sim 30\text{--}50 \text{ cm}$ ) [285, 290]. The accrual of peat over millennia leads to the formation of deep peat deposits, which may reach depths of 15–20 m [291–293]. We discuss peatlands by bioregion (tropical, temperate, and boreal). Considering peatlands by climatic region is necessary due to the latitudinal gradient in carbon accumulation, with colder regions having higher peat accumulation rates to a point [294, 295], also higher in tropical mountain peatlands [296]. We have grouped our synthesis of the status of carbon monitoring in peatlands into five sections: (a) tropical peatlands, (b) temperate peatlands, (c) boreal peatlands and permafrost, (d) peatland fires, and (e) data and uncertainty.

#### 3.2.2.1. Tropical

Tropical peatland carbon indicators included AGB, degradation, subsidence, and canopy height. Southeast Asia ( $n = 34$ ) was the primary focus of tropical peatland research, with additional studies focused on South America and Africa. South American studies mapped carbon stocks [296–299], extent and degradation [300], and mountain peatland stocks using SAR and multispectral imagery [301, 302]. In Africa, research focused on mapping the extent, depth [302, 303] and estimating carbon stocks [304]. In Southeast Asia, degradation, loss, and recovery were major research topics enabled by lidar, SAR, and multispectral imagery. Studies have used lidar to detect illegal logging and carbon sequestration [305], map peat depth [306], and estimate AGB for tropical peatlands [307]. Minasny *et al* detail an open data and mapping methodology with the ability to predict peat depth at a lower cost than lidar [308]. SAR particularly useful in tropical peatlands due to cloud and forest canopy penetration and its sensitivity to inundation and biomass [290, 296]. SAR applications included dinSAR to map subsidence across Southeast Asia

**Table 4.** Global carbon monitoring values for inland wetlands from the literature. Method refers to categories: modeled, extrapolation (*in situ* combined with extent to upscale estimates), data synthesis, and remote sensing (mapping or predicting spatial heterogeneity for an indicator).

| Carbon indicator  | System   | Value   | Units                           | Method                      | Source    |
|---|--|---------|---------------------------------|-----------------------------|-----------|
| System extent   | Global Inland Wetlands on Alluvial Soils                 | 3.7     | 10 <sup>6</sup> km <sup>2</sup> | Remote Sensing              | [13, 279] |
|   | North America Inland Mineral Soil Wetlands               | 0.93    | 10 <sup>6</sup> km <sup>2</sup> | Mixed                       | [241]     |
| System extent change  | Global Long-term (Pre-1900s to 2000)                     | −0.39   | % yr <sup>−1</sup>              | Extrapolation               | [29]      |
|   | Global Short-term (1990 to 2000s)                        | −0.48   | % yr <sup>−1</sup>              |                             |           |
|   | Total loss of North America Inland Mineral Soil Wetlands | 28.62   | %                               | Extrapolation               | [241]     |
| Carbon burial (sediment accumulation)                             | Inland Freshwater Mineral Soil Wetlands                  | 39 ± 39 | TgC yr <sup>−1</sup>            | Extrapolation               | [11]      |
| Carbon stock (Soil)   | Inland Freshwater Mineral Soil Wetlands                  | 46 ± 9  | PgC                             | Extrapolation               | [11]      |
|   | North America Inland Mineral Soil Wetlands               | 29.3    | PgC                             | Mixed                       | [241]     |
|   | Inland Freshwater Mineral Soil Wetlands                  | 2.2     | PgC yr <sup>−1</sup>            | Extrapolation               | [282]     |
| Carbon emissions (CO <sub>2</sub> Flux)                           | North America Inland Mineral Soil Wetlands               | −64.3   | TgC yr <sup>−1</sup>            | Mixed                       | [241]     |
| Net Ecosystem CO <sub>2</sub> Exchange (Net CO <sub>2</sub> flux) | Inland Freshwater Mineral Soil Wetlands                  | 68 ± 68 | TgC yr <sup>−1</sup>            | Remote Sensing and Modeling | [11]      |
| CH <sub>4</sub> Flux  | North America Inland Mineral Soil Wetlands               | 25.2    | TgC yr <sup>−1</sup>            | Mixed                       | [241]     |
|   | Inland Freshwater Mineral Soil Wetlands                  | 3.2     | PgC yr <sup>−1</sup>            | Extrapolation               | [282]     |
| Net Primary Productivity  | Inland Freshwater Mineral Soil Wetlands                  |         |                                 |                             |           |

[309] and predict AGB [310]. Studies have addressed remote sensing limitations by using multiple satellites to expand spatial and temporal coverage of fires [311] and the utilization of lidar to expand training data [310]. Despite the significant research interest, tropical peatlands lack regional and global scale monitoring due in part to data availability, extent uncertainty, and resources.

### 3.2.2.2. Temperate

Historically, temperate peatlands have frequently been managed for fuel, drained for agriculture, or other land-use [288, 312, 313]. Temperate peatland indicators included GPP [313, 314], water table dynamics [315], erosion [316], disturbance [317], peat depth [318], and moisture [313, 314]. Due to the prevalence of past anthropogenic disturbance, restoration and recovery are common research topics [319–322]. High-resolution imagery is common for site-scale studies, including satellite [316, 323, 324], UAS [325], aerial [326], and handheld spectrometers [314]. Aitkenhead and Coull [318] conducted a regional carbon monitoring system creating a national map of peat depth and Scotland's carbon content. The variety of temperate peatland vegetation and the importance of subsurface carbon stocks are challenges for regional and global monitoring.

### 3.2.2.3. Boreal and permafrost peatlands

The boreal and tundra regions ( $n = 35$ ) are data-poor due to remoteness and the short field season limiting *in situ* data collection. There are also significant human development pressures in parts of the boreal zone for petroleum exploration, mining, forestry, agriculture, and infrastructure operations. Even low impact disturbances such as seismic lines will increase the fragmentation of wetlands and have ecological impacts [345]. Most degraded peatlands are tropical [288] but boreal peatlands and permafrost will change significantly with warming and changes to precipitation [346].

Optical remote sensing data in boreal environments is limited due to sun angle, cloud cover, and the short growing season [347]. The floristic similarity between peatlands and non-peatland ecotypes makes identifying landform and hydrology with active sensors particularly important. The focus on topography and landform included identifying permafrost peat mound degradation with aerial and high-resolution imagery [348], classifying boreal bogs with microtopographic variation from lidar [349], mapping thermokarst lakes with spectral imagery [350, 351], detecting freeze thaw dynamics with SAR [352], detecting permafrost extent with electromagnetic imaging [353], and mapping

**Table 5.** Existing global carbon monitoring indicator values for peatlands and permafrost. Method refers to the categories, modeled, data synthesis, extrapolation (*in situ* combined with extent to upscale estimates), and remote sensing (mapping including remote sensing derived spatial heterogeneity). No isolated values for CH<sub>4</sub> flux or carbon export found.

| Carbon indicator     | System                     | Value                                   | Units  | Method          | Source     |
|----------------------|----------------------------|---|--|-----------------|------------|
| System Extent        | Total Peatlands            | 4.2                                     | 10 <sup>6</sup> km <sup>2</sup>              | Various         | [285]      |
|                      | Tropical Peatlands         | 0.387–1.7                               | 10 <sup>6</sup> km <sup>2</sup>              | Various         | [327, 338] |
|                      | Temperate/Boreal Peatlands | 4.06                                    | 10 <sup>6</sup> km <sup>2</sup>              | Various         | [287]      |
|                      | Permafrost                 | 22.0                                    | 10 <sup>6</sup> km <sup>2</sup>              | Modeled         | [339]      |
| System Extent Change | Peatlands                  | 0.5                                     | % yr <sup>-1</sup> (1990–2008)               | Various methods | [13, 340]  |
| Carbon burial        | Peatlands                  | 0.14 ± 0.007                            | PgC yr <sup>-1</sup>                         | Extrapolation   | [341]      |
|                      | Tropical Peatlands         | 0.02                                    | PgC yr <sup>-1</sup>                         | Extrapolation   | [287]      |
|                      | Temperate/Boreal Peatlands | 0.09                                    | PgC yr <sup>-1</sup>                         | Extrapolation   | [287]      |
|                      | Permafrost                 | –0.55                                   | PgC yr <sup>-1</sup>                         | Modeled         | [342]      |
| Carbon stock         | Tropical peatlands         | 81.7–91.9                               | PgC  | Extrapolation   | [343]      |
|                      | Temperate/Boreal Peatlands | 473–621                                 | PgC  | Various         | [287]      |
|                      | Permafrost                 | 1700                                    | PgC  | Extrapolation   | [9]        |
| Carbon emissions     | Tropical peatlands         | 1.26 ± 0.77 (includes CH <sub>4</sub> ) | Pg CO <sub>2</sub> e yr <sup>-1</sup> (2015) | Extrapolation   | [344]      |
|                      | Temperate/Boreal peatlands | 0.27 ± 0.03 (includes CH <sub>4</sub> ) | Pg CO <sub>2</sub> e yr <sup>-1</sup> (2015) | Extrapolation   | [344]      |
|                      | Permafrost                 | Not available                           |  |                 |            |

lake extent with multispectral imagery [354]. An integration of multi-season SAR and multispectral imagery was complementary in detecting vegetation and hydrologic differences in bogs versus fens in the boreal zone [290, 355]. Carbon monitoring efforts included modeling gas fluxes [272, 328, 356], upscaling *in situ* emission estimates with land cover maps [350, 329, 330, 357], and peat extent [358]. Major change drivers within the system include increasing temperatures [351, 331, 332, 359] and fire [333, 360]. Boreal systems are critical for understanding the global carbon cycle, and unique challenges to *in situ* and remote sensing data collection are being addressed by science programs such as the NASA Artic-Boreal Vulnerability Experiment [361].

#### 3.2.2.4. Fires

The global importance of peatland fires in Southeast Asia has long been acknowledged, with peak yearly emissions equaling 13%–40% of the mean annual global carbon emissions from fossil fuels [23]. Earth observation has enabled and verified peatland fires. Page *et al* [23] primarily used fire extent mapped from Landsat to understand peatland fires carbon emissions (2002). Lidar has been used to map fire scars and burn depth improving emission estimates [362]. Emission estimates and burn area models have used satellite-derived peatland fire data from the Global Fire Emissions Database for verification [334, 335, 363]. SMAP soil moisture data has been used to provide fire warnings, predict burn area [364], and as an input in emission models [365]. Drought can worsen emissions from forest fires within temperate/subtropical peatlands (0.32 PgC) [366]. Thus,

earth observation is critical for modeling and verifying this important source of CO<sub>2</sub> emission. CMS has supported several fire mapping efforts of which peatlands are the focus [367] or included in more general fire data [368].

Fires in permafrost regions are also a major climate concern with remote sensing monitoring applications. Remote sensing has identified fires as the most prevalent disturbance in the permafrost region [369], leading to widespread permafrost thawing [370]. SAR has been used to track subsidence following vegetation loss in permafrost regions, including subsidence of 0.5–3 cm yr<sup>-1</sup> in deforested areas [371] and the rapidly developed thermokarst following fires with rates of subsidence up to 6.2 cm yr<sup>-1</sup> [372]. Studies have used SAR interferometry to model recovery and loss estimating that 4 m of permafrost is lost in a fire event and recovery takes up to 70 years [373]. For wildfire effects, algorithms were developed for assessing peat burn severity (depth) using Landsat-5 [293] and Landsat-8 [374]. Projections suggest rapid thawing will release 60–100 PgC, and gradual thaw regions will release another 200 PgC by 2030 [375]. Permafrost thawing will release significant mercury into the environment [376].

#### 3.2.2.5. Data and uncertainty

Globally, peatlands represent a massive SOC stock (table 5) and a remote sensing challenge due to their disparate data needs and global range. Peatland extent is  $\sim 4.0106 \times 10^6$  km<sup>2</sup> and  $4.5104 \times 10^4$  km<sup>2</sup> in the northern and southern hemispheres, respectively [287, 290]. Boreal regions of the northern hemisphere are 25%–30% peatland and comprise most of the

global extent [290, 377]. Tropical peatland carbon (88.6 Pg) is estimated to be 15% of the global peatland carbon, with boreal and temperate peatland carbon estimated to be 521.4 Pg [343]. Temperate peatland carbon is understudied and as a result has high uncertainty in the carbon estimates [378]. The area of tropical peatlands is uncertain (387 201–657 430 km<sup>2</sup>), and the largest area (56%) and most of the carbon stock (77%) are in Southeast Asia [327], followed by the Amazon basin [379]. Africa's lowland peatland area is largely unknown except for the Congo Basin [303]. Tropical alpine peatlands are numerous in the Andes, many islands, and Africa [290, 380, 381]. Permafrost peatlands are estimated to contain 277 PgC and are changing rapidly due to global warming and fire [336, 337, 382]. The carbon store within the permafrost region is estimated to be ~1300 Pg (1100–1500 Pg) with 500 Pg within the active layer [383].

### 3.3. Inland waterbodies

#### 3.3.1. Lakes and ponds

In total, we found 64 papers relevant to carbon monitoring with remote sensing in lakes and ponds. Freshwater lakes are an important component of the global carbon cycle, but this has not always been acknowledged [384–388]. This oversight is primarily due to the small fraction of the earth's surface area covered by lakes, the large number, the diversity of freshwater lake type, and the complex carbon cycle of individual lakes [384, 386, 387, 389]. Recent work suggests that the carbon cycle of individual lakes can vary significantly across time and space depending on thermal stratification, allochthonous loading, trophic state, and degree of anthropogenic influence [15, 388, 390, 391]. Large lakes are common in the boreal region and freshwater lakes play a crucial role in transforming and storing carbon [386]. We have grouped our synthesis of the status of carbon monitoring in lakes into two sections: (a) carbon monitoring status and (b) data and applications.

##### 3.3.1.1. Carbon monitoring status

Phytoplankton photosynthesis is the primary process by which carbon dioxide is fixed from the water column and overlying atmosphere. Remote sensing applications to estimate phytoplankton photosynthesis or primary production in the marine environment are numerous (see section 3.4). However due to the spatial variability and optical complexity, applications to freshwater systems are scarce. Advances in remote sensing platforms and algorithm development have allowed for the characterization of phytoplankton abundance and productivity in various freshwater environments [e.g. 392–397]. Remote sensing approaches hold much promise for sampling many lakes on the planet [398] and understanding global trends in phytoplankton [399].

Globally, freshwater lakes exhibit a wide range in size and shape, creating a unique challenge for

applying remote sensing methods. Accurate estimates of freshwater phytoplankton biomass require remote sensing data with specific wavelengths associated with spectrally narrow chlorophyll-*a* absorption features and high signal-to-noise ratios [400]. Satellite sensors with these spectral requirements often target oceans and typically have a coarser spatial resolution (300 m–1000 m), limiting their ability to observe smaller freshwater features. These requirements limit how carbon monitoring of freshwater lakes. The Plankton, Aerosol, Clouds, ocean Ecosystem will address spectral needs of ocean color remote sensing but is still too coarse (<1 km<sup>2</sup>) to discern small-scale waterbodies [401]. Instead, data fusion using high-resolution imagery and ocean color remote sensing are likely necessary to improve mapping of phytoplankton biomass in lakes and ponds.

##### 3.3.1.2. Carbon fixation

Several recent works have used a mechanistic carbon fixation model adapted for use in the Laurentian Great Lakes [396, 397] to estimate carbon fixation in the world's large lakes [402]. Additionally, a simple depth integrated model approach (DIM) was refined to estimate growing season carbon fixation of ~80 000 freshwater lakes [403]. The DIM approach relies on the light-utilization index, which relates to latitude providing a straightforward method to estimate carbon fixation rates when minimal limnological data is available. The marine standard Vertically Generalized Production Model has also been applied to estimate carbon fixation in large lakes [409]. Remote sensing approaches to estimate freshwater phytoplankton carbon fixation have been developed and applied for small lakes [410, 411].

Lake carbon budgets are highly dependent on carbon fixation rates, yet these rates are unknown for most lakes. McDonald *et al* [412] estimated that there are over 60 million lakes. Estimating carbon fixation in all these lakes would be impossible with *in situ* methods. Therefore, the development of remote sensing methods to estimate carbon fixation rates is a current focus. Still, global-scale estimates remain elusive due to the lack of readily available remote sensing products appropriate for optically and spatially complex inland lakes. However, several recent works have estimated global scale freshwater carbon fixation for satellite observable lakes [402, 403]. These works also examined carbon fixation on multiple temporal scales ranging from a single year growing season snapshot for ~80 000 lakes [403] to a 15 year time-series for the world's eleven largest lakes [402]. The latter work revealed significant changes in carbon fixation for several lakes, likely in response to changes in climate. The use of remote sensing to understand spatial variability across lakes is lacking in many of the existing global carbon monitoring values (table 6).

Additionally, common carbon monitoring measurements in lakes include chlorophyll-*a*, DOC, CO<sub>2</sub>



**Table 6.** Global carbon monitoring values for lakes. Method refers to the categories, modeled, extrapolation (*in situ* combined with extent to upscale estimates), data synthesis, and remote sensing (mapping including remote sensing derived spatial heterogeneity).

| Carbon indicator                      | System               | Value            | Units                                  | Method         | Source     |
|---------------------------------------|----------------------|------------------|--|----------------|------------|
| System extent                         | Lakes                | 5                | 10 <sup>6</sup> km <sup>2</sup>        | Remote sensing | [404]      |
| Carbon burial (sediment accumulation) | Lakes and Reservoirs | 0.15 (0.06–0.25) | Pg CO <sub>2</sub> –C yr <sup>−1</sup> | Modeling       | [405]      |
| Carbon fixation                       | Lakes                | 0.376            | PgC yr <sup>−1</sup>                   | Remote sensing | [403]      |
| Carbon fixation                       | Lakes                | 1.3              | PgC yr <sup>−1</sup>                   | Modeling       | [406]      |
| Carbon storage                        | Lakes                | 820              | PgC                                    | Extrapolation  | [384, 407] |
| Carbon Flux                           | Lakes                | 0.75–1.65        | PgC yr <sup>−1</sup>                   | Extrapolation  | [384]      |
| CH <sub>4</sub> Flux                  | Lakes                | 71.6             | Tg CH <sub>4</sub> yr <sup>−1</sup>    | Extrapolation  | [408]      |

flux, and GPP. Kuhn *et al* [413] calculated boreal lake GPP with aerial and satellite imagery and verified the result with *in situ* measurements. Remote sensing combined with *in situ* measurements clarified that boreal lakes may have a limited role in carbon mineralization [414]. Lake color in the region has been tracked with the satellite record identifying increased connection with the surrounding landscape [415]. The combination of electromagnetic imaging and satellite imagery has mapped the temporal dynamics of hydrological connectivity between boreal lakes and permafrost [416]. Remote sensing is critical for understanding the effect of climate change on the carbon cycle in permafrost regions.

Methods to estimate chlorophyll-*a* concentrations range from empirical and semi-analytical approaches and, more recently, machine learning and artificial intelligence-based techniques (Reviews in [417, 418]). Initial work has been done to estimate global freshwater lake chlorophyll concentrations [398]. However, more robust methods to account for the varying optical complexity of lakes should be developed. The GloboLakes initiative has developed a freshwater chlorophyll retrieval algorithm, generated a global time-series of chlorophyll concentrations for ~1000 lakes, and provided monitoring products for the ESA Climate Change Initiative [419].

DOC and CDOM are also frequently monitored in lake environments with remote sensing. CDOM algorithm comparisons found that remote sensing algorithms did not predict the highs or lows well [420], but continued algorithm refinements are promising [421]. Brezonik *et al* [422] demonstrated a strong relationship between CDOM and DOC but were cautious about assuming a consistent relationship. Geographically diverse study sites suggest the possibility of applying these methods globally [423].

CO<sub>2</sub> flux has been estimated with partial pressure of CO<sub>2</sub> (*p*CO<sub>2</sub>) in coastal oceans [424]. Simple relationships have also been developed between bio-geochemical properties and freshwater carbon flux through comparisons with Eddy-covariance flux tower measurements [425]. While these methods show promise, applications in freshwater lakes are infrequent. Similarly, very few efforts have been made

to fully characterize carbon fractions in freshwater systems, although initial efforts seem promising [426] and are worthy of continued research.

### 3.3.2. Rivers

In total, we found 33 papers relevant to carbon monitoring with remote sensing of rivers. Rivers and streams receive a large amount of carbon from terrestrial ecosystems and actively cycle carbon through them by outgassing CO<sub>2</sub> and CH<sub>4</sub> into the atmosphere, burying particulate carbon in the riverbed, and exporting organic and inorganic carbon into estuaries and coasts [15, 384, 427–434]. Meanwhile, the flowing waters in river networks link the carbon cycle in non-flowing (or slowly flowing) waterbodies and wetlands. Here we summarize and discuss carbon monitoring of rivers and streams based on the literature. We do not include terrestrial carbon inputs due to the lack of direct observations as that carbon flux is often inferred through mass balance analysis by assuming no accumulation of carbon in inland waters [435]. We have grouped our synthesis of the status of carbon monitoring in rivers into three sections: (a) carbon export, (b) outgassing of CO<sub>2</sub> and CH<sub>4</sub>, and (c) carbon burial.

#### 3.3.2.1. Carbon export

Riverine C export is well constrained using global streamflow discharge and measurements of aqueous carbon concentrations [384, 433]. Stream gauge and water quality data can provide the necessary data for the extrapolation of C export at continental scales [436] and global scales [437, 438]. Mass balance analysis and data initiatives have refined global estimates [15, 439]. Many studies have established empirical relationships between surface organic C concentrations (e.g. POC, DOC, and phytoplankton) and remote sensing data across various aquatic systems, including river reaches [e.g. 440–447].

Remote sensing derived C concentrations have been used to estimate riverine export to estuaries and coasts. For example, Chunhock *et al* [448] calculated river-to-ocean fluxes with remote sensing derived DOC concentrations near the river mouth in conjunction with discharge data. Liu *et al* [449] used

Landsat-derived POC concentrations and monthly river discharges near the mouth of the Yangtze River to assess long-term patterns of riverine POC fluxes from 2000 to 2017. Successful application of remote sensing methods requires continual monitoring of constituent concentrations and a large enough water body (e.g. river with a width larger than 90 m) to be observed from satellite imagery [450], making it challenging to apply them in small rivers and streams. High-resolution UAS imagery was applied to detect water quality parameters in small rivers/streams, such as chlorophyll-*a*, Secchi disc depth, and turbidity, with limited success [451, 452]. Therefore, carbon monitoring of rivers and small streams with remote sensing requires further research and technological advancement.

### 3.3.2.2. Outgassing of CO<sub>2</sub> and CH<sub>4</sub>

In the past two decades, quantification of regional and global CO<sub>2</sub> outgassing from streams and rivers has made great progress. Richey *et al* [453] in a pioneering study of regional-scale CO<sub>2</sub> outgassing in the Amazon River basin, used field observations to estimate CO<sub>2</sub> emissions per unit area in mainstem and floodplains. They used JERS-1 L-band SAR to estimate areal coverage and inundation status of rivers and floodplains (>100 m in width) and developed empirical relationships for smaller streams. Since then, multiple studies have continued to use remote sensing to refine estimates of CO<sub>2</sub> emissions from the running waters in the Amazon. For example, Johnson *et al* [454] constrained their analysis to seasonally inundated areas based on SAR detected high and low water periods. De Fátima *et al* [455, 456] used a 100 m DEM to improve the surface area calculation. Recently, Sawakuchi *et al* [431] used model estimates of surface area to estimate outgassing in the lower Amazon River Basin. These advances have resulted in an estimate of  $\sim 0.96 \text{ PgC yr}^{-1}$  CO<sub>2</sub>-C outgassing from the rivers and streams in the Amazon [433], nearly double the estimate by Richey *et al* [453], which included both rivers and floodplains. In another salient example of regional carbon accounting, Butman and Raymond [457] used numerous USGS field observations and the National Hydrography Dataset plus [458] river networks to estimate surface water area. These studies demonstrate the need for high-resolution river networks and water surface area data to monitor CO<sub>2</sub> outgassing from rivers reliably.

At the global scale, Richey *et al* [453] upscaled their estimates of CO<sub>2</sub> outgassing in the Amazon River Basin to calculate outgassing from rivers and floodplains in the global humid tropics. This was much higher than contemporary estimates not informed by remote sensing [384, 459]. Battin *et al* [460] analyzed the net heterotrophy (respiration—GPP) of 130 rivers and streams and extrapolated the results to the global scale by multiplying average

emissions of streams and rivers by global surface area. Utilizing remote sensing data including hydrological data derived from the SRTM, Raymond *et al* [430] reported a  $1.8 \text{ PgC yr}^{-1}$  of CO<sub>2</sub> outgassing from global streams and rivers. Recently, the global relevance of dry inland waters to the carbon cycle has been identified [461–463], representing unreported CO<sub>2</sub> emissions [430].

Progress has also been made for accounting CH<sub>4</sub> emissions from global freshwaters. Bastviken *et al* [408] synthesized and calculated average areal field observations of CH<sub>4</sub> fluxes of various types of freshwaters (including lakes, reservoirs, wetlands, and lakes) by different latitudes to estimate a total of  $103.3 \text{ Tg CH}_4 \text{ yr}^{-1}$ , of which rivers contributed  $\sim 1.5 \text{ Tg CH}_4 \text{ yr}^{-1}$  (or  $\sim 10 \text{ Tg C (CO}_2\text{-e) yr}^{-1}$ ). The scarcity of observed data points and the exclusion of small streams in the river surface area likely contributed to low river flux [464]. Overall, CH<sub>4</sub> emissions from streams and rivers are less studied than CO<sub>2</sub> emissions.

In general, current riverine CO<sub>2</sub> and CH<sub>4</sub> outgassing estimates are subject to large uncertainties due to difficulty in accurately measuring surface water area, partial pressure of CO<sub>2</sub>, and gas exchange rates [427]. More field data and high spatial resolution remote sensing are needed to refine surface water area and gas exchange rates. The global studies rely on river networks primarily based on NASA's global SRTM DEM at 90 m. In the US, 10 m DEM-derived high-resolution hydrological data is available [465]. Still, higher resolution lidar derived DEM with ( $\sim 2 \text{ m}$ ) can improve river network delineation [466]. Additionally, SAR, multispectral, and hyperspectral data collected from aerial, satellite, and UAS, have been used to map surface water area and characterize river channel morphology [467–470]. Although those applications achieved noticeable success, upscaling them to continental or global scales face many challenges [471].

The Surface Water and Ocean Topography (SWOT) satellite mission [472], will measure terrestrial water at a spatial resolution of 50 m and provide river vector products that represent reaches with a collection of nodes spanning every 200 m [473, 474]. Researchers estimate gas exchange coefficient with remote sensing derived width and water surface slope measurements, while surface water area can be multiplied with estimated gas emissions per unit area to estimate total C degassing. Note that small streams are difficult to discern at SWOT's spatial resolution; therefore, data fusion of SWOT river vectors with high-resolution DEMs holds promise to provide more accurate data regarding rivers and streams.

### 3.3.2.3. Carbon burial

Global estimates of aquatic organic C burial are between  $0.15$  and  $1.6 \text{ Pg CO}_2\text{-C yr}^{-1}$  [405, 475]. These studies focus on sedimentation in reservoirs,



**Table 7.** Global carbon monitoring values for rivers. Method refers to three broad categories, modeled, extrapolation (*in situ* combined with extent to upscale estimates), data synthesis (combination of data sources and methods), and remote sensing (mapping including remote sensing derived spatial heterogeneity).

| Carbon indicator           | System             | Value            | Units                            | Method   | Source              |
|----------------------------|--------------------|------------------|----------------------------------|--|---------------------|
| System extent              | Rivers and streams | $0.773 \pm 0.08$ | $10^6 \text{ km}^2$              | Remote sensing/modeling for rivers less than 90 m in width | [478]               |
| Carbon input               | Inland waters      | 2.7–5.1          | $\text{PgC yr}^{-1}$             | Data synthesis   | [15, 385, 427, 433] |
| Carbon export to estuaries | Rivers and streams | 1.06             | $\text{PgC yr}^{-1}$             | Data synthesis   | [439]               |
| Carbon flux to atmosphere  | Rivers and streams | $1.8 \pm 0.25$   | $\text{PgCO}_2 \text{ yr}^{-1}$  | Extrapolation  | [430]               |
| CH <sub>4</sub> Flux       | Rivers and streams | ~1.5             | $\text{Tg CH}_4 \text{ yr}^{-1}$ | Extrapolation  | [408]               |

lakes, and wetlands, without explicit global-scale C burial in rivers and streams. Watershed models that explicitly integrate terrestrial and aquatic carbon cycling processes are being developed to quantify the burial of particulate organic carbon (OC) in rivers. For example, Qi *et al* [476, 477] incorporated OC deposition, resuspension, and diagenesis processes in the soil and water assessment tool and showed that a significant fraction of terrestrially originated POC is deposited on the bed of small streams and further decomposes into CO<sub>2</sub> and CH<sub>4</sub>. These results indicate that the inclusion of C burial in rivers and streams would improve the accounting of global C burial in inland waters. High-resolution riverine networks will be critical for updating and improving existing carbon monitoring (table 7). Additionally, certain carbon pathways are relatively unknown, e.g. how much carbon enters wetlands and subsequently enters rivers.

### 3.4. Ocean and shelves

In total, we found 102 papers relevant to carbon monitoring with remote sensing of oceans. Earth observation-derived oceanic carbon indicators have been used to characterize a variety of carbon-related properties and processes. The global oceans represent a substantial sink for anthropogenic CO<sub>2</sub>, accounting for more than 40% of the global sink of anthropogenically produced CO<sub>2</sub> (figure 1) [9]. Moreover, the magnitude of the ocean sink appears to be increasing with the buildup of CO<sub>2</sub> in our planet's atmosphere. Approaches to estimate the ocean sink have relied on a combination of global ocean biogeochemistry models (GOBMs) along with comparison to observation-based estimates, including *p*CO<sub>2</sub>-based interpolations. These interpolations, in some cases, have relied on remote sensing products as described in Rödenbeck *et al* [479], involving regression to remotely sensed external drivers such as sea surface temperature, sea surface salinity, and chlorophyll-*a* concentration. Many of the GOBMs also use remote sensing for model implementation and model-data comparisons [e.g. 480–482].

Several studies have examined regional time-series changes in values averaged over the 17 biomes of Fay and McKinley [483], which were defined based on various environmental datasets including the SeaWiFS chlorophyll-*a* product. These time-series have revealed substantial interannual and decadal variability as well as regional patterns in atmosphere-ocean CO<sub>2</sub> fluxes [9, 484, 485]. Interannual and multi-year variability can be related to climate oscillations including El Niño as well as decadal scale oscillations in the North Pacific and Southern Ocean, as described by Liao *et al* [486] in a NASA CMS-supported study. The Liao *et al* [486] simulations expanded on prior observational studies that have identified negative anomalies in eastern Pacific surface *p*CO<sub>2</sub> during El Niño events as well as other seasonal and interannual variations and regional patterns [e.g. 479, 487–489]. More recently, Watson *et al* [490] provided a revised estimate of observation-based CO<sub>2</sub> atmosphere-ocean fluxes, accounting for temperature gradients between the surface and sampling at a few meters' depth, or for the effect of the cool ocean surface skin. Their estimate resulted in an upward revision of the net flux into the oceans of  $0.8\text{--}0.9 \text{ PgC yr}^{-1}$ , with a best estimate for the period 1994–2007 of  $-2.5 \pm 0.4 \text{ PgC yr}^{-1}$  (where negative values denote net uptake into the ocean) that is consistent with ocean interior inventory increases [491]. This estimate is considerably less than that of Wang *et al* [492], who applied an atmospheric inversion approach to GOSAT and *in situ* observations of atmospheric CO<sub>2</sub> and derived estimates for ocean fluxes of  $-3.1 \pm 0.5 \text{ PgC yr}^{-1}$ . Considerable progress has been made in the assessment of oceanic CO<sub>2</sub> flux, with different approaches converging.

#### 3.4.1. Sedimentation/benthic-pelagic coupling

Satellite observations have also been used to observe coupling between surface and benthic biogeochemical processes with implications for carbon transport from the surface to the deep ocean. Waga *et al* [493] found evidence of linkages between surface phytoplankton size structure, derived with ocean color

proxies, and deep ocean benthic macrofaunal distributions. Corliss *et al* [494] reported lower benthic foraminiferal diversity in North Atlantic latitudes coinciding with high seasonality in primary production as inferred from SeaWiFS satellite imagery. Surface patterns of SeaWiFS-derived chlorophyll-*a* were also found to be related to regional differences in macrobenthic community structure in the deep Gulf of Mexico [495]. Satellite observations have also been used to assess transport to offshore waters of unattached benthic algae and found to be associated with a substantial carbon footprint [496]. These studies highlight the apparent coupling between surface ocean carbon dynamics, as observed by remote sensing, and deep ocean biogeochemistry.

### 3.4.2. Ocean chlorophyll and primary production

Oceanic NPP, estimated as diurnal photosynthesis minus diel respiration, is responsible for almost half of global NPP ( $\sim 50$  PgC yr $^{-1}$ ) and is the primary source of energy for marine food webs [497]. NPP draws down CO $_2$  levels in the surface ocean, thus shifting net fluxes from the atmosphere to the ocean and thereby exerting an important control on global climate [498]. The export of fixed carbon from the surface ocean by sinking particles to the deep through the 'biological pump' stores carbon on time scales ranging from seasons to centuries and is a critical estimate of how oceans regulate our planet's climate [499–501]. Thus, accurate and well-characterized regional, basin, and global scale NPP products are essential for understanding how ocean biology influences ocean carbon dynamics.

NPP estimates derived from satellite data, have the advantage of providing unprecedented spatial and temporal coverage. However, despite considerable progress over the past two decades, remotely sensed NPP estimates continue to suffer from large uncertainties [502–505]. At present, satellite-based global annual NPP estimates range from 32 to 79 PgC yr $^{-1}$  [502], and annual carbon export fluxes range from 5 to  $>12$  PgC yr $^{-1}$  [506, 507]. The uncertainties associated with these measurements are clearly as large as the annual anthropogenic CO $_2$  emission rates of between  $\sim 7$  and 11 PgC yr $^{-1}$  [508]. Necessitating that we continue improving remote sensing methods to estimate NPP.

Satellite-based NPP models span a wide range of complexity from empirical [509] to semi-analytical models [510, 511], but can be generally categorized into one of three modeling strategies [512]. Two of these, are the biology-based models, of which one uses phytoplankton biomass (chlorophyll-*a*) derived from remote sensing reflectance ( $R_{rs}$ ) [502, 513–519], while the other, the carbon based Productivity Model, uses phytoplankton carbon stock ( $C_{phyto}$ ) retrieved from backscattering coefficients at 443 nm ( $b_{bp}(443)$ ). The latter is also derived from  $R_{rs}$ . The term ocean color is described with the spectrum of

$R_{rs}(\lambda)$  and defined as the ratio of water-leaving radiance to downwelling irradiance just above the surface. A major problem in using chlorophyll-*a* as a critical input parameter is the disparate and often opposing responses of cellular chlorophyll-*a* content to nutrient availability, light limitations, and temperature conditions that can confound any simple relationship between NPP and chlorophyll-*a*. To alleviate this, Behrenfeld *et al* [520] used the 'carbon-based approach' and replaced chlorophyll-*a* with  $C_{phyto}$ . However, this method includes a new uncertainty due to scattering by non-phytoplankton particles including bubbles [521–523].

The third category is the absorption-based models (AbPMs), which rely on the absorption coefficient of phytoplankton ( $a_{ph}$ ) an inherent optical property, derived directly from  $R_{rs}$ . The recent model, Carbon Absorption Fluorescence Euphotic resolving [505], belongs to this category. AbPMs derive NPP as the product of  $a_{ph}$ , photosynthetically active radiation (PAR) [524] and the efficiency ( $\phi$ ) with which absorbed energy is converted into carbon biomass [525–533]. Currently, broad use of AbPM models has been hampered by the lack of adequate *in situ*  $\phi$  measurements, forcing reliance on estimates that ignore large, temporal (diurnal, seasonal) and spatial (regional and vertical) variability [526, 529, 534–536]. One approach to circumventing this problem is via modeling  $\phi$  as a function of PAR and temperature [533, 537]. While this approach will continue to be useful for application to ocean color from polar orbiting satellites, full realization of AbPM for use with the new generation of geostationary ocean color satellites such as GOCI-1, GOCI-2 and NASA GLIMR will rely on our ability to measure diurnal variability in  $\phi$ . In conclusion, while it is clear AbPM models will help reduce uncertainty in deriving NPP from satellite data, their usefulness for obtaining NPP will require community efforts to accurately derive  $a_{ph}$ , diurnal PAR, and  $\phi$ .

Satellite observations have improved global estimates of organic carbon export from the surface ocean. DeVries and Weber [538] combined satellite and ship-based observations in an assimilative global carbon cycle model to estimate a global POC flux out of the euphotic zone of  $\sim 9$  PgC yr $^{-1}$ . Their study showed that carbon export ratios (ratios of NPP to carbon export) were highest in higher latitudes, even though export from lower latitudes was higher than previously estimated. Satellite-derived NPP and particle size as variables in a food web model enabled estimation of a climatological mean global carbon export from the euphotic zone of  $\sim 6$  PgC yr $^{-1}$  [508]. Regional and basin-scale estimates of carbon export with satellite-derived NPP and empirical relationships are prevalent [495, 539–541]. The NASA Exports program [542] focused on developing new approaches to characterize global carbon export using satellite observations of ocean surface properties,

**Table 8.** Existing carbon monitoring indicators for oceans and continental shelves. Method refers to broad categories, modeled, extrapolation (*in situ* combined with extent to upscale estimates), data synthesis, and remote sensing (mapping or predicting spatial heterogeneity for an indicator).

| Carbon indicator  | System                  | Value                | Units  | Method   | Source              |
|---|-------------------------|----------------------|--|--|---------------------|
| Carbon stocks   | Ocean                   |                      |  |  |                     |
|   | POC (upper mixed layer) | 0.77–1.9             | PgC  | Remote Sensing                                 | [547, 548]          |
|   | Total Organic C         | 700                  | PgC  | Extrapolation                                  | [9]                 |
|   | DIC                     | 38 000               | PgC  | Extrapolation                                  | [9]                 |
|   | PIC (euphotic zone)     | 0.63–0.7             | PgC  | Remote Sensing                                 | [545]               |
|   | Surface Sediments       | 1750                 | PgC  | Extrapolation                                  | [9]                 |
|   | Carbonate Rock Shelf    | $60 \times 10^6$     | PgC  | Extrapolation                                  | [550]               |
| Carbon export from upper mixed layer                                  | Ocean                   |                      |  |  |                     |
|   | Organic Carbon          | 5→12                 | PgC yr <sup>-1</sup>                         | Extrapolation and Remote Sensing               | [506–508, 551, 552] |
|   | PIC Shelf               | 0.59                 | PgC yr <sup>-1</sup>                         | Model  | [553]               |
| Carbon Burial   | Ocean                   | 0.012 ± 0.02         | PgC yr <sup>-1</sup>                         | Extrapolation                                  | [551]               |
|   | Shelf                   | 0.29 ± 0.15          | PgC yr <sup>-1</sup>                         | Extrapolation                                  | [551]               |
| CO <sub>2</sub> flux (negative values correspond to net ocean uptake) | Ocean                   | –2.5 ± 0.4           | PgC yr <sup>-1</sup>                         | Remote Sensing and Extrapolation               | [490]               |
|   |                         | –3.1 ± 0.5           | PgC yr <sup>-1</sup>                         | Remote Sensing (inversion)                     | [492]               |
|   | Shelf                   | –1.6–2.8<br>–0.1–0.2 | PgC yr <sup>-1</sup><br>PgC yr <sup>-1</sup> | Various<br>Extrapolation and Model             | [9]<br>[556, 557]   |
| Primary Production  | Ocean                   | 32–79                | PgC yr <sup>-1</sup>                         | Remote Sensing ( <i>in situ</i> extrapolation) | [502]               |
|   | Shelf                   | 9–11                 | PgC yr <sup>-1</sup>                         | Remote Sensing; Extrapolation                  | [554, 555, 558]     |
| Calcification   | Ocean                   | 1.1–1.6              | PgC yr <sup>-1</sup>                         | Remote Sensing; Model                          | [545, 553, 559]     |

specifically considering different mechanisms. These include settling of particulate carbon in the form of intact phytoplankton, aggregates, and zooplankton byproducts; net vertical transport of suspended particulate and DOC by physical and microbial processes; and vertical transport of organic carbon associated with migration of zooplankton and their predators.

#### 3.4.3. Satellite assessments of ocean carbon stocks

Remotely sensed observations have also been used to derive stocks of different forms of carbon in ocean waters (table 8). Estimations of basin scale DOC have been explored on the basis of relationships to satellite-observable optical properties, specifically CDOM absorption [e.g. 543]. The method requires *a priori* knowledge of the relationship between DOC and CDOM, the latter comprising only a small portion of the total DOC pool. Various approaches have also been developed to estimate global satellite-based estimates of total surface POC [e.g. 522, 544] and PIC [560, 545, 546]. Estimates of mixed-layer integrated global POC range between 0.77 and 1.3 PgC of

carbon [547]. Cloud-Aerosol Lidar with Orthogonal Polarization (CALIOP), a space-based lidar system, was used to derive global average mixed-layer standing stocks of phytoplankton carbon ( $C_{\text{phyto}}$ ) and total POC, with estimated values of 0.44 PgC for  $C_{\text{phyto}}$  and 1.9 PgC for POC [548]. Balch *et al* [549] extended the PIC surface algorithms by developing approaches for estimation of PIC concentrations integrated over both the upper 100 m and the euphotic zone depths, based on relationships between ship-based PIC concentrations.

#### 3.4.4. Coastal and continental shelf seas

Coastal and continental shelf seas make up 7%–11% of the total area of the ocean, yet have a significant impact on the global carbon cycle relative to their size [561]. Shelf seas are estimated to contribute almost a third of the total marine primary production, up to 50% of the inorganic carbon burial, and up to 80% of the organic carbon burial [550, 551, 554, 555, 558, 562], and therefore significantly contribute to oceanic-atmosphere carbon exchange [556, 563]. Each coastal region is different,

and carbon monitoring tends to focus on each one individually, but there are a number of robust synthesis and review papers on coastal carbon cycling [e.g. 561, 562, 564] and we refer the reader to those for recent coastal carbon budgets. Here, we review the status of carbon monitoring in these regions ( $n = 30$ ).

#### 3.4.4.1. Carbon monitoring status

The carbon cycle in coastal shelf seas is very similar to that of the open oceans. Thus, carbon monitoring methods in shelf seas tend to overlap with oceanic approaches. However, the coastal shelf has unique data needs i.e. spatial resolution to discern coastal features, spectral influence of depth and terrestrial hydrology. Thus, oceanic remote sensing methods require alteration for use in coastal shelf regions. NPP monitoring has used methods derived for ocean systems both directly and with slight modifications [504, 554], but the performance of these methods is lowest in coastal shelf seas [504]. One region of particular focus is the Arctic Ocean and its surrounding shelf seas, where many regional algorithms exist [e.g. 514, 565, 566]. Lee *et al* [512] provide an assessment of 32 Arctic NPP satellite models, finding the models performing relatively well in low-productivity seasons and deep-water regions. However, the algorithms tended to overestimate NPP, but yielded underestimates when a subsurface chlorophyll-*a* maximum was present.

Given that the shelf sea represents the continuum between terrestrial and ocean ecosystems, there are additional factors to be considered compared to carbon monitoring in ocean systems. NASA CMS studies have focused on improved observation and modeling of lateral transport of terrestrial carbon into the watershed and ultimately to the coasts [567–574]. Other studies have focused on the estimation of DOC and CDOM [188, 575–578]. As described in section 3.3.1, CDOM only makes up a fraction of the total DOC pool, but in coastal systems dominated by terrestrial discharge, CDOM and DOC co-vary. The exact form of the relationship between CDOM and DOC varies both temporally and spatially, driven by terrestrial source characteristics and biogeochemical processes, thus the need for regional approaches. However, Vantrepotte *et al* [579] demonstrated the potential of a generalized approach in deriving DOC from CDOM in very contrasting coastal environments.

The CMS program has supported carbon monitoring in the northern Gulf of Mexico and the region influenced by the Mississippi River. This included efforts to map  $p\text{CO}_2$  and estimate fluxes [580–584], model simulations using a coupled physical-biogeochemical model [585] and satellite-derived estimation of  $p\text{CO}_2$  and air-sea flux of  $\text{CO}_2$  [424]. Studies have also examined patterns in

phytoplankton community composition and potential relationships to carbon dynamics [586, 587]. Other CMS program efforts examined carbon properties in both the Gulf of Mexico and the Atlantic coast [564, 588], and other studies have focused on sedimentation and flux of various carbon forms to the seafloor [554, 589–592].

There remains considerable uncertainty in the estimate of global coastal ocean uptake of  $\text{CO}_2$ . Some of this is related to differences in the extent to which estuarine and inland waters are included in the inventory. However, estimates based on *in situ* extrapolations as well as global models have generally converged around  $-0.1$  to  $-0.3$   $\text{PgC yr}^{-1}$  [556, 557, 593].

## 4. Stakeholders

Although there are different approaches for monitoring WC systems, the full potential of satellite WC products requires and thrives with stakeholder involvement to utilize and disseminate the resulting maps and perpetuate monitoring. WC stakeholders are diverse across systems, scales, and studies. In general, stakeholders for carbon monitoring and climate action are cities, international organizations, non-government organizations (NGOs), and other governing bodies. Several international agreements include carbon monitoring such as The UN Sustainable Development Goals, which encourages national monitoring. The IPCC outlines carbon monitoring methods and the Paris Agreements NDCs, which outline carbon monitoring and mitigation activities.

The inclusion of WC systems within these agreements varies. In 1997, the Kyoto protocol had no mention of wetlands [594], in 2006, the first IPCC guidelines included only peatlands and flooded lands [20], and in 2013, a supplement added recommendations for monitoring additional WC systems [595]. Oceans were conspicuously absent [596] but have subsequently been addressed in a special report [597] due in part to their importance for achieving climate goals [4]. The IPCC methods are focused on anthropogenic emissions and recommend isolating these by identifying a change in managed lands [20]. Defining managed lands is straightforward in forestry and agriculture; however, the term is ambiguous in WC systems. Therefore, national monitoring programs have addressed this ambiguity by considering all wetlands managed [173]. Codifying this approach within an update to the IPCC protocols would ensure a uniform application of WC monitoring. Many countries cite the IPCC guidelines in their NDCs and seek to report and mitigate land-use, land-use change, and forestry emissions; however, only a few directly stated their intention to track wetland restoration [598]. Enhanced stakeholder capacity will improve the MRV of carbon stocks and fluxes for NDCs, and



carbon markets [599]. The gaps in WC monitoring within international agreements and resulting national monitoring leave a critical role for NGOs, universities, and subnational governing bodies to fill.

The transition from remote sensing methodology, often prototyped over a subnational region, to globally consistent time-series is difficult and requires stakeholder involvement. For example, the Global Mangrove Watch, a scientific data initiative has mapped mangrove change, provided carbon monitoring data, and disseminated data [35]. Carbon monitoring can inform management of protected areas, as an example, with no intervention, the Great Dismal Swamp would have emitted 6.5 million tons of CO<sub>2</sub> through 2062 (Net Present Value (NPV): \$232 million) but due to informed management practices, it is expected to offset 9.9 million tons of CO<sub>2</sub> emissions (NPV: \$326 million) [600]. Similarly, peatland restoration approaches, project size, and stakeholder involvement have advanced over the last 25 years [601]. Local, regional, and international stakeholders are critical for taking the science from space to policy.

## 5. Recommendations

Upon review of the status of WC monitoring, clear gaps exist. Several systems lack fundamental remote sensing baselines, such as, location, extent, and change. Complete global extent maps are a priority for seagrass, tidal marsh, and mineral wetlands. Similarly, peatlands could benefit from an improved extent map, e.g. peatlands in Africa [304]. There are additional systems that were not a focus of this review due to limited remote sensing-based carbon monitoring research that would benefit from global mapping forested wetlands, freshwater tidal marshes, and riparian wetlands. Also, thematic classifications that focus on differences in carbon storage, e.g. separating mineral wetlands and peatlands or species of mangroves. Existing wetland inventories can have high classification errors, and omission bias for wetlands that are difficult to detect, e.g. forested wetlands obscured by tree canopy. Another major challenge in understanding carbon stocks and fluxes is the limited availability of data on the factors contributing to the variability of carbon stocks and fluxes, such as the hydroperiod, hydrologic connectivity, plant and microbial communities, soil properties, chemical characteristics, and disturbance. This data would improve the ability to quantify change uncertainty and outcomes as they relate to carbon stocks and flows. Remote sensing research can fill these gaps by providing improved up to date wetland inventories [602], reconstruction of both seasonal and long-term changes in wetland hydroperiod [248, 552], monitoring disturbance [130, 603], and improving

subsurface measurements [230]. Terrestrial and coastal carbon budgets can be enhanced by determining the type of disturbance [40] and quantifying the carbon impacts of varied change processes including degradation, loss, and restoration [604]. Poulter *et al* [378] proposed reducing global-scale wetland carbon uncertainty with additional field collection, continuous flux measurements, new satellite data sources, improved modeling of biogeochemical processes, and harnessing high-performance computing. While initially proposed for wetlands, these methods for reducing uncertainty are helpful for all WC monitoring.

Carbon fluxes are an area of research across WC systems. The flows and interactions between systems are still understudied, e.g. ocean carbon fluxes and linkages across the terrestrial-shelf-ocean continuum as a constraint on terrestrial carbon fluxes. Remote sensing has the potential to reduce carbon stock and flux uncertainty by optimizing and fusing techniques that take advantage of the spatial, e.g. morphology, spectral, e.g. species, and temporal, e.g. phenology and change, remote sensing resolution domains, including the limitations and tradeoffs of applying these techniques. The next generation of carbon monitoring will capture the complex linkages between WC systems, e.g. the linked permafrost and boreal lake carbon cycle [414–416]. As we address these challenges and opportunities, our ability to understand WC storage and fluxes will improve, and in turn, our understanding of how these ecosystems function, allowing for sustainable management and conservation. Our suggestions and recommendations to accelerate the development of WC monitoring fall into four categories remote sensing, *in situ*, terrestrial and blue carbon and aquatic recommendations (table 9).

As noted by Shutler *et al* [611] satellite observations, international collaboration, and methodological advancement have resulted in accurate and robust oceanic carbon monitoring. Following a similar roadmap robust carbon monitoring can be achieved in all WC systems. The global-scale WC monitoring relies on remote sensing often as ancillary data. Our remote sensing WC agenda prioritizes the integration of remote sensing within WC monitoring at local to global scales identifying the importance of change locations and types. To summarize, major priorities are: (a) mapping or improving existing baselines will benefit all systems and the ability to understand their interconnections (b) determining linkages between systems and how climate change will alter these, (c) leveraging local remote sensing and *in situ* measurements to facilitate global analysis, and (d) continued and expanded global-scale remote sensing-based MRV to enable, subnational, national, and international carbon budgets.

**Table 9.** Recommendations for future wet carbon monitoring with remote sensing.

| Type                        | Recommendation  | Potential outcome   |
|-----------------------------|---|---|
| Remote Sensing              | Continued evaluation of new sensors and technology for WC monitoring.   | Increased temporal, spatial, and thematic coverage. Reduced uncertainty.  |
| Remote Sensing              | The perpetuation of long running earth observation missions to ensure a continuous observation of global carbon processes.                              | Improved monitoring reporting and verification  |
| Remote Sensing              | Access to long-term archives to resolve trends, regional patterns, and their underlying mechanisms  | Elucidate climate effects on carbon cycle   |
| Remote Sensing              | Data consistency to support development of remote sensing algorithms and model data assimilation.   | Improved accuracy and applicability of methodologies  |
| Remote Sensing              | The use of spatial-temporal data to determine fine-phase temporal effects (e.g. extreme events, river plumes, drought) and how these affect WC systems. | Improved carbon budgets and understanding of carbon cycle interactions  |
| Remote Sensing              | Increased spatial and temporal coverage of lidar [548, 605].  | Expanded understanding of vegetation and landscape structure and change   |
| Remote Sensing              | Coordination of carbon monitoring across boundaries including terrestrial-aquatic boundary, fresh-saline gradient, and peat-mineral wetlands.           | Determination of WC linkages  |
| <i>In situ</i>              | Open access to <i>in situ</i> data.   | Reducing barriers to carbon monitoring research and expanded impact of <i>in situ</i> data  |
| <i>In situ</i>              | Methods for scaling the limited <i>in situ</i> data for use in prediction and modeling of carbon products from satellite data.                          | Reduced uncertainty and spatial biases in carbon monitoring   |
| <i>In situ</i>              | Greater geographic distribution of <i>in situ</i> samples collection.   | Global data products with reduced uncertainty and spatial biases in carbon monitoring e.g. $p\text{CO}_2$ across ocean basins [606] |
| Terrestrial and Blue carbon | Spatial variability of belowground carbon [34, 607]   | Improved spatial estimates of carbon stock and change impacts   |
| Terrestrial and Blue carbon | Impact of disturbance and recovery [8, 115, 607–609]  | Determine carbon stock stability and major change drivers   |
| Terrestrial and Blue carbon | Concurrent loss, gain [49], and restoration monitoring [610]  | Improved change maps and extents  |
| Aquatic                     | Development and refinement of ocean color remote sensing methods in optically complex coastal shelf sea and nearshore environments                      | Improved carbon budgets and understanding of carbon cycle interactions in coastal margins   |

## 6. Conclusions

Carbon monitoring depends heavily on *in situ* measurements (e.g. shipboard water and spectral sampling, soil cores, allometric equations, and biomass collection). These data are limited in WC systems due to inaccessibility and cost. Global carbon monitoring often uses mass balance equations and modeling with limited need for measurements of individual systems. Local estimates rely on *in situ* samples to estimate site-level carbon budgets. The gap between these scales will increasingly rely on

earth observation. System-specific estimates are often extrapolated from limited *in situ* data, but remote sensing can capture spatial variability, quantify uncertainty, and improve carbon estimates. Remote sensing is critical for national carbon monitoring programs that fulfill IPCC level 3 data requirements. Therefore, NDCs supplement the existing need for remote sensing monitoring of WC systems. All these recommendations culminate in a primary goal for all WC systems, quantifying their contribution to global and national carbon budgets with associated uncertainties.



## Data availability statement

Any data that support the findings of this study are included within the article or supplemental.

## Acknowledgments

This research was in part supported by NASA Carbon Monitoring Systems Program (Grant Nos. 18-CMS18-0052, 16-CMS16-0073, 80NSSC17K0712, 80NSSC20K0013, NNH18 ZDA001-CMP, 80NSSC20K0084, 80NSSC20K0427, NNX14AO73G). This research was supported in part by the U.S. Department of Agriculture, Agricultural Research Service. This work was partly conducted by the Jet Propulsion Laboratory, California Institute of Technology, under contract with the National Aeronautics and Space Administration. Anthony Campbell was supported by the NASA Postdoctoral Program administered by the University Space Research Association.

## ORCID iDs


Anthony D Campbell  <https://orcid.org/0000-0001-8379-9513>

Temilola Fatoyinbo  <https://orcid.org/0000-0002-1130-6748>

James Holmquist  <https://orcid.org/0000-0003-2546-6766>

Catherine Mitchell  <https://orcid.org/0000-0001-9932-3050>

Han Qiu  <https://orcid.org/0000-0001-9962-2472>

Marc Simard  <https://orcid.org/0000-0002-9442-4562>

Jinghui Wu  <https://orcid.org/0000-0002-6788-1055>

Xuesong Zhang  <https://orcid.org/0000-0003-4711-7751>

## References

- [1] Walsh B, Ciaïs P, Janssens I A, Penuelas J, Riahi K, Rydzak E, Van Vuuren D P and Obersteiner M 2017 Pathways for balancing CO<sub>2</sub> emissions and sinks *Nat. Commun.* **8** 1–12
- [2] Herold M and Skutsch M 2011 Monitoring, reporting and verification for national REDD programmes: two proposals *Environ. Res. Lett.* **6** 014002
- [3] Joseph S, Herold M, Sunderlin W D and Verchot L V 2013 REDD readiness: early insights on monitoring, reporting and verification systems of project developers *Environ. Res. Lett.* **8** 034038
- [4] Hoegh-Guldberg O, Northrop E and Lubchenco J 2019 The ocean is key to achieving climate and societal goals *Science* **365** 1372–4
- [5] Seifollahi-Aghmiuni S, Nockrach M and Kalantari Z 2019 The potential of wetlands in achieving the sustainable development goals of the 2030 Agenda *Water* **11** 609
- [6] Moomaw W R, Chmura G L, Davies G T, Finlayson C M, Middleton B A, Natali S M, Perry J E, Roulet N and Sutton-Grier A E 2018 Wetlands in a changing climate: science, policy and management *Wetlands* **38** 183–205
- [7] Saintilan N, Rogers K, Kelleway J J, Ens E and Sloane D R 2019 Climate change impacts on the coastal wetlands of Australia *Wetlands* **39** 1145–54
- [8] Taillie P J, Roman-Cuesta R, Lagomasino D, Cifuentes-Jara M, Fatoyinbo T, Ott L E and Poulter B 2020 Widespread mangrove damage resulting from the 2017 Atlantic mega hurricane season *Environ. Res. Lett.* **15** 064010
- [9] Friedlingstein P, O'Sullivan M, Jones M W, Andrew R M, Hauck J, Olsen A, Peters G P, Peters W, Pongratz J and Sitch S 2020 Global carbon budget 2020 *Earth Syst. Sci. Data* **12** 3269–340
- [10] Odum H T 1983 *Systems Ecology; an Introduction* (Hoboken, NJ: Wiley) 644
- [11] Bridgman S D, Megonigal J P, Keller J K, Bliss N B and Trettin C 2006 The carbon balance of North American wetlands *Wetlands* **26** 889–916
- [12] Macreadie P I, Anton A, Raven J A, Beaumont N, Connolly R M, Friess D A, Kelleway J J, Kennedy H, Kuwae T and Lavery P S 2019 The future of Blue Carbon science *Nat. Commun.* **10** 1–13
- [13] Davidson N C and Finlayson C M 2018 Extent, regional distribution and changes in area of different classes of wetland *Mar. Freshw. Res.* **69** 1525–33
- [14] Tootchi A, Jost A and Ducharme A 2019 Multi-source global wetland maps combining surface water imagery and groundwater constraints *Earth Syst. Sci. Data* **11** 189–220
- [15] Regnier P, Friedlingstein P, Ciaïs P, Mackenzie F T, Gruber N, Janssens I A, Laruelle G G, Lauerwald R, Luyssaert S and Andersson A J 2013 Anthropogenic perturbation of the carbon fluxes from land to ocean *Nat. Geosci.* **6** 597–607
- [16] Krug J H 2018 Accounting of GHG emissions and removals from forest management: a long road from Kyoto to Paris *Carbon Balance Manage.* **13** 1–11
- [17] UNFCCC 2016 Canada intended nationally determined contributions (INDCs) *United Nations Framework Convention on Climate Change (15 May 2015)*
- [18] Hurtt G, Wickland D, Jucks K, Bowman K, Brown M E, Duren R M, Hagen S and Verdy A 2014 NASA carbon monitoring system: prototype monitoring, reporting, and verification
- [19] Pendleton L, Donato D C, Murray B C, Crooks S, Jenkins W A, Sifleet S, Craft C, Fourqurean J W, Kauffman J B and Marbà N 2012 Estimating global “blue carbon” emissions from conversion and degradation of vegetated coastal ecosystems *PLoS One* **7** e43542
- [20] Eggleston H S, Buendia L, Miwa K, Ngara T and Tanabe K 2006 2006 IPCC Guidelines for National Greenhouse Gas Inventories
- [21] Sanderman J, Hengl T, Fiske G, Solvik K, Adame M F, Benson L, Bukoski J J, Carnell P, Cifuentes-Jara M and Donato D 2018 A global map of mangrove forest soil carbon at 30 m spatial resolution *Environ. Res. Lett.* **13** 055002
- [22] Nellemann C, Corcoran E, Duarte C M, Valdes L, DeYoung C, Fonseca L and Grimsditch G 2009 *Blue Carbon: The Role of Healthy Oceans in Binding Carbon* Center for Coastal and Ocean Mapping
- [23] Page S E, Siegert F, Rieley J O, Boehm H, Jaya A and Limin S 2002 The amount of carbon released from peat and forest fires in Indonesia during 1997 *Nature* **420** 61–65
- [24] Mcleod E, Chmura G L, Bouillon S, Salm R, Björk M, Duarte C M, Lovelock C E, Schlesinger W H and Silliman B R 2011 A blueprint for blue carbon: toward an improved understanding of the role of vegetated coastal habitats in sequestering CO<sub>2</sub> *Front. Ecol. Environ.* **9** 552–60
- [25] Duarte C M, Dennison W C, Orth R J and Carruthers T J 2008 The charisma of coastal ecosystems: addressing the imbalance *Estuar. Coasts* **31** 233–8

- [26] Aria M and Cuccurullo C 2017 Bibliometrix: an R-tool for comprehensive science mapping analysis *J. Informetr.* **11** 959–75
- [27] Cobo M J, López-Herrera A G, Herrera-Viedma E and Herrera F 2011 An approach for detecting, quantifying, and visualizing the evolution of a research field: a practical application to the fuzzy sets theory field *J. Informetr.* **5** 146–66
- [28] Perillo G, Wolanski E, Cahoon D R and Hopkinson C S 2018 *Coastal Wetlands: An Integrated Ecosystem Approach* (Amsterdam: Elsevier)
- [29] Davidson N C 2014 How much wetland has the world lost? Long-term and recent trends in global wetland area *Mar. Freshw. Res.* **65** 934–41
- [30] Rovai A S, Coelho-Jr C, de Almeida R, Cunha-Lignon M, Menghini R P, Twilley R R, Cintrón-Molero G and Schaeffer-Novelli Y 2021 Ecosystem-level carbon stocks and sequestration rates in mangroves in the Cananéia-Iguape lagoon estuarine system, southeastern Brazil *For. Ecol. Manage.* **479** 118553
- [31] Donato D C, Kauffman J B, Murdiyarto D, Kurnianto S, Stidham M and Kanninen M 2011 Mangroves among the most carbon-rich forests in the tropics *Nat. Geosci.* **4** 293–7
- [32] Jardine S L and Siikamäki J V 2014 A global predictive model of carbon in mangrove soils *Environ. Res. Lett.* **9** 104013
- [33] Keenan R J, Reams G A, Achard F, de Freitas J V, Grainger A and Lindquist E 2015 Dynamics of global forest area: results from the FAO global forest resources assessment 2015 *For. Ecol. Manage.* **352** 9–20
- [34] Atwood T B et al 2017 Global patterns in mangrove soil carbon stocks and losses *Nat. Clim. Change* **7** 523–8
- [35] Bunting P, Rosenqvist A, Lucas R M, Rebelo L, Hilarides L, Thomas N, Hardy A, Itoh T, Shimada M and Finlayson C M 2018 The global mangrove watch—a new 2010 global baseline of mangrove extent *Remote Sens.* **10** 1669
- [36] Simard M, Fatoyinbo L, Smetanka C, Rivera-Monroy V H, Castañeda-Moya E, Thomas N and Van der Stocken T 2019 Mangrove canopy height globally related to precipitation, temperature and cyclone frequency *Nat. Geosci.* **12** 40–45
- [37] Worthington T A, Andradi-Brown D A, Bhargava R, Buelow C, Bunting P, Duncan C, Fatoyinbo L, Friess D A, Goldberg L and Hilarides L 2020 Harnessing big data to support the conservation and rehabilitation of mangrove forests globally *One Earth* **2** 429–43
- [38] Richards D R and Friess D A 2016 Rates and drivers of mangrove deforestation in Southeast Asia, 2000–2012 *Proc. Natl Acad. Sci.* **113** 344–9
- [39] Thomas N, Lucas R, Bunting P, Hardy A, Rosenqvist A and Simard M 2017 Distribution and drivers of global mangrove forest change, 1996–2010 *PLoS One* **12** e0179302
- [40] Goldberg L, Lagomasino D, Thomas N and Fatoyinbo T 2020 Global declines in human-driven mangrove loss *Glob. Change Biol.* **26** 5844–55
- [41] Twilley R R, Chen R H and Hargis T 1992 Carbon sinks in mangroves and their implications to carbon budget of tropical coastal ecosystems *Water Air Soil Pollut.* **64** 265–88
- [42] Chmura G L, Anisfeld S C, Cahoon D R and Lynch J C 2003 Global carbon sequestration in tidal, saline wetland soils *Glob. Biogeochem. Cycles* **17** 4
- [43] Alongi D M 2002 Present state and future of the world's mangrove forests *Environ. Conserv.* **29** 331–49
- [44] Alongi D M 2014 Carbon cycling and storage in mangrove forests *Annu. Rev. Mar. Sci.* **6** 195–219
- [45] Bouillon S, Borges A V, Castañeda-Moya E, Diele K, Dittmar T, Duke N C, Kristensen E, Lee S Y, Marchand C and Middelburg J J 2008 Mangrove production and carbon sinks: a revision of global budget estimates *Glob. Biogeochem. Cycles* **22** 1–12
- [46] Giri C, Ochieng E, Tieszen L L, Zhu Z, Singh A, Loveland T, Masek J and Duke N 2011 Status and distribution of mangrove forests of the world using earth observation satellite data *Glob. Ecol. Biogeogr.* **20** 154–9
- [47] Hamilton S E and Casey D 2016 Creation of a high spatio-temporal resolution global database of continuous mangrove forest cover for the 21st century (CGMFC-21) *Glob. Ecol. Biogeogr.* **25** 729–38
- [48] Hamilton S E and Friess D A 2018 Global carbon stocks and potential emissions due to mangrove deforestation from 2000 to 2012 *Nat. Clim. Change* **8** 240–4
- [49] Lagomasino D, Fatoyinbo T, Lee S, Feliciano E, Trettin C, Shapiro A and Mangora M M 2019 Measuring mangrove carbon loss and gain in deltas *Environ. Res. Lett.* **14** 025002
- [50] Zhu Y, Liu K, Liu L, Myint S W, Wang S, Cao J and Wu Z 2020 Estimating and mapping mangrove biomass dynamic change using worldview-2 images and digital surface models *IEEE J. Sel. Top. Appl. Earth Obs. Remote Sens.* **13** 2123–34
- [51] Zhu Y, Liu K, Myint S W, Du Z, Li Y, Cao J, Liu L and Wu Z 2020 Integration of GF2 optical, GF3 SAR, and UAV data for estimating aboveground biomass of China's largest artificially planted Mangroves *Remote Sens.* **12** 2039
- [52] Salum R B, Souza-Filho P, Simard M, Silva C A, Fernandes M E B, Cougo M F, Do Nascimento Junior W and Rogers K 2020 Improving mangrove above-ground biomass estimates using LiDAR *Estuar. Coast. Shelf Sci.* **236** 106585
- [53] Ghosh S M, Behera M D and Paramanik S 2020 Canopy height estimation using sentinel series images through machine learning models in a Mangrove forest *Remote Sens.* **12** 1519
- [54] Anand A, Pandey P C, Petropoulos G P, Pavlides A, Srivastava P K, Sharma J K and Malhi R K M 2020 Use of hyperion for Mangrove forest carbon stock assessment in bhitaranika forest reserve: a contribution towards blue carbon initiative *Remote Sens.* **12** 597
- [55] Shrestha S, Miranda I, Kumar A, Pardo M L E, Dahal S, Rashid T, Remillard C and Mishra D R 2019 Identifying and forecasting potential biophysical risk areas within a tropical mangrove ecosystem using multi-sensor data *Int. J. Appl. Earth Obs. Geoinf.* **74** 281–94
- [56] Simard M, Zhang K, Rivera-Monroy V H, Ross M S, Ruiz P L, Castañeda-Moya E, Twilley R R and Rodriguez E 2006 Mapping height and biomass of mangrove forests in Everglades National park with SRTM elevation data *Photogramm. Eng. Remote Sens.* **72** 299–311
- [57] Elmahdy S I, Ali T A, Mohamed M M, Howari F M, Abouleish M and Simonet D 2020 Spatiotemporal mapping and monitoring of Mangrove forests changes from 1990 to 2019 in the Northern Emirates, UAE using random forest, Kernel logistic regression and Naive Bayes tree models *Front. Environ. Sci.* **8** 102
- [58] Nwobi C, Williams M and Mitchard E T 2020 Rapid Mangrove forest loss and Nipa Palm (*Nypa fruticans*) expansion in the Niger Delta, 2007–2017 *Remote Sens.* **12** 2344
- [59] Suyadi J G, Lundquist C J and Schwendenmann L 2020 Aboveground carbon stocks in rapidly expanding Mangroves in New Zealand: regional assessment and economic valuation of blue carbon *Estuar. Coasts* **43** 1456–69
- [60] Lucas R, De Kerchove R V, Otero V, Lagomasino D, Fatoyinbo L, Omar H, Satyanarayana B and Dandouh-Guebas F 2020 Structural characterisation of mangrove forests achieved through combining multiple sources of remote sensing data *Remote Sens. Environ.* **237** 111543
- [61] Jones A R, Raja Segaran R, Clarke K D, Waycott M, Goh W S and Gillanders B M 2020 Estimating Mangrove tree biomass and carbon content: a comparison of forest inventory techniques and drone imagery *Front. Mar. Sci.* **6** 784
- [62] Fatoyinbo T E and Simard M 2013 Height and biomass of mangroves in Africa from ICESat/GLAS and SRTM *Int. J. Remote Sens.* **34** 668–81

- [63] Hutchison J, Manica A, Swetnam R, Balmford A and Spalding M 2014 Predicting global patterns in mangrove forest biomass *Conserv. Lett.* **7** 233–40
- [64] Taureau F, Robin M, Proisy C, Fromard F C, Imbert D and Debaine F C 2019 Mapping the mangrove forest canopy using spectral unmixing of very high spatial resolution satellite images *Remote Sens.* **11** 367
- [65] Tang W, Zheng M, Zhao X, Shi J, Yang J and Trettin C C 2018 Big geospatial data analytics for global mangrove biomass and carbon estimation *Sustainability* **10** 472
- [66] Rovai A S, Twilley R R, Castañeda-Moya E, Riul P, Cifuentes-Jara M, Manrow-Villalobos M, Horta P A, Simonassi J C, Fonseca A L and Pagliosa P R 2018 Global controls on carbon storage in mangrove soils *Nat. Clim. Change* **8** 534–8
- [67] Kauffman J B et al 2020 Total ecosystem carbon stocks of mangroves across broad global environmental and physical gradients *Ecol. Monogr.* **90** 01405
- [68] Jones T G, Ratsimba H R, Ravaoarinoshoarana L, Cripps G and Bey A 2014 Ecological variability and carbon stock estimates of mangrove ecosystems in northwestern Madagascar *Forests* **5** 177–205
- [69] Pandey P C, Anand A and Srivastava P K 2019 Spatial distribution of mangrove forest species and biomass assessment using field inventory and earth observation hyperspectral data *Biodivers. Conserv.* **28** 2143–62
- [70] Li Z, Zan Q, Yang Q, Zhu D, Chen Y and Yu S 2019 Remote estimation of mangrove aboveground carbon stock at the species level using a low-cost unmanned aerial vehicle system *Remote Sens.* **11** 1018
- [71] Rahman M M, Lagomasino D, Lee S, Fatoyinbo T, Ahmed I and Kanzaki M 2019 Improved assessment of mangrove forests in Sundarbans East Wildlife Sanctuary using WorldView 2 and Tan DEM-X high resolution imagery *Remote Sens. Ecol. Conserv.* **5** 136–49
- [72] Wicaksono P, Danoedoro P, Hartono and Nehren U 2016 Mangrove biomass carbon stock mapping of the Karimunjawa Islands using multispectral remote sensing *Int. J. Remote Sens.* **37** 26–52
- [73] Pham L T H and Brabyn L 2017 Monitoring mangrove biomass change in Vietnam using SPOT images and an object-based approach combined with machine learning algorithms *ISPRS J. Photogramm. Remote Sens.* **128** 86–97
- [74] Pham T D, Yoshino K, Nga N L and Dieu T B 2018 Estimating aboveground biomass of a mangrove plantation on the Northern coast of Vietnam using machine learning techniques with an integration of ALOS-2 PALSAR-2 and Sentinel-2A data *Int. J. Remote Sens.* **39** 7761–88
- [75] Shapiro A C, Trettin C C, Kuchly H, Alavinapanah S and Bandiera S 2015 The mangroves of the Zambezi Delta from 1995 to 2013 increase in extent observed via satellite *Remote Sens.* **7** 16504–18
- [76] Sannigrahi S 2017 Modeling terrestrial ecosystem productivity of an estuarine ecosystem in the Sundarban biosphere region, India using seven ecosystem models *Ecol. Model.* **356** 73–90
- [77] Lu W, Xiao J, Cui X, Xu F, Lin G and Lin G 2019 Insect outbreaks have transient effects on carbon fluxes and vegetative growth but longer-term impacts on reproductive growth in a mangrove forest *Agric. For. Meteorol.* **279** 107747
- [78] Wicaksono P, Danoedoro P, Hartono H, Nehren U and Ribbe L 2011 Preliminary work of mangrove ecosystem carbon stock mapping in small island using remote sensing: above and below ground carbon stock mapping on medium resolution satellite image *Remote Sensing for Agriculture, Ecosystems, and Hydrology XIII Prague, Czech Republic* 81741B
- [79] Oostdijk M, Santos M J, Whigham D, Verhoeven J and Silvestri S 2018 Assessing rehabilitation of managed mangrove ecosystems using high resolution remote sensing *Estuar. Coast. Shelf Sci.* **211** 238–47
- [80] Wang M, Cao W, Jiang C, Yan Y and Guan Q 2018 Potential ecosystem service values of mangrove forests in southeastern China using high-resolution satellite data *Estuar. Coast. Shelf Sci.* **209** 30–40
- [81] Wang M, Cao W, Guan Q, We G and Wang F 2018 Assessing changes of mangrove forest in a coastal region of southeast China using multi-temporal satellite images *Estuar. Coast. Shelf Sci.* **207** 283–92
- [82] Lee S and Fatoyinbo T E 2015 TanDEM-X Pol-InSAR inversion for mangrove canopy height estimation *IEEE J. Sel. Top. Appl. Earth Obs. Remote Sens.* **8** 3608–18
- [83] Lagomasino D, Fatoyinbo T, Lee S and Simard M 2015 High-resolution forest canopy height estimation in an African blue carbon ecosystem *Remote Sens. Ecol. Conserv.* **1** 51–60
- [84] Lagomasino D, Fatoyinbo T, Lee S, Feliciano E, Trettin C and Simard M 2016 A comparison of Mangrove canopy height using multiple independent measurements from land, air, and space *Remote Sens.* **8** 327
- [85] Stringer C E, Trettin C C and Zarnoch S J 2016 Soil properties of mangroves in contrasting geomorphic settings within the Zambezi River Delta, Mozambique *Wetl. Ecol. Manage.* **24** 139–52
- [86] Feliciano E A, Wdowinski S, Potts M D, Lee S and Fatoyinbo T E 2017 Estimating Mangrove canopy height and above-ground biomass in the everglades national park with Airborne LiDAR and TanDEM-X data *Remote Sens.* **9** 702
- [87] Fatoyinbo T, Feliciano E A, Lagomasino D, Lee S K and Trettin C 2018 Estimating mangrove aboveground biomass from airborne LiDAR data: a case study from the Zambezi River delta *Environ. Res. Lett.* **13** 025012
- [88] Yin D and Wang L 2019 Individual mangrove tree measurement using UAV-based LiDAR data: possibilities and challenges *Remote Sens. Environ.* **223** 34–49
- [89] Lee S, Fatoyinbo T E, Lagomasino D, Feliciano E and Trettin C 2018 Multibaseline TanDEM-X Mangrove height estimation: the selection of the vertical wavenumber *IEEE J. Sel. Top. Appl. Earth Obs. Remote Sens.* **11** 3434–42
- [90] Hansen M C et al 2013 High-resolution global maps of 21st-century forest cover change *Science* **342** 850–3
- [91] Hamdan O, Aziz H K and Hasmadi I M 2014 L-band ALOS PALSAR for biomass estimation of Matang Mangroves, Malaysia *Remote Sens. Environ.* **155** 69–78
- [92] Lucas R, Otero V, Van De Kerchove R, Lagomasino D, Satyanarayana B, Fatoyinbo T and Dahdouh-Guebas F 2021 Monitoring Matang's Mangroves in Peninsular Malaysia through Earth observations: a globally relevant approach *Land Degrad. Dev.* **32** 354–73
- [93] Wang D, Wan B, Liu J, Su Y, Guo Q, Qiu P and Wu X 2020 Estimating aboveground biomass of the mangrove forests on northeast Hainan Island in China using an upscaling method from field plots, UAV-LiDAR data and Sentinel-2 imagery *Int. J. Appl. Earth Obs. Geoinf.* **85** 101986
- [94] Navarro J A, Algeet N, Fernández-Landa A, Esteban J, Rodríguez-Noriega P and Guillén-Climent M L 2019 Integration of UAV, sentinel-1, and sentinel-2 data for mangrove plantation aboveground biomass monitoring in Senegal *Remote Sens.* **11** 77
- [95] Hartoko A et al 2015 Carbon biomass algorithms development for Mangrove vegetation in Kemujan, Parang Island Karimunjawa National Park and Demak coastal area—Indonesia *Procedia Environ. Sci.* **23** 39
- [96] Hickey S M, Callow N J, Phinn S, Lovelock C E and Duarte C M 2018 Spatial complexities in aboveground carbon stocks of a semi-arid mangrove community: a remote sensing height-biomass-carbon approach *Estuar. Coast. Shelf Sci.* **200** 194–201
- [97] Barr J G, Engel V, Smith T J and Fuentes J D 2012 Hurricane disturbance and recovery of energy balance, CO<sub>2</sub> fluxes and canopy structure in a Mangrove forest of the Florida everglades *Agric. For. Meteorol.* **153** 54–66

- [98] Adame M F *et al* 2021 Future carbon emissions from global mangrove forest loss *Glob. Change Biol.* **27** 2856–66
- [99] Dai Z, Trettin C C, Birdsie R and Froelking S 2018 Mangrove carbon assessment tool: model development and sensitivity analyses *Estuar. Coast. Shelf Sci.* **208** 23–35
- [100] Bournazel J, Kumara M P, Jayatissa L P, Viergever K, Morel V and Huxham M 2015 The impacts of shrimp farming on land-use and carbon storage around Puttalam lagoon, Sri Lanka *Ocean Coast. Manage.* **113** 18–28
- [101] Duncan C, Primavera J H, Pettorelli N, Thompson J R, Loma R J A and Koldewey H J 2016 Rehabilitating mangrove ecosystem services: a case study on the relative benefits of abandoned pond reversion from Panay Island, Philippines *Mar. Pollut. Bull.* **109** 772–82
- [102] Yang J, Gao J, Cheung A, Liu B, Schwendenmann L and Costello M J 2013 Vegetation and sediment characteristics in an expanding mangrove forest in New Zealand *Estuar. Coast. Shelf Sci.* **134** 11–18
- [103] Ellegaard M, Nguyen N T G, Andersen T J, Michelsen A, Nguyen N L, Doan N H, Kristensen E, Weckström K, Son T P H and Lund-Hansen L C 2014 Temporal changes in physical, chemical and biological sediment parameters in a tropical estuary after mangrove deforestation *Estuar. Coast. Shelf Sci.* **142** 32–40
- [104] Anne N J, Abd-Elrahman A H, Lewis D B and Hewitt N A 2014 Modeling soil parameters using hyperspectral image reflectance in subtropical coastal wetlands *Int. J. Appl. Earth Obs. Geoinf.* **33** 47–56
- [105] Huang T, Fu Y, Pan P and Chen C A 2012 Fluvial carbon fluxes in tropical rivers *Curr. Opin. Environ. Sustain.* **4** 162–9
- [106] Bauer J E, Cai W-J, Raymond P A, Bianchi T S, Hopkinson C S and Regnier P A G 2013 The changing carbon cycle of the coastal ocean *Nature* **504** 61–70
- [107] Alongi D M 2020 Carbon balance in salt marsh and mangrove ecosystems: a global synthesis *J. Mar. Sci. Eng.* **8** 767
- [108] Breithaupt J L, Smoak J M, Smith T J III, Sanders C J and Hoare A 2012 Organic carbon burial rates in mangrove sediments: strengthening the global budget *Glob. Biogeochem. Cycles* **26** GB3011
- [109] Hansen A M, Kraus T E C, Pellerin B A, Fleck J A, Downing B D and Bergamaschi B A 2016 Optical properties of dissolved organic matter (DOM): effects of biological and photolytic degradation *Limnol. Oceanogr.* **61** 1015–32
- [110] Lu C J, Benner R, Fichot C G, Fukuda H, Yamashita Y and Ogawa H 2016 Sources and transformations of dissolved lignin phenols and chromophoric dissolved organic matter in Otsuchi Bay, Japan *Front. Mar. Sci.* **3** 85
- [111] Sanyal P, Ray R, Paul M, Gupta V K, Acharya A, Bakshi S, Jana T K and Mukhopadhyay S K 2020 Assessing the dynamics of dissolved organic matter (DOM) in the coastal environments dominated by mangroves, Indian Sundarbans *Front. Earth Sci.* **8** 218
- [112] Friess D A, Rogers K, Lovelock C E, Krauss K W, Hamilton S E, Lee S Y, Lucas R, Primavera J, Rajkaran A and Shi S 2019 The state of the world's mangrove forests: past, present, and future *Annu. Rev. Environ. Resour.* **44** 89–115
- [113] Krauss K W, From A S, Doyle T W, Doyle T J and Barry M J 2011 Sea-level rise and landscape change influence mangrove encroachment onto marsh in the Ten Thousand Islands region of Florida, USA *J. Coast. Conserv.* **15** 629–38
- [114] Ross M S, Meeder J F, Sah J P, Ruiz P L and Telesnicki G J 2000 The southeast saline Everglades revisited: 50 years of coastal vegetation change *J. Veg. Sci.* **11** 101–12
- [115] Osland M J, Day R H and Michot T C 2020 Frequency of extreme freeze events controls the distribution and structure of black mangroves (*Avicennia germinans*) near their northern range limit in coastal Louisiana *Divers. Distrib.* **26** 1366–82
- [116] Charles S P, Kominoski J S, Armitage A R, Guo H, Weaver C A and Pennings S C 2020 Quantifying how changing mangrove cover affects ecosystem carbon storage in coastal wetlands *Ecology* **101** e02916
- [117] Doughty C L, Langley J A, Walker W S, Feller I C, Schaub R and Chapman S K 2016 Mangrove range expansion rapidly increases coastal wetland carbon storage *Estuar. Coasts* **39** 385–96
- [118] Yando E S, Osland M J, Willis J M, Day R H, Krauss K W and Hester M W 2016 Salt marsh-mangrove ecotones: using structural gradients to investigate the effects of woody plant encroachment on plant–soil interactions and ecosystem carbon pools *J. Ecol.* **104** 1020–31
- [119] Worthington T A *et al* 2020 A global biophysical typology of mangroves and its relevance for ecosystem structure and deforestation *Sci. Rep.* **10** 1–11
- [120] Simard M, Fatoyinbo T, Smetanka C, Rivera-Monroy V H, Castaneda E, Thomas N and Van Der Stocken T 2019 *Global Mangrove Distribution, Aboveground Biomass, and Canopy Height* (<https://doi.org/10.3334/ORNLDAA/1665>)
- [121] Rosentreter J A, Maher D T, Erler D V, Murray R H and Eyre B D 2018 Methane emissions partially offset “blue carbon” burial in mangroves *Sci. Adv.* **4** eaao4985
- [122] Richards D R, Thompson B S and Wijedasa L 2020 Quantifying net loss of global mangrove carbon stocks from 20 years of land cover change *Nat. Commun.* **11** 1–7
- [123] Twilley R R, Castañeda-Moya E, Rivera-Monroy V H and Rovai A 2017 Productivity and carbon dynamics in mangrove wetlands *Mangrove Ecosystems: A Global Biogeographic Perspective* (Berlin: Springer) pp 113–62
- [124] Duarte C M and Cebrián J 1996 The fate of marine autotrophic production *Limnol. Oceanogr.* **41** 1758–66
- [125] Duarte C M, Losada I J, Hendriks I E, Mazarrasa I and Marbà N 2013 The role of coastal plant communities for climate change mitigation and adaptation *Nat. Clim. Change* **3** 961–8
- [126] Maher D T, Santos I R, Golsby-Smith L, Gleeson J and Eyre B D 2013 Groundwater-derived dissolved inorganic and organic carbon exports from a mangrove tidal creek: the missing mangrove carbon sink? *Limnol. Oceanogr.* **58** 475–88
- [127] Sippo J Z, Maher D T, Tait D R, Holloway C and Santos I R 2016 Are mangroves drivers or buffers of coastal acidification? Insights from alkalinity and dissolved inorganic carbon export estimates across a latitudinal transect *Glob. Biogeochem. Cycles* **30** 753–66
- [128] Barbier E B, Hacker S D, Kennedy C, Koch E W, Stier A C and Silliman B R 2011 The value of estuarine and coastal ecosystem services *Ecol. Monogr.* **81** 169–93
- [129] Mcowen C J, Weatherdon L V, Van Bochove J, Sullivan E, Blyth S, Zockler C, Stanwell-Smith D, Kingston N, Martin C S and Spalding M 2017 A global map of saltmarshes *Biodivers. Data J.* **5** e11764
- [130] Murray N J, Phinn S R, DeWitt M, Ferrari R, Johnston R, Lyons M B, Clinton N, Thau D and Fuller R A 2019 The global distribution and trajectory of tidal flats *Nature* **565** 222–5
- [131] Sager P E, Richman S, Harris H J and Fewless G 1985 Preliminary observations on the seiche-induced flux of carbon, nitrogen, and phosphorus in a Great Lakes coastal marsh *Coastal Wetlands* (Chelsea: Lewis Publishers) pp 59–68
- [132] Watson E B, Wigand C, Davey E W, Andrews H M, Bishop J and Raposa K B 2017 Wetland loss patterns and inundation-productivity relationships prognosticate widespread Salt Marsh loss for Southern New England *Estuar. Coasts* **40** 662–81
- [133] Deegan L A, Johnson D S, Warren R S, Peterson B J, Fleeger J W, Fagherazzi S and Wollheim W M 2012 Coastal eutrophication as a driver of salt marsh loss *Nature* **490** 388–92
- [134] Wang H, Ge Z, Yuan L and Zhang L 2014 Evaluation of the combined threat from sea-level rise and sedimentation



- reduction to the coastal wetlands in the Yangtze Estuary, China *Ecol. Eng.* **71** 346–54
- [135] Blum M D and Roberts H H 2009 Drowning of the Mississippi Delta due to insufficient sediment supply and global sea-level rise *Nat. Geosci.* **2** 488–91
- [136] Syvitski J P, Vörösmarty C J, Kettner A J and Green P 2005 Impact of humans on the flux of terrestrial sediment to the global coastal ocean *Science* **308** 376–80
- [137] Poffenbarger H J, Needelman B A and Megonigal J P 2011 Salinity influence on methane emissions from tidal marshes *Wetlands* **31** 831–42
- [138] Kroeger K D, Crooks S, Moseman-Valtierra S and Tang J 2017 Restoring tides to reduce methane emissions in impounded wetlands: a new and potent Blue Carbon climate change intervention *Sci. Rep.* **7** 1–12
- [139] Powell E B, Krause J R, Martin R M and Watson E B 2020 Pond excavation reduces coastal wetland carbon dioxide assimilation *J. Geophys. Res. Biogeosci.* **125** e2019JG005187
- [140] Hopkinson C S, Morris J T, Fagherazzi S, Wollheim W M and Raymond P A 2018 Lateral marsh edge erosion as a source of sediments for vertical marsh accretion *J. Geophys. Res. Biogeosci.* **123** 2444–65
- [141] Ghosh S, Mishra D R and Gitelson A A 2016 Long-term monitoring of biophysical characteristics of tidal wetlands in the northern Gulf of Mexico—a methodological approach using MODIS *Remote Sens. Environ.* **173** 39–58
- [142] Kromkamp J C, Morris E and Forster R M 2020 Microscale variability in biomass and photosynthetic activity of microphytobenthos during a spring–neap tidal cycle *Front. Mar. Sci.* **7** 562
- [143] Méléder V, Savelli R, Barnett A, Polsenaere P, Gernez P, Cugier P, Lerouxel A, Le Bris A, Dupuy C and Le Fouest V 2020 Mapping the intertidal microphytobenthos gross primary production part I: coupling multispectral remote sensing and physical modeling *Front. Mar. Sci.* **7** 520
- [144] Gao Y, Ouyang Z, Shao C, Chu H, Su Y, Guo H, Chen J and Zhao B 2018 Field observation of lateral detritus carbon flux in a coastal wetland *Wetlands* **38** 613–25
- [145] Tao J, Mishra D R, Cotten D L, O’Connell J, Leclerc M, Nahrawi H B, Zhang G and Pahari R 2018 A comparison between the MODIS product (MOD17A2) and a tide-robust empirical GPP model evaluated in a Georgia wetland *Remote Sens.* **10** 1831
- [146] Yan Y, Zhao B, Chen J, Guo H, Gu Y, Wu Q and Li B 2008 Closing the carbon budget of estuarine wetlands with tower-based measurements and MODIS time series *Glob. Change Biol.* **14** 1690–702
- [147] Feagin R A, Forbrich I, Huff T P, Barr J G, Ruiz-Plancarte J, Fuentes J D, Najjar R G, Vargas R, Vázquez-Lule A and Windham-Myers L 2020 Tidal wetland gross primary production across the continental United States, 2000–2019 *Glob. Biogeochem. Cycles* **34** e2019GB006349
- [148] Feagin R A, Forbrich I, Huff T P, Barr J G, Ruiz-Plancarte J, Fuentes J D, Najjar R G, Vargas R, Vázquez-Lule A and Windham-Myers L 2020b *Gross Primary Production Maps of Tidal Wetlands across Conterminous USA, 2000–2019* (<https://doi.org/10.3334/ORNLDAAAC/1792>)
- [149] O’Connell J L, Mishra D R, Cotten D L, Wang L and Alber M 2017 The Tidal Marsh Inundation Index (TMII): an inundation filter to flag flooded pixels and improve MODIS tidal marsh vegetation time-series analysis *Remote Sens. Environ.* **201** 34–46
- [150] Gross M F, Klemas V and Levasseur J E 1986 Remote sensing of *Spartina anglica* biomass in five French salt marshes *Int. J. Remote Sens.* **7** 657–64
- [151] Gross M F, Hardisky M A, Klemas V and Wolf P L 1987 Quantification of biomass of the marsh grass *Spartina alterniflora* Loisel using Landsat Thematic Mapper imagery *Photogramm. Eng. Remote Sens.* **53** 11
- [152] Hardisky M A, Daiber F C, Roman C T and Klemas V 1984 Remote sensing of biomass and annual net aerial primary productivity of a salt marsh *Remote Sens. Environ.* **16** 91–106
- [153] Jensen D, Cavanaugh K C, Simard M, Christensen A, Rovai A and Twilley R 2021 Aboveground biomass distributions and vegetation composition changes in Louisiana’s Wax Lake Delta *Estuar. Coast. Shelf Sci.* **250** 107139
- [154] Doughty C L and Cavanaugh K C 2019 Mapping coastal wetland biomass from high resolution unmanned aerial vehicle (UAV) imagery *Remote Sens.* **11** 540
- [155] Buffington K J, Dugger B D and Thorne K M 2018 Climate-related variation in plant peak biomass and growth phenology across Pacific Northwest tidal marshes *Estuar. Coast. Shelf Sci.* **202** 212–21
- [156] Rasel S M, Chang H, Ralph T J, Saintilan N and Diti I J 2019 Application of feature selection methods and machine learning algorithms for saltmarsh biomass estimation using Worldview-2 imagery *Geocarto Int.* **36** 1–25
- [157] Miller G J, Morris J T and Wang C 2019 Estimating aboveground biomass and its spatial distribution in coastal wetlands utilizing planet multispectral imagery *Remote Sens.* **11** 2020
- [158] Byrd K B, O’Connell J L, Di Tommaso S and Kelly M 2014 Evaluation of sensor types and environmental controls on mapping biomass of coastal marsh emergent vegetation *Remote Sens. Environ.* **149** 166–80
- [159] Zhang C, Denka S, Cooper H and Mishra D R 2018 Quantification of sawgrass marsh aboveground biomass in the coastal Everglades using object-based ensemble analysis and Landsat data *Remote Sens. Environ.* **204** 366–79
- [160] Kulawardhana R W, Popescu S C and Feagin R A 2014 Fusion of lidar and multispectral data to quantify salt marsh carbon stocks *Remote Sens. Environ.* **154** 345–57
- [161] Byrd K B, Ballanti L, Thomas N, Nguyen D, Holmquist J R, Simard M and Windham-Myers L 2018a *Aboveground Biomass High-Resolution Maps for Selected US Tidal Marshes, 2015* (<https://doi.org/10.3334/ORNLDAAAC/1879>)
- [162] Byrd K B, Ballanti L, Thomas N, Nguyen D, Holmquist J R, Simard M and Windham-Myers L 2018b A remote sensing-based model of tidal marsh aboveground carbon stocks for the conterminous United States *ISPRS J. Photogramm. Remote Sens.* **139** 255–71
- [163] Byrd K B, Ballanti L, Thomas N, Nguyen D, Holmquist J R, Simard M and Windham-Myers L 2020 Corrigendum to “A remote sensing-based model of tidal marsh aboveground carbon stocks for the conterminous United States” [ISPRS J. Photogramm. Rem. Sens. 139 (2018) 255–271] *ISPRS J. Photogramm. Remote Sens.* **166** 63–67
- [164] Xiangzhen Q, Huiyu L, Zhenshan L, Xiang L and Haibo G 2019 Impacts of age and expansion direction of invasive *Spartina alterniflora* on soil organic carbon dynamics in coastal salt marshes along eastern China *Estuar. Coasts* **42** 1858–67
- [165] Kulawardhana R W, Feagin R A, Popescu S C, Boutton T W, Yeager K M and Bianchi T S 2015 The role of elevation, relative sea-level history and vegetation transition in determining carbon distribution in *Spartina alterniflora* dominated salt marshes *Estuar. Coast. Shelf Sci.* **154** 48–57
- [166] Campbell A D and Wang Y 2020 Salt marsh monitoring along the mid-Atlantic coast by google earth engine enabled time series *PLoS One* **15** e0229605
- [167] Li X, Ren L, Liu Y, Craft C, Mander Ü and Yang S 2014 The impact of the change in vegetation structure on the ecological functions of salt marshes: the example of the Yangtze estuary *Reg. Environ. Change* **14** 623–32
- [168] Thomas N, Simard M, Castañeda-Moya E, Byrd K B, Windham-Myers L, Bevington A and Twilley R 2019 High-resolution mapping of biomass and distribution of marsh and forested wetlands in southeastern coastal Louisiana *Int. J. Appl. Earth Obs. Geoinf.* **80** 257–67
- [169] Zhao G, Ye S, Li G, Yu X and McClellan S A 2017 Soil organic carbon storage changes in coastal wetlands of the Liaohe Delta, China, based on landscape patterns *Estuar. Coasts* **40** 967–76



- [170] Jensen L A, Schmidt L B, Hollesen J and Elberling B 2006 Accumulation of soil organic carbon linked to Holocene sea-level changes in west Greenland *Arct. Antarct. Alp. Res.* **38** 378–83
- [171] Braun K N, Theuerkauf E J, Masterson A L, Curry B B and Horton D E 2019 Modeling organic carbon loss from a rapidly eroding freshwater coastal wetland *Sci. Rep.* **9** 1–13
- [172] Bianchi T S, Allison M A, Zhao J, Li X, Comeaux R S, Feagin R A and Kulawardhana R W 2013 Historical reconstruction of mangrove expansion in the Gulf of Mexico: linking climate change with carbon sequestration in coastal wetlands *Estuar. Coast. Shelf Sci.* **119** 7–16
- [173] Crooks S, Sutton-Grier A E, Troxler T G, Herold N, Bernal B, Schile-Beers L and Wirth T 2018 Coastal wetland management as a contribution to the US National greenhouse gas inventory *Nat. Clim. Change* **8** 1109–12
- [174] Holmquist J R et al 2018 Uncertainty in United States coastal wetland greenhouse gas inventorying *Environ. Res. Lett.* **13** 115005
- [175] Holmquist J R et al 2018 Accuracy and precision of tidal wetland soil carbon mapping in the conterminous United States *Sci. Rep.* **8** 1–16
- [176] Holmquist J R, Windham-Myers L, Bliss N, Crooks S, Morris J T, Megonigal J P, Troxler T, Weller D E, Callaway J and Drexler J 2019 *Tidal Wetland Soil Carbon Stocks for the Conterminous United States, 2006–2010* (<https://doi.org/10.3334/ORNLDAAC/1612>)
- [177] Callaway J C, Borgnis E L, Turner R E and Milan C S 2012 Carbon sequestration and sediment accretion in San Francisco Bay tidal wetlands *Estuar. Coasts* **35** 1163–81
- [178] Peck E K, Wheatcroft R A and Brophy L S 2020 Controls on sediment accretion and blue carbon burial in tidal saline wetlands: insights from the Oregon coast, USA *J. Geophys. Res. Biogeosci.* **125** e2019JG005464
- [179] Rogers K et al 2019 Wetland carbon storage controlled by millennial-scale variation in relative sea-level rise *Nature* **567** 91–95
- [180] Duarte C M 2017 Reviews and syntheses: hidden forests, the role of vegetated coastal habitats in the ocean carbon budget *Biogeosciences* **14** 301–10
- [181] Costanza R, d'Arge R, De Groot R, Farber S, Grasso M, Hannon B, Limburg K, Naeem S, O'Neill R V and Paruelo J 1997 The value of the world's ecosystem services and natural capital *Nature* **387** 253–60
- [182] Duarte C M, Middelburg J J and Caraco N 2005 Major role of marine vegetation on the oceanic carbon cycle *Biogeosciences* **2** 1–8
- [183] Al-Haj A N and Fulweiler R W 2020 A synthesis of methane emissions from shallow vegetated coastal ecosystems *Glob. Change Biol.* **26** 2988–3005
- [184] Lin W, Wu J and Lin H 2020 Contribution of unvegetated tidal flats to coastal carbon flux *Glob. Change Biol.* **26** 3443–54
- [185] Teal J M 1962 Energy flow in the salt marsh ecosystem of Georgia *Ecology* **43** 614–24
- [186] Childers D L, Day J W and Mckellar H N 2002 Twenty more years of marsh and estuarine flux studies: revisiting Nixon (1980) *Concepts and Controversies in Tidal Marsh Ecology* (New York: Kluwer Academic Publishers) pp 391–423
- [187] Tobias C and Neubauer S C 2019 Salt marsh biogeochemistry—an overview *Coastal Wetlands: An Integrated Ecosystem Approach* (Amsterdam: Elsevier) ed G M E Perillo, E Wolanski, D R Cahoon and M M Brinson pp 539–96
- [188] Cao F, Tzortziou M, Hu C, Mannino A, Fichot C G, Del Vecchio R, Najjar R G and Novak M 2018 Remote sensing retrievals of colored dissolved organic matter and dissolved organic carbon dynamics in North American estuaries and their margins *Remote Sens. Environ.* **205** 151–65
- [189] Short F, Carruthers T, Dennison W and Waycott M 2007 Global seagrass distribution and diversity: a bioregional model *J. Exp. Mar. Biol. Ecol.* **350** 3–20
- [190] Fourqurean J W, Duarte C M, Kennedy H, Marbà N, Holmer M, Mateo M A, Apostolaki E T, Kendrick G A, Krause-Jensen D and McGlathery K J 2012 Seagrass ecosystems as a globally significant carbon stock *Nat. Geosci.* **5** 505–9
- [191] Salinas C, Duarte C M, Lavery P S, Masque P, Arias-Ortiz A, Leon J X, Callaghan D, Kendrick G A and Serrano O 2020 Seagrass losses since mid-20th century fuelled CO<sub>2</sub> emissions from soil carbon stocks *Glob. Change Biol.* **26** 4772–84
- [192] Pollard P C and Greenway M 2013 Seagrasses in tropical Australia, productive and abundant for decades decimated overnight *J. Biosci.* **38** 157–66
- [193] Zhang M, English D, Hu C, Carlson P, Muller-Karger F E, Toro-Farmer G and Herwitz S R 2016 Short-term changes of remote sensing reflectance in a shallow-water environment: observations from repeated airborne hyperspectral measurements *Int. J. Remote Sens.* **37** 1620–38
- [194] Lyons M, Roelfsema C, Kovacs E, Samper-Villarreal J, Saunders M, Maxwell P and Phinn S 2015 Rapid monitoring of seagrass biomass using a simple linear modelling approach, in the field and from space *Mar. Ecol. Prog. Ser.* **530** 1–14
- [195] Munir M and Wicaksono P 2019 Support vector machine for seagrass percent cover mapping using PlanetScope image in Labuan Bajo, East Nusa Tenggara *Sixth Int. Symp. on LAPAN-IPB Satellite* (International Society for Optics and Photonics)
- [196] Misbari S and Hashim M 2016 Change detection of submerged seagrass biomass in shallow coastal water *Remote Sens.* **8** 200
- [197] Tamondong A, Cruz C, Quides R R, Garcia M, Cruz J A, Guihawan J and Blanco A 2018 Remote sensing-based estimation of seagrass percent cover and LAI for above ground carbon sequestration mapping *Remote Sensing of the Open and Coastal Ocean and Inland Waters Honolulu, Hawaii, United States October 2018* p 1077803
- [198] Tamondong A M, Blanco A C, Fortes M D and Nadaoka K 2013 Mapping of seagrass and other benthic habitats in Bolinao, Pangasinan using Worldview-2 satellite image *2013 IEEE Int. Geoscience and Remote Sensing Symp. -IGARSS (IEEE)* p 1579
- [199] Kakuta S, Takeuchi W and Prathep A 2016 Seaweed and seagrass mapping in thailand measured using Landsat 8 optical and textural image properties *J. Mar. Sci. Technol.* **24** 1155–60
- [200] Dierssen H M, Chlus A and Russell B 2015 Hyperspectral discrimination of floating mats of seagrass wrack and the macroalgae Sargassum in coastal waters of Greater Florida Bay using airborne remote sensing *Remote Sens. Environ.* **167** 247–58
- [201] Dierssen H M, Zimmerman R C, Drake L A and Burdige D 2010 Benthic ecology from space: optics and net primary production in seagrass and benthic algae across the Great Bahama Bank *Mar. Ecol. Prog. Ser.* **411** 1–15
- [202] Jayathilake D R and Costello M J 2018 A modelled global distribution of the seagrass biome *Biol. Conserv.* **226** 120–6
- [203] Duffy J E, Benedetti-Cecchi L, Trinanés J, Muller-Karger F E, Ambo-Rappe R, Boström C, Buschmann A H, Byrnes J, Coles R G and Creed J 2019 Toward a coordinated global observing system for seagrasses and marine macroalgae *Front. Mar. Sci.* **6** 317
- [204] McKenzie L J, Nordlund L M, Jones B L, Cullen-Unsworth L C, Roelfsema C and Unsworth R K 2020 The global distribution of seagrass meadows *Environ. Res. Lett.* **15** 074041
- [205] Pergent G, Pergent-Martini C, de Florinier M and Valette-Sansevin A 2015 Assessment of carbon sequestration in Posidonia meadow *Medcoast 2015 Varna, Bulgaria October 2015* p 231–38
- [206] Lefcheck J S, Wilcox D J, Murphy R R, Marion S R and Orth R J 2017 Multiple stressors threaten the imperiled

- coastal foundation species eelgrass (*Zostera marina*) in Chesapeake Bay, USA *Glob. Change Biol.* **23** 3474–83
- [207] Sousa A I, da Silva J F, Azevedo A and Lillebø A I 2019 Blue carbon stock in *Zostera noltei* meadows at Ria de Aveiro coastal lagoon (Portugal) over a decade *Sci. Rep.* **9** 1–13
- [208] Zoffoli M L, Gernez P, Rosa P, Le Bris A, Brando V E, Barillé A, Harin N, Peters S, Poser K and Spaias L 2020 Sentinel-2 remote sensing of *Zostera noltei*-dominated intertidal seagrass meadows *Remote Sens. Environ.* **251** 112020
- [209] Hedley J and Enriquez S 2010 Optical properties of canopies of the tropical seagrass *Thalassia testudinum* estimated by a three-dimensional radiative transfer model *Limnol. Oceanogr.* **55** 1537–50
- [210] Hedley J, Russell B, Randolph K and Dierssen H 2016 A physics-based method for the remote sensing of seagrasses *Remote Sens. Environ.* **174** 134–47
- [211] Greene A, Rahman A F, Kline R and Rahman M S 2018 Side scan sonar: a cost-efficient alternative method for measuring seagrass cover in shallow environments *Estuar. Coast. Shelf Sci.* **207** 250–8
- [212] Rende S F, Bosman A, Di Mento R, Bruno F, Lagudi A, Irving A D, Dattola L, Giambattista L D, Lanera P and Proietti R 2020 Ultra-High-Resolution Mapping of *Posidonia oceanica* (L.) Delile Meadows through acoustic, optical data and object-based image classification *J. Mar. Sci. Eng.* **8** 647
- [213] Beca-Carretero P, Varela S and Stengel D B 2020 A novel method combining species distribution models, remote sensing, and field surveys for detecting and mapping subtidal seagrass meadows *Aquat. Conserv.: Mar. Freshw. Ecosyst.* **30** 1098–110
- [214] Poursanidis D, Traganos D, Teixeira L, Shapiro A and Muaves L 2020 Cloud-native seascape mapping of Mozambique's Quirimbas National park with sentinel-2 *Remote Sens. Ecol. Conserv.* **7** 275–91
- [215] UNEP-WCMC, Short FT 2021 *Global Distribution of Seagrasses (Version 7.1). Seventh Update to the Data Layer Used in Green and Short (2003)* (Cambridge: UN Environment World Conservation Monitoring Centre) Data (<https://doi.org/10.34892/x6r3-d211>)
- [216] Waycott M, Duarte C M, Carruthers T J, Orth R J, Dennison W C, Olyarnik S, Calladine A, Fourqurean J W, Heck K L and Hughes A R 2009 Accelerating loss of seagrasses across the globe threatens coastal ecosystems *Proc. Natl Acad. Sci.* **106** 12377–81
- [217] Duffy J P, Pratt L, Anderson K, Land P E and Shutler J D 2018 Spatial assessment of intertidal seagrass meadows using optical imaging systems and a lightweight drone *Estuar. Coast. Shelf Sci.* **200** 169–80
- [218] Ballard M S, Lee K M, Sagers J D, Venegas G R, McNeese A R, Wilson P S and Rahman A F 2020 Application of acoustical remote sensing techniques for ecosystem monitoring of a seagrass meadow *J. Acoust. Soc. Am.* **147** 2002–19
- [219] Hays G C, Alcoverro T, Christianen M J, Duarte C M, Hamann M, Macreadie P I, Marsh H D, Rasheed M A, Thums M and Unsworth R K 2018 New tools to identify the location of seagrass meadows: marine grazers as habitat indicators *Front. Mar. Sci.* **5** 9
- [220] Traganos D, Aggarwal B, Poursanidis D, Topouzelis K, Chrysoulakis N and Reinartz P 2018 Towards global-scale seagrass mapping and monitoring using sentinel-2 on google earth engine: the case study of the Aegean and Ionian seas *Remote Sens.* **10** 1227
- [221] Ha N T, Manley-Harris M, Pham T D and Hawes I 2020 A comparative assessment of ensemble-based machine learning and maximum likelihood methods for mapping seagrass using sentinel-2 imagery in tauranga harbor, New Zealand *Remote Sens.* **12** 355
- [222] Brock J C, Yates K K, Halley R B, Kuffner I B, Wright C W and Hatcher B G 2006 Northern Florida reef tract benthic metabolism scaled by remote sensing *Mar. Ecol. Prog. Ser.* **312** 123–39
- [223] Moses C S, Andréfouët S, Kranenburg C J and Muller-Karger F E 2009 Regional estimates of reef carbonate dynamics and productivity using Landsat 7 ETM, and potential impacts from ocean acidification *Mar. Ecol. Prog. Ser.* **380** 103–15
- [224] Clavier J, Chauvaud L, Carlier A, Amice E, Van der Geest M, Labrosse P, Diagne A and Hily C 2011 Aerial and underwater carbon metabolism of a *Zostera noltii* seagrass bed in the Banc d'Arguin, Mauritania *Aquat. Bot.* **95** 24–30
- [225] Van Dam B, Zeller M, Lopes C, Smyth A, Böttcher M, Osburn C, Zimmerman T, Pröfrock D, Fourqurean J and Thomas H 2021 Calcification-driven CO<sub>2</sub> emissions exceed "Blue Carbon" sequestration in a carbonate seagrass meadow *Sci. Adv.* **7** eabj1372
- [226] Polsenaere P, Lamaud E, Lafon V, Bonnefond J, Bretel P, Delille B, Deborde J, Loustau D and Abril G 2012 Spatial and temporal CO<sub>2</sub> exchanges measured by Eddy Covariance over a temperate intertidal flat and their relationships to net ecosystem production *Biogeosciences* **9** 249–68
- [227] Samper-Villarreal J, Lovelock C E, Saunders M I, Roelfsema C and Mumby P J 2016 Organic carbon in seagrass sediments is influenced by seagrass canopy complexity, turbidity, wave height, and water depth *Limnol. Oceanogr.* **61** 938–52
- [228] Serrano O, Lavery P S, Rozaimi M and Mateo M Á 2014 Influence of water depth on the carbon sequestration capacity of seagrasses *Glob. Biogeochem. Cycles* **28** 950–61
- [229] Traganos D and Reinartz P 2018 Machine learning-based retrieval of benthic reflectance and *Posidonia oceanica* seagrass extent using a semi-analytical inversion of Sentinel-2 satellite data *Int. J. Remote Sens.* **39** 9428–52
- [230] Thomas N, Pertiwi A P, Traganos D, Lagomasino D, Poursanidis D, Moreno S and Fatoyinbo L 2021 Space-borne cloud-native satellite-derived Bathymetry (SDB) models using ICESat-2 and sentinel-2 *Geophys. Res. Lett.* **48** e2020GL092170
- [231] Saunders M I, Bayraktarov E, Roelfsema C M, Leon J X, Samper-Villarreal J, Phinn S R, Lovelock C E and Mumby P J 2015 Spatial and temporal variability of seagrass at Lizard Island, Great Barrier Reef *Bot. Mar.* **58** 35–49
- [232] Ouisse V, Marchand-Jouravleff I, Fiandrino A, Feunteun E and Ysnel F 2020 Swinging boat moorings: spatial heterogeneous damage to eelgrass beds in a tidal ecosystem *Estuar. Coast. Shelf Sci.* **235** 106581
- [233] Glasby T M and West G 2018 Dragging the chain: quantifying continued losses of seagrasses from boat moorings *Aquat. Conserv.: Mar. Freshw. Ecosyst.* **28** 383–94
- [234] Kelly J J, Orr D and Takekawa J Y 2019 Quantification of damage to eelgrass (*Zostera marina*) beds and evidence-based management strategies for boats anchoring in San Francisco Bay *Environ. Manage.* **64** 20–26
- [235] Thorhaug A, Berlyn G P, Poulos H M and Goodale U M 2015 Pollutant tracking for 3 Western North Atlantic sea grasses by remote sensing: preliminary diminishing white light responses of *Thalassia testudinum*, *Halodule wrightii*, and *Zostera marina* *Mar. Pollut. Bull.* **97** 460–9
- [236] Carnell P E, Ierodiaconou D, Atwood T B and Macreadie P I 2020 Overgrazing of seagrass by sea urchins diminishes blue carbon stocks *Ecosystems* **23** 1437–48
- [237] Arias-Ortiz A, Serrano O, Masqué P, Lavery P S, Mueller U, Kendrick G A, Rozaimi M, Esteban A, Fourqurean J W and Marbà N 2018 A marine heatwave drives massive losses from the world's largest seagrass carbon stocks *Nat. Clim. Change* **8** 338–44
- [238] Davenport A E, Davis J D, Woo I, Grossman E E, Barham J, Ellings C S and Takekawa J Y 2017 Comparing automated classification and digitization approaches to detect change in eelgrass bed extent during restoration of a large river delta *Northwest Sci.* **91** 272–82

- [239] McGlathery K J, Reynolds L K, Cole L W, Orth R J, Marion S R and Schwarzschild A 2012 Recovery trajectories during state change from bare sediment to eelgrass dominance *Mar. Ecol. Prog. Ser.* **448** 209–21
- [240] Valdez S R, Zhang Y S, van der Heide T, Vanderklift M A, Tarquinio F, Orth R J and Silliman B R 2020 Positive ecological interactions and the success of seagrass restoration *Front. Mar. Sci.* **7** 91
- [241] Kolka R et al 2018 Terrestrial wetlands *Second State of the Carbon Cycle Report (SOCCR2): A Sustained Assessment Report* ed N Cavallaro, G Shrestha, R Birdsey, A M Mayes, R G Najjar, S C Reed, P Romero-Lankao and Z Zhu (Washington, DC: U.S. Global Change Research Program) pp 507–67 Ch 13
- [242] Cowardin L M, Carter V, Golet F C and LaRoe E T 1979 *Classification of Wetlands and Deepwater Habitats of the United States* (Washington, DC: US Department of the Interior, US Fish and Wildlife Service)
- [243] Dahl T E 1990 *Wetlands Losses in the United States, 1780's to 1980's* (St. Petersburg, FL: Report to the Congress, National Wetlands Inventory)
- [244] Lal R 2008 Carbon sequestration *Phil. Trans. R. Soc. B* **363** 815–30
- [245] Nahlik A M and Fennessy M S 2016 Carbon storage in US wetlands *Nat. Commun.* **7** 1–9
- [246] Davidson N C, Fluet-Chouinard E and Finlayson C M 2018 Global extent and distribution of wetlands: trends and issues *Mar. Freshw. Res.* **69** 620–7
- [247] Dahl T E, Johnson C E and Frayer W E 1991 *Wetlands, Status and Trends in the Conterminous United States Mid-1970's to Mid-1980's* U.S. Department of the Interior, Fish and Wildlife Service
- [248] Halabisky M, Moskal L M, Gillespie A and Hannam M 2016 Reconstructing semi-arid wetland surface water dynamics through spectral mixture analysis of a time series of Landsat satellite images (1984–2011) *Remote Sens. Environ.* **177** 171–83
- [249] Kissel A M, Halabisky M, Scherer R D, Ryan M E and Hansen E C 2020 Expanding wetland hydroperiod data via satellite imagery for ecological applications *Front. Ecol. Environ.* **18** 432–8
- [250] Lang M, McCarty G, Oesterling R and Yeo I 2013 Topographic metrics for improved mapping of forested wetlands *Wetlands* **33** 141–55
- [251] O'Neil G L, Saby L, Band L E and Goodall J L 2019 Effects of LiDAR DEM smoothing and conditioning techniques on a topography-based wetland identification model *Water Resour. Res.* **55** 4343–63
- [252] Adeli S, Salehi B, Mahdianpari M, Quackenbush L J, Brisco B, Tamiminia H and Shaw S 2020 Wetland monitoring using SAR data: a meta-analysis and comprehensive review *Remote Sens.* **12** 2190
- [253] Descloux S, Chanudet V, Poilvé H and Grégoire A 2011 Co-assessment of biomass and soil organic carbon stocks in a future reservoir area located in Southeast Asia *Environ. Monit. Assess.* **173** 723–41
- [254] Suchenwirth L, Stümer W, Schmidt T, Förster M and Kleinschmit B 2014 Large-scale mapping of carbon stocks in riparian forests with self-organizing maps and the k-nearest-neighbor algorithm *Forests* **5** 1635–52
- [255] Sanders L M, Taffs K, Stokes D, Sanders C J, Enrich-Prast A, Amora-Nogueira L and Marotta H 2018 Historic carbon burial spike in an Amazon floodplain lake linked to riparian deforestation near Santarém, Brazil *Biogeosciences* **15** 447–55
- [256] Graves B P, Ralph T J, Hesse P P, Westaway K E, Kobayashi T, Gadd P S and Mazumder D 2019 Macro-charcoal accumulation in floodplain wetlands: problems and prospects for reconstruction of fire regimes and environmental conditions *PLoS One* **14** e0224011
- [257] Fluet-Chouinard E, Lehner B, Rebelo L, Papa F and Hamilton S K 2015 Development of a global inundation map at high spatial resolution from topographic downscaling of coarse-scale remote sensing data *Remote Sens. Environ.* **158** 348–61
- [258] Fernandes M R, Aguiar F C, Martins M J, Rico N, Ferreira M T and Correia A C 2020 Carbon stock estimations in a mediterranean Riparian forest: a case study combining field data and UAV Imagery *Forests* **11** 376
- [259] McClellan M, Comas X, Benschoter B, Hinkle R and Sumner D 2017 Estimating belowground carbon stocks in isolated wetlands of the Northern Everglades Watershed, central Florida, using ground penetrating radar and aerial imagery *J. Geophys. Res. Biogeosci.* **122** 2804–16
- [260] Buma B, Krapek J and Edwards R T 2016 Watershed-scale forest biomass distribution in a perhumid temperate rainforest as driven by topographic, soil, and disturbance variables *Can. J. For. Res.* **46** 844–54
- [261] Buras A, Thevs N, Zerbe S and Wilmking M 2013 Productivity and carbon sequestration of *Populus euphratica* at the Amu River, Turkmenistan *Forestry* **86** 429–39
- [262] Filippi A M, Güneralp İ and Randall J 2014 Hyperspectral remote sensing of aboveground biomass on a river meander bend using multivariate adaptive regression splines and stochastic gradient boosting *Remote Sens. Lett.* **5** 432–41
- [263] Chabi A, Lautenbach S, Orekan V O A and Kyei-Baffour N 2016 Allometric models and aboveground biomass stocks of a West African Sudan Savannah watershed in Benin *Carbon Balance Manage.* **11** 1–18
- [264] Riegel J B, Bernhardt E and Swenson J 2013 Estimating above-ground carbon biomass in a newly restored coastal plain wetland using remote sensing *PLoS One* **8** e68251
- [265] Taddeo S, Dronova I and Depsky N 2019 Spectral vegetation indices of wetland greenness: responses to vegetation structure, composition, and spatial distribution *Remote Sens. Environ.* **234** 111467
- [266] Lumbierres M, Méndez P F, Bustamante J, Soriguer R and Santamaría L 2017 Modeling biomass production in seasonal wetlands using MODIS NDVI land surface phenology *Remote Sens.* **9** 392
- [267] O'Connell J L, Byrd K B and Kelly M 2014 Remotely-sensed indicators of N-related biomass allocation in *Schoenoplectus acutus* *PLoS One* **9** e90870
- [268] Ling C, Sun H, Zhang H, Lin H, Ju H and Liu H 2014 Study on above-ground biomass estimation of East Dong Ting lake wetland based on Worldview-2 data 2014 *Third Int. Workshop on Earth Observation and Remote Sensing Applications (EORSA)* (IEEE) p 428
- [269] Budzynska M, Dabrowska-Zielinska K, Kowalik W, Malek I and Turlej K 2010 Study in Biebrza Wetlands using optical and microwave satellite data 2010 *IEEE Int. Geoscience and Remote Sensing Symp.* (IEEE) p 393
- [270] Knox S H, Dronova I, Sturtevant C, Oikawa P Y, Matthes J H, Verfaillie J and Baldocchi D 2017 Using digital camera and Landsat imagery with eddy covariance data to model gross primary production in restored wetlands *Agric. For. Meteorol.* **237** 233–45
- [271] Mendez-Estrella R, Romo-Leon J R and Castellanos A E 2017 Mapping changes in carbon storage and productivity services provided by riparian ecosystems of semi-arid environments in Northwestern Mexico *ISPRS Int. J. Geo-Inf.* **6** 298
- [272] Poulter B, Bousquet P, Canadell J G, Ciais P, Pregon A, Saunois M, Arora V K, Beerling D J, Brovkin V and Jones C D 2017 Global wetland contribution to 2000–2012 atmospheric methane growth rate dynamics *Environ. Res. Lett.* **12** 094013
- [273] Potter C, Klooster S, Hiatt S, Fladeland M, Genovese V and Gross P 2006 Methane emissions from natural wetlands in the United States: satellite-derived estimation based on ecosystem carbon cycling *Earth Interact.* **10** 1–12
- [274] Melton J R, Wania R, Hodson E L, Poulter B, Ringeval B, Spahni R, Bohn T, Avis C A, Beerling D J and Chen G 2013 Present state of global wetland extent and wetland methane



- modelling: conclusions from a model inter-comparison project (WETCHIMP) *Biogeosciences* **10** 753–88
- [275] Wania R, Melton J R, Hodson E L, Poulter B, Ringeval B, Spahni R, Bohn T, Avis C A, Chen G and Eliseev A V 2013 Present state of global wetland extent and wetland methane modelling: methodology of a model inter-comparison project (WETCHIMP) *Geosci. Model Dev.* **6** 617–41
- [276] Hondula K L, DeVries B, Jones C N and Palmer M A 2021 Effects of using high resolution satellite-based inundation time series to estimate methane fluxes from forested Wetlands *Geophys. Res. Lett.* **48** e2021GL092556
- [277] Lu W, Xiao J, Liu F, Zhang Y, Liu C and Lin G 2017 Contrasting ecosystem CO<sub>2</sub> fluxes of inland and coastal wetlands: a meta-analysis of eddy covariance data *Glob. Change Biol.* **23** 1180–98
- [278] Prigent C, Papa F, Aires F, Rossow W B and Matthews E 2007 Global inundation dynamics inferred from multiple satellite observations, 1993–2000 *J. Geophys. Res. Atmos.* **112** D12107
- [279] Lehner B and Döll P 2004 Development and validation of a global database of lakes, reservoirs and wetlands *J. Hydrol.* **296** 1–22
- [280] Aselmann I and Crutzen P J 1989 Global distribution of natural freshwater wetlands and rice paddies, their net primary productivity, seasonality and possible methane emissions *J. Atmos. Chem.* **8** 307–58
- [281] Matthews E and Fung I 1987 Methane emission from natural wetlands: global distribution, area, and environmental characteristics of sources *Glob. Biogeochem. Cycles* **1** 61–86
- [282] Roehm C L 2005 Respiration in wetland ecosystems respiration in aquatic ecosystems (Oxford University Press) pp 83–102 (available at: <https://oxford.universitypressscholarship.com/view/10.1093/acprof:oso/9780198527084.001.0001/acprof-9780198527084-chapter-6>)
- [283] Campbell C, Vitt D H, Halsey L A, Campbell I D, Thormann M N and Bayley S E 2000 *Net Primary Production and Standing Biomass in Northern Continental Wetlands* NOR-X-369 Northern Forestry Centre
- [284] Mitsch W J and Gosselink J G 2000 The value of wetlands: importance of scale and landscape setting *Ecol. Econ.* **35** 25–33
- [285] Xu J, Morris P J, Liu J and Holden J 2018 PEATMAP: refining estimates of global peatland distribution based on a meta-analysis *Catena* **160** 134–40
- [286] Hodgkins S B, Richardson C J, Dommann R, Wang H, Glaser P H, Verbeke B, Winkler B R, Cobb A R, Rich V I and Missilmani M 2018 Tropical peatland carbon storage linked to global latitudinal trends in peat recalcitrance *Nat. Commun.* **9** 1–13
- [287] Yu Z, Loisel J, Brosseau D P, Beilman D W and Hunt S J 2010 Global peatland dynamics since the Last Glacial Maximum *Geophys. Res. Lett.* **37** 13
- [288] Leifeld J and Menichetti L 2018 The underappreciated potential of peatlands in global climate change mitigation strategies *Nat. Commun.* **9** 1–7
- [289] Loisel J, Gallego-Sala A V, Amesbury M J, Magnan G, Anshari G, Beilman D W, Benavides J C, Blewett J, Camill P and Charman D J 2021 Expert assessment of future vulnerability of the global peatland carbon sink *Nat. Clim. Change* **11** 70–77
- [290] Bourgeau-Chavez L L, Endres S L, Graham J A, Hribljan J A, Chimner R A, Lilleskov E A and Battaglia M J 2018 Mapping peatlands in boreal and tropical ecoregions *Comprehensive Remote Sensing* vol 6, ed S Liang (Amsterdam: Elsevier) pp 24–44
- [291] Limpens J, Berendse F, Blodau C, Canadell J G, Freeman C, Holden J, Roulet N, Rydin H and Schaepman-Strub G 2008 Peatlands and the carbon cycle: from local processes to global implications—a synthesis *Biogeosciences* **5** 1475–91
- [292] Turunen J, Tomppo E, Tolonen K and Reinikainen A 2002 Estimating carbon accumulation rates of undrained mires in Finland—application to boreal and subarctic regions *Holocene* **12** 69–80
- [293] Bourgeau-Chavez L L, Grelik S L, Billmire M G, Jenkins L, Kasischke E S and Turetsky M R 2020 Assessing boreal peat fire severity and vulnerability of peatlands to early season wildland fire *Front. For. Glob. Change* **3** 20
- [294] Craft C, Washburn C and Parker A 2008 Latitudinal trends in organic carbon accumulation in temperate freshwater peatlands *Wastewater Treatment, Plant Dynamics and Management in Constructed and Natural Wetlands* (Berlin: Springer) pp 23–31
- [295] Charman D J, Beilman D W, Blaauw M, Booth R K, Brewer S, Chambers F M, Christen J A, Gallego-Sala A, Harrison S P and Hughes P D 2013 Climate-related changes in peatland carbon accumulation during the last millennium *Biogeosciences* **10** 929–44
- [296] Bourgeau-Chavez L L et al 2021 Advances in amazonian peatland discrimination with multi-temporal PALSAR Refines estimates of Peatland distribution, C stocks and deforestation *Front. Earth Sci.* **9** 676748
- [297] Draper F C, Roucoux K H, Lawson I T, Mitchard E T, Coronado E N H, Lähteenoja O, Montenegro L T, Sandoval E V, Zarate R and Baker T R 2014 The distribution and amount of carbon in the largest peatland complex in Amazonia *Environ. Res. Lett.* **9** 124017
- [298] Silva M L D, Silva A C, Silva B P C, Barral U M, Soares P G and Vidal-Torrado P 2013 Surface mapping, organic matter and water stocks in peatlands of the Serra do Espinhaço Meridional-Brazil *Rev. Bras. Cienc. Solo* **37** 1149–57
- [299] Lähteenoja O, Reátegui Y R, Räsänen M, Torres D D C, Oinonen M and Page S 2012 The large Amazonian peatland carbon sink in the subsiding Pastaza-Marañón foreland basin, Peru *Glob. Change Biol.* **18** 164–78
- [300] Hergoualc'h K, Gutiérrez-Vélez V H, Menton M and Verhot L V 2017 Characterizing degradation of palm swamp peatlands from space and on the ground: an exploratory study in the Peruvian Amazon *For. Ecol. Manage.* **393** 63–73
- [301] Chimner R A, Bourgeau-Chavez L, Grelik S, Hribljan J A, Clarke A M P, Polk M H, Lilleskov E A and Fuentealba B 2019 Mapping mountain peatlands and wet meadows using multi-date, multi-sensor remote sensing in the Cordillera Blanca, Peru *Wetlands* **39** 1057–67
- [302] Hribljan J A, Suarez E, Bourgeau-Chavez L, Endres S, Lilleskov E A, Chimbolema S, Wayson C, Serocki E and Chimner R A 2017 Multidate, multisensor remote sensing reveals high density of carbon-rich mountain peatlands in the páramo of Ecuador *Glob. Change Biol.* **23** 5412–25
- [303] Davenport I J, McNicol I, Mitchard E T, Dargie G, Suspense I, Milongo B, Bocko Y E, Hawthorne D, Lawson I and Baird A J 2020 First evidence of peat domes in the Congo Basin using LiDAR from a fixed-Wing Drone *Remote Sens.* **12** 2196
- [304] Dargie G C, Lewis S L, Lawson I T, Mitchard E T, Page S E, Bocko Y E and Ifo S A 2017 Age, extent and carbon storage of the central Congo Basin peatland complex *Nature* **542** 86–90
- [305] Wedeux B, Dalponte M, Schlund M, Hagen S, Cochrane M, Graham L, Usup A, Thomas A and Coomes D 2020 Dynamics of a human-modified tropical peat swamp forest revealed by repeat lidar surveys *Glob. Change Biol.* **26** 3947–64
- [306] Vernimmen R, Hooijer A, Akmalia R, Fitriyananegara N, Mulyadi D, Yuherdha A, Andreas H and Page S 2020 Mapping deep peat carbon stock from a LiDAR based DTM and field measurements, with application to eastern Sumatra *Carbon Balance Manage.* **15** 1–18
- [307] Thapa R B, Watanabe M, Motohka T, Shiraiishi T and Shimada M 2014 Calibration of aboveground forest carbon stock models for major tropical forests in central Sumatra using airborne LiDAR and field measurement data *IEEE J. Sel. Top. Appl. Earth Obs. Remote Sens.* **8** 661–73

- [308] Minasnay B, Sulaeman Y and Setiawan B I 2019 Open digital mapping for accurate assessment of tropical peatlands *Tropical Wetlands-Innovation in Mapping and Management: Proc. of the Int. Workshop on Tropical Wetlands: Innovation in Mapping and Management (Banjarmasin, Indonesia, 19–20 October 2018)* (CRC Press) p 3
- [309] Hoyt A M, Chaussard E, Seppalainen S S and Harvey C F 2020 Widespread subsidence and carbon emissions across Southeast Asian peatlands *Nat. Geosci.* **13** 435–40
- [310] Enghart S, Keuck V and Siegert F 2011 Modeling aboveground biomass in tropical forests using multi-frequency SAR data—a comparison of methods *IEEE J. Sel. Top. Appl. Earth Obs. Remote Sens.* **5** 298–306
- [311] Noojipady P, Morton D C, Schroeder W, Carlson K M, Huang C, Gibbs H K, Burns D, Walker N F and Prince S D 2017 Managing fire risk during drought: the influence of certification and El Niño on fire-driven forest conversion for oil palm in Southeast Asia *Earth Syst. Dyn.* **8** 749–71
- [312] Adesiji A R, Mohammed T A, Daud N N, Saari M, Gbadebo A O and Jacdonmi I 2015 Impacts of land use change on peatland degradation: a review *Ethiop. J. Environ. Stud. Manage.* **8** 225–34
- [313] Tsvetkov P S 2017 The history, present status and future prospects of the Russian fuel peat industry *Mires Peat* **19** 1–12
- [314] Lees K J, Artz R R, Khomik M, Clark J M, Ritson J, Hancock M H, Cowie N R and Quaife T 2020 Using spectral indices to estimate water content and GPP in Sphagnum moss and other peatland vegetation *IEEE Trans. Geosci. Remote Sens.* **58** 4547–57
- [315] Tampuu T, Praks J, Uiboupin R and Kull A 2020 Long term interferometric temporal coherence and DInSAR phase in Northern Peatlands *Remote Sens.* **12** 1566
- [316] Medcalf K A, Jarman M W and Keyworth S J 2010 Assessing the extent and severity of erosion on the upland organic soils of Scotland using earth observation and object orientated classification methods *Int Soc Photogrammetry and Remote Sensing* ed E A Addink and F VanCoillie (Gottingen: Copernicus Gesellschaft mbH) p 37081
- [317] Connolly J, Holden N M, Connolly J, Seaquist J W and Ward S M 2011 Detecting recent disturbance on Montane blanket bogs in the Wicklow Mountains, Ireland using the MODIS enhanced vegetation index *Int. J. Remote Sens.* **32** 2377–93
- [318] Aitkenhead M and Coull M 2020 Mapping soil profile depth, bulk density and carbon stock in Scotland using remote sensing and spatial covariates *Eur. J. Soil Sci.* **71** 553–67
- [319] Lees K J, Quaife T, Artz R, Khomik M, Sottocornola M, Kiely G, Hambley G, Hill T, Saunders M and Cowie N R 2019 A model of gross primary productivity based on satellite data suggests formerly afforested peatlands undergoing restoration regain full photosynthesis capacity after five to ten years *J. Environ. Manage.* **246** 594–604
- [320] Williamson J, Rowe E, Reed D, Ruffino L, Jones P, Dolan R, Buckingham H, Norris D, Astbury S and Evans C D 2017 Historical peat loss explains limited short-term response of drained blanket bogs to rewetting *J. Environ. Manage.* **188** 278–86
- [321] Patberg W, Baaijens G J, Smolders A J, Grootjans A P and Elzenga J T M 2013 The importance of groundwater-derived carbon dioxide in the restoration of small Sphagnum bogs *Preslia* **85** 389–403
- [322] Henman J and Poulter B 2008 Inundation of freshwater peatlands by sea-level rise: uncertainty and potential carbon cycle feedbacks *J. Geophys. Res. Biogeosci.* **113** G01011
- [323] Connolly J and Holden N M 2011 Mapping peatland disturbance in Ireland: an object oriented approach *Remote Sensing for Agriculture, Ecosystems, and Hydrology XIII Prague, Czech Republic 2011* 81740G
- [324] Gunnarsson U, Boresjö Brongre L, Rydin H and Ohlson M 2008 Near-zero recent carbon accumulation in a bog with high nitrogen deposition in SW Sweden *Glob. Change Biol.* **14** 2152–65
- [325] Scholefield P, Morton D, McShane G, Carrasco L, Whitfield M G, Rowland C, Rose R, Wood C, Tebbs E and Dodd B 2019 Estimating habitat extent and carbon loss from an eroded northern blanket bog using UAV derived imagery and topography *Prog. Phys. Geogr.: Earth Environ.* **43** 282–98
- [326] Borge A F, Westermann S, Solheim I and Eitzelmüller B 2017 Strong degradation of palsas and peat plateaus in northern Norway during the last 60 years *Cryosphere* **11** 1–16
- [327] Rieley J and Page S 2016 *Tropical peatland of the world Tropical Peatland Ecosystems* (Berlin: Springer) pp 3–32
- [328] Tan Z, Zhuang Q, Henze D K, Frankenberg C, Dlugokencky E, Sweeney C, Turner A J, Sasakawa M and Machida T 2016 Inverse modeling of pan-Arctic methane emissions at high spatial resolution: what can we learn from assimilating satellite retrievals and using different process-based wetland and lake biogeochemical models? *Atmos. Chem. Phys.* **16** 12649–66
- [329] Hugelius G, Kuhry P, Tarnocai C and Virtanen T 2010 Soil organic carbon pools in a periglacial landscape: a case study from the central Canadian Arctic *Permafrost. Periglac. Process.* **21** 16–29
- [330] Sheng Y, Smith L C, MacDonald G M, Kremenski K V, Frey K E, Velichko A A, Lee M, Beilman D W and Dubinin P 2004 A high-resolution GIS-based inventory of the west Siberian peat carbon pool *Glob. Biogeochem. Cycles* **18** GB3004
- [331] McPartland M Y, Falkowski M J, Reinhardt J R, Kane E S, Kolka R, Turetsky M R, Douglas T A, Anderson J, Edwards J D and Palik B 2019a Characterizing boreal peatland plant composition and species diversity with hyperspectral remote sensing *Remote Sens.* **11** 1685
- [332] McPartland M Y, Kane E S, Falkowski M J, Kolka R, Turetsky M R, Palik B and Montgomery R A 2019b The response of boreal peatland community composition and NDVI to hydrologic change, warming, and elevated carbon dioxide *Glob. Change Biol.* **25** 93–107
- [333] Potter C 2018 Recovery rates of wetland vegetation greenness in severely burned ecosystems of Alaska derived from satellite image analysis *Remote Sens.* **10** 1456
- [334] Van der Werf G R, Randerson J T, Giglio L, Collatz G J, Mu M, Kasibhatla P S, Morton D C, DeFries R S, Jin Y V and van Leeuwen T T 2010 Global fire emissions and the contribution of deforestation, savanna, forest, agricultural, and peat fires (1997–2009) *Atmos. Chem. Phys.* **10** 11707–35
- [335] Fokeeva E V, Safronov A N, Rakitin V S, Yurganov L N, Grechko E I and Shumskii R A 2011 Investigation of the 2010 July–August fires impact on carbon monoxide atmospheric pollution in Moscow and its outskirts, estimating of emissions *Izv. Atmos. Ocean. Phys.* **47** 682–98
- [336] Schuur E A, Bockheim J, Canadell J G, Euskirchen E, Field C B, Goryachkin S V, Hagemann S, Kuhry P, Lafleur P M and Lee H 2008 Vulnerability of permafrost carbon to climate change: implications for the global carbon cycle *Bioscience* **58** 701–14
- [337] Schuur E A, McGuire A D, Schädel C, Grosse G, Harden J W, Hayes D J, Hugelius G, Koven C D, Kuhry P and Lawrence D M 2015 Climate change and the permafrost carbon feedback *Nature* **520** 171–9
- [338] Gumbrecht T, Roman-Cuesta R M, Verchot L, Herold M, Wittmann F, Householder E, Herold N and Murdiyarso D 2017 An expert system model for mapping tropical wetlands and peatlands reveals South America as the largest contributor *Glob. Change Biol.* **23** 3581–99
- [339] Gruber S 2012 Derivation and analysis of a high-resolution estimate of global permafrost zonation *Cryosphere* **6** 221–33
- [340] Joosten H 2009 *The Global Peatland CO<sub>2</sub> Picture: Peatland Status and Drainage Related Emissions in All Countries of the World* Wetlands International



- [341] Gallego-Sala A V, Charman D J, Brewer S, Page S E, Prentice I C, Friedlingstein P, Moreton S, Amesbury M J, Beilman D W and Björck S 2018 Latitudinal limits to the predicted increase of the peatland carbon sink with warming *Nat. Clim. Change* **8** 907–13
- [342] Schaphoff S, Heyder U, Ostberg S, Gerten D, Heinke J and Lucht W 2013 Contribution of permafrost soils to the global carbon budget *Environ. Res. Lett.* **8** 014026
- [343] Page S E, Rieley J O and Banks C J 2011 Global and regional importance of the tropical peatland carbon pool *Glob. Change Biol.* **17** 798–818
- [344] Leifeld J, Wüst-Galley C and Page S 2019 Intact and managed peatland soils as a source and sink of GHGs from 1850 to 2100 *Nat. Clim. Change* **9** 945–7
- [345] Chasmer L, Lima E M, Mahoney C, Hopkinson C, Montgomery J and Cobbaert D 2021 Shrub changes with proximity to anthropogenic disturbance in boreal wetlands determined using bi-temporal airborne lidar in the Oil Sands Region, Alberta Canada *Sci. Total Environ.* **780** 146638
- [346] Chaudhary N, Westermann S, Lamba S, Shurpali N, Sannel A B K, Schurgers G, Miller P A and Smith B 2020 Modelling past and future peatland carbon dynamics across the pan-Arctic *Glob. Change Biol.* **26** 4119–33
- [347] Beamish A, Reynolds M K, Epstein H, Frost G V, Macander M J, Bergstedt H, Bartsch A, Kruse S, Miles V and Tanis C M 2020 Recent trends and remaining challenges for optical remote sensing of Arctic tundra vegetation: a review and outlook *Remote Sens. Environ.* **246** 111872
- [348] Kirkwood A, Roy-Léveillé P, Packalen M, McLaughlin J and Basiliko N 2019 Evolution of Palsas and Peat Plateaus in the Hudson Bay Lowlands: permafrost degradation and the production of greenhouse gases *Cold Regions Engineering 2019 American Society of Civil Engineers Quebec City, Quebec, Canada August, 18–22, 2019* pp 597–606
- [349] Korpela I, Haapanen R, Korrensalo A, Tuittila E S and Vesala T 2020 Fine-resolution mapping of microforms of a boreal bog using aerial images and waveform-recording LiDAR *Mires Peat* **26** 1–24
- [350] Jones M C, Grosse G, Jones B M and Walter Anthony K 2012 Peat accumulation in drained thermokarst lake basins in continuous, ice-rich permafrost, northern Seward Peninsula, Alaska *J. Geophys. Res. Biogeosci.* **117** G00M07
- [351] Sannel A and Kuhry P 2011 Warming-induced destabilization of peat plateau/thermokarst lake complexes *J. Geophys. Res. Biogeosci.* **116** G03035
- [352] Podest E, McDonald K C and Kimball J S 2014 Multisensor microwave sensitivity to freeze/thaw dynamics across a complex boreal landscape *IEEE Trans. Geosci. Remote Sens.* **52** 6818–28
- [353] Minsley B J, Abraham J D, Smith B D, Cannia J C, Voss C I, Jorgenson M T, Walvoord M A, Wylie B K, Anderson L and Ball L B 2012 Airborne electromagnetic imaging of discontinuous permafrost *Geophys. Res. Lett.* **39** L02503
- [354] Cooley S W, Smith L C, Ryan J C, Pitcher L H and Pavelsky T M 2019 Arctic-Boreal lake dynamics revealed using CubeSat imagery *Geophys. Res. Lett.* **46** 2111–20
- [355] Bourgeau-Chavez L L, Endres S, Powell R, Battaglia M J, Benscoter B, Turetsky M, Kasischke E S and Banda E 2017 Mapping boreal peatland ecosystem types from multitemporal radar and optical satellite imagery *Can. J. For. Res.* **47** 545–59
- [356] Watts J D, Kimball J S, Bartsch A and McDonald K C 2014 Surface water inundation in the boreal-Arctic: potential impacts on regional methane emissions *Environ. Res. Lett.* **9** 075001
- [357] Takeuchi W, Nakano T, Ochi S and Yasuoka Y 2002 Estimation of methane emission from West Siberian Lowland with sub-pixel land cover characterization *IEEE Int. Geoscience and Remote Sensing Symp. (IEEE)* p 2351
- [358] DeLancey E R, Kariyeva J, Bried J T and Hird J N 2019 Large-scale probabilistic identification of boreal peatlands using google earth engine, open-access satellite data, and machine learning *PLoS One* **14** e0218165
- [359] Warren R K, Pappas C, Helbig M, Chasmer L E, Berg A A, Baltzer J L, Quinton W L and Sonnentag O 2018 Minor contribution of overstorey transpiration to landscape evapotranspiration in boreal permafrost peatlands *Ecology* **11** e1975
- [360] Evangelou N, Kylling A, Eckhardt S, Myroniuk V, Stebel K, Paugam R, Zibtev S and Stohl A 2019 Open fires in Greenland in summer 2017: transport, deposition and radiative effects of BC, OC and BrC emissions *Atmos. Chem. Phys.* **19** 1393–411
- [361] Kasischke E S, Goetz S J, Kimball J S and Mack M M 2010 The arctic-boreal vulnerability experiment (ABoVE): a concise plan for a NASA-sponsored field campaign *Final Report on the VuRSAL/ABoVE Scoping Study*
- [362] Ballhorn U, Siebert F, Mason M and Limin S 2009 Derivation of burn scar depths and estimation of carbon emissions with LIDAR in Indonesian peatlands *Proc. Natl Acad. Sci.* **106** 21213–8
- [363] Shi Y, Sasai T and Yamaguchi Y 2014 Spatio-temporal evaluation of carbon emissions from biomass burning in Southeast Asia during the period 2001–2010 *Ecol. Model.* **272** 98–115
- [364] Dadap N C, Cobb A R, Hoyt A M, Harvey C F and Konings A G 2019 Satellite soil moisture observations predict burned area in Southeast Asian peatlands *Environ. Res. Lett.* **14** 094014
- [365] Kiely L, Spracklen D V, Wiedinmyer C, Conibear L, Reddington C L, Archer-Nicholls S, Lowe D, Arnold S R, Knote C and Khan M F 2019 New estimate of particulate emissions from Indonesian peat fires in 2015 *Atmos. Chem. Phys.* **19** 11105–21
- [366] Poulter B, Christensen N L Jr and Halpin P N 2006 Carbon emissions from a temperate peat fire and its relevance to interannual variability of trace atmospheric greenhouse gases *J. Geophys. Res. Atmos.* **111** D06301
- [367] Vetrina Y and Cochrane M A 2019 *Annual Burned Area from Landsat, Mawas, Central Kalimantan, Indonesia, 1997–2015* (<https://doi.org/10.3334/ORNLDAAC/1708>)
- [368] Andela N, Morton D C, Giglio L and Randerson J T 2019 *Global Fire Atlas with Characteristics of Individual Fires, 2003–2016* (<https://doi.org/10.3334/ORNLDAAC/1642>)
- [369] Nitze I, Grosse G, Jones B M, Romanovsky V E and Boike J 2018 Remote sensing quantifies widespread abundance of permafrost region disturbances across the Arctic and Subarctic *Nat. Commun.* **9** 1–11
- [370] Jones B M, Grosse G, Arp C D, Miller E, Liu L, Hayes D J and Larsen C F 2015 Recent Arctic tundra fire initiates widespread thermokarst development *Sci. Rep.* **5** 1–13
- [371] Abe T, Iwahana G, Efremov P V, Desyatkin A R, Kawamura T, Fedorov A, Zhegusov Y, Yanagiya K and Tadono T 2020 Surface displacement revealed by L-band InSAR analysis in the Mayya area, Central Yakutia, underlain by continuous permafrost *Earth Planets Space* **72** 1–16
- [372] Iwahana G, Uchida M, Liu L, Gong W, Meyer F J, Guritz R, Yamanokuchi T and Hinzman L 2016 InSAR detection and field evidence for thermokarst after a tundra wildfire, using ALOS-PALSAR *Remote Sens.* **8** 218
- [373] Michaelides R J, Schaefer K, Zebker H A, Parsekian A, Liu L, Chen J, Natali S, Ludwig S and Schaefer S R 2019 Inference of the impact of wildfire on permafrost and active layer thickness in a discontinuous permafrost region using the remotely sensed active layer thickness (ReSALT) algorithm *Environ. Res. Lett.* **14** 035007
- [374] French N H, Graham J, Whitman E and Bourgeau-Chavez L L 2020 Quantifying surface severity of the 2014 and 2015 fires in the Great Slave Lake area of Canada *Int. J. Wildland Fire* **29** 892–906
- [375] Turetsky M R, Abbott B W, Jones M C, Anthony K W, Olefeldt D, Schuur E A, Koven C, McGuire A D, Grosse G

- and Kuhry P 2019 Permafrost collapse is accelerating carbon release *Nature* **569** 32–34
- [376] Schaefer K, Elshorbany Y, Jafarov E, Schuster P F, Striegl R G, Wickland K P and Sunderland E M 2020 Potential impacts of mercury released from thawing permafrost *Nat. Commun.* **11** 1–6
- [377] Wieder R K, Vitt D H and Benscoter B W 2006 Peatlands and the boreal forest *Boreal Peatland Ecosystems* (Berlin: Springer) pp 1–8
- [378] Poulter B, Fluet-Chouinard E, Hugelius G, Koven C, Fatoyinbo L, Page S E, Rosentretre J A, Smart L S, Taillie P J and Thomas N 2021 A review of global wetland carbon stocks and management challenges *Wetland Carbon and Environmental Management* (Hoboken, NJ: John Wiley & Sons) pp 1–20
- [379] Lähteenoja O, Ruokolainen K, Schulman L and Oinonen M 2009 Amazonian peatlands: an ignored C sink and potential source *Glob. Change Biol.* **15** 2311–20
- [380] Chimner R A 2004 Soil respiration rates of tropical peatlands in Micronesia and Hawaii *Wetlands* **24** 51–56
- [381] Chimner R A and Karberg J M 2008 Long-term carbon accumulation in two tropical mountain peatlands, Andes Mountains, Ecuador *Mires Peat* **3** 1–10
- [382] Gibson C M, Chasmer L E, Thompson D K, Quinton W L, Flannigan M D and Olefeldt D 2018 Wildfire as a major driver of recent permafrost thaw in boreal peatlands *Nat. Commun.* **9** 1–9
- [383] Hugelius G, Strauss J, Zubrzycki S, Harden J W, Schuur E, Ping C, Schirmer L, Grosse G, Michaelson G J and Koven C D 2014 Estimated stocks of circumpolar permafrost carbon with quantified uncertainty ranges and identified data gaps *Biogeosciences* **11** 6573–93
- [384] Cole J J, Prairie Y T, Caraco N F, McDowell W H, Tranvik L J, Striegl R G, Duarte C M, Kortelainen P, Downing J A and Middelburg J J 2007 Plumbing the global carbon cycle: integrating inland waters into the terrestrial carbon budget *Ecosystems* **10** 172–85
- [385] Tranvik L J, Downing J A, Cotner J B, Loiselle S A, Striegl R G, Ballatore T J, Dillon P, Finlay K, Fortino K and Knoll L B 2009 Lakes and reservoirs as regulators of carbon cycling and climate *Limnol. Oceanogr.* **54** 2298–314
- [386] Williamson C E, Saros J E, Vincent W F and Smol J P 2009 Lakes and reservoirs as sentinels, integrators, and regulators of climate change *Limnol. Oceanogr.* **54** 2273–82
- [387] Buffam I, Turner M G, Desai A R, Hanson P C, Rusak J A, Lottig N R, Stanley E H and Carpenter S R 2011 Integrating aquatic and terrestrial components to construct a complete carbon budget for a north temperate lake district *Glob. Change Biol.* **17** 1193–211
- [388] Bennington V, McKinley G A, Urban N R and McDonald C P 2012 Can spatial heterogeneity explain the perceived imbalance in Lake Superior's carbon budget? A model study *J. Geophys. Res. Biogeosci.* **117** G03020
- [389] Lohila A, Tuovinen J, Hatakka J, Aurela M, Vuorenmaa J, Haakana M and Laurila T 2015 Carbon dioxide and energy fluxes over a northern boreal lake *Boreal Env. Res* **20** 474–88
- [390] Larsen S, Andersen T and Hessen D O 2011 Climate change predicted to cause severe increase of organic carbon in lakes *Glob. Change Biol.* **17** 1186–92
- [391] Moss B, Kosten S, Meerhoff M, Battarbee R W, Jeppesen E, Mazzeo N, Havens K, Lacerot G, Liu Z and De Meester L 2011 Allied attack: climate change and eutrophication *Inland Waters* **1** 101–5
- [392] Bergmann T, Fahnenstiel G, Lohrenz S, Millie D and Schofield O 2004 Impacts of a recurrent resuspension event and variable phytoplankton community composition on remote sensing reflectance *J. Geophys. Res. Oceans* **109** C10S15
- [393] Gons H J, Auer M T and Effler S W 2008 MERIS satellite chlorophyll mapping of oligotrophic and eutrophic waters in the Laurentian Great Lakes *Remote Sens. Environ.* **112** 4098–106
- [394] Lohrenz S E, Fahnenstiel G L, Schofield O and Millie D F 2008 Coastal sediment dynamics and river discharge as key factors influencing: coastal ecosystem productivity in Southeastern Lake Michigan *Oceanography* **21** 60–69
- [395] Hunter P D, Tyler A N, Carvalho L, Codd G A and Maberly S C 2010 Hyperspectral remote sensing of cyanobacterial pigments as indicators for cell populations and toxins in eutrophic lakes *Remote Sens. Environ.* **114** 2705–18
- [396] Shuchman R A, Sayers M, Fahnenstiel G L and Leshkevich G 2013 A model for determining satellite-derived primary productivity estimates for Lake Michigan *J. Great Lakes Res.* **39** 46–54
- [397] Fahnenstiel G L, Sayers M J, Shuchman R A, Yousef F and Pothoven S A 2016 Lake-wide phytoplankton production and abundance in the upper great lakes: 2010–2013 *J. Great Lakes Res.* **42** 619–29
- [398] Sayers M J, Grimm A G, Shuchman R A, Deines A M, Bunnell D B, Raymer Z B, Rogers M W, Woelmer W, Bennion D H and Brooks C N 2015 A new method to generate a high-resolution global distribution map of lake chlorophyll *Int. J. Remote Sens.* **36** 1942–64
- [399] Ho J C, Michalak A M and Pahlevan N 2019 Widespread global increase in intense lake phytoplankton blooms since the 1980s *Nature* **574** 667–70
- [400] Mouw C B, Greb S, Aurin D, DiGiacomo P M, Lee Z, Twardowski M, Binding C, Hu C, Ma R and Moore T 2015 Aquatic color radiometry remote sensing of coastal and inland waters: challenges and recommendations for future satellite missions *Remote Sens. Environ.* **160** 15–30
- [401] Werdell P J et al 2019 The Plankton, Aerosol, Cloud, ocean Ecosystem mission: status, science, advances *Bull. Am. Meteorol. Soc.* **100** 1775–94
- [402] Sayers M, Bosse K, Fahnenstiel G and Shuchman R 2020 Carbon fixation trends in eleven of the World's largest lakes: 2003–2018 *Water* **12** 3500
- [403] Sayers M J, Fahnenstiel G L, Shuchman R A and Bosse K R 2021 A new method to estimate global freshwater phytoplankton carbon fixation using satellite remote sensing: initial results *Int. J. Remote Sens.* **42** 3708–30
- [404] Verpoorter C, Kutser T, Seekell D A and Tranvik L J 2014 A global inventory of lakes based on high-resolution satellite imagery *Geophys. Res. Lett.* **41** 6396–402
- [405] Mendonça R, Müller R A, Clow D, Verpoorter C, Raymond P, Tranvik L J and Sobek S 2017 Organic carbon burial in global lakes and reservoirs *Nat. Commun.* **8** 1–7
- [406] Lewis W M Jr 2011 Global primary production of lakes: 19th Baldi Memorial Lecture *Inland Waters* **1** 1–28
- [407] Einsele G, Yan J and Hinderer M 2001 Atmospheric carbon burial in modern lake basins and its significance for the global carbon budget *Glob. Planet. Change* **30** 167–95
- [408] Bastviken D, Tranvik L J, Downing J A, Crill P M and Enrich-Prast A 2011 Freshwater methane emissions offset the continental carbon sink *Science* **331** 50
- [409] Warner D M and Lesht B M 2015 Relative importance of phosphorus, invasive mussels and climate for patterns in chlorophyll a and primary production in Lakes Michigan and Huron *Freshw. Biol.* **60** 1029–43
- [410] Kauer T, Kutser T, Arst H, Danckaert T and Nöges T 2015 Modelling primary production in shallow well mixed lakes based on MERIS satellite data *Remote Sens. Environ.* **163** 253–61
- [411] Soomets T, Kutser T, Wüest A and Bouffard D 2019 Spatial and temporal changes of primary production in a deep peri-alpine lake *Inland Waters* **9** 49–60
- [412] McDonald C P, Rover J A, Stets E G and Striegl R G 2012 The regional abundance and size distribution of lakes and reservoirs in the United States and implications for estimates of global lake extent *Limnol. Oceanogr.* **57** 597–606
- [413] Kuhn C, Bogard M, Johnston S E, John A, Vermote E, Spencer R, Dornblaser M, Wickland K, Striegl R and Butman D 2020 Satellite and airborne remote sensing of

- gross primary productivity in boreal Alaskan lakes *Environ. Res. Lett.* **15** 105001
- [414] Bogard M J, Kuhn C D, Johnston S E, Striegl R G, Holtgrieve G W, Dornblaser M M, Spencer R G, Wickland K P and Butman D E 2019 Negligible cycling of terrestrial carbon in many lakes of the arid circumpolar landscape *Nat. Geosci.* **12** 180–5
- [415] Kuhn C and Butman D 2021 Declining greenness in Arctic-boreal lakes *Proc. Natl Acad. Sci.* **118** e2021219118
- [416] Rey D M, Walvoord M, Minsley B, Rover J and Singha K 2019 Investigating lake-area dynamics across a permafrost-thaw spectrum using airborne electromagnetic surveys and remote sensing time-series data in Yukon Flats, Alaska *Environ. Res. Lett.* **14** 025001
- [417] Palmer S C, Kutser T and Hunter P D 2015 Remote sensing of inland waters: challenges, progress and future directions *Remote Sens. Environ.* **157** 1–8
- [418] Mishra D R, Ogashawara I and Gitelson A A 2017 *Bio-optical Modeling and Remote Sensing of Inland Waters* (Amsterdam: Elsevier)
- [419] Tyler A N, Hunter P D, Spyarakos E, Neil C, Simis S, Groom S, Merchant C J, Miller C A, O'Donnell R and Scott E M 2017 A global observatory of lake water quality *EGU General Assembly Conf. Abstracts* p 10609
- [420] Zhu W, Yu Q, Tian Y Q, Becker B L, Zheng T and Carrick H J 2014 An assessment of remote sensing algorithms for colored dissolved organic matter in complex freshwater environments *Remote Sens. Environ.* **140** 766–78
- [421] Li J, Yu Q, Tian Y Q, Becker B L, Siqueira P and Torbick N 2018 Spatio-temporal variations of CDOM in shallow inland waters from a semi-analytical inversion of Landsat-8 *Remote Sens. Environ.* **218** 189–200
- [422] Brezonik P L, Olmanson L G, Finlay J C and Bauer M E 2015 Factors affecting the measurement of CDOM by remote sensing of optically complex inland waters *Remote Sens. Environ.* **157** 199–215
- [423] Kutser T, Casal Pascual G, Barbosa C, Paavel B, Ferreira R, Carvalho L and Toming K 2016 Mapping inland water carbon content with Landsat 8 data *Int. J. Remote Sens.* **37** 2950–61
- [424] Lohrenz S E, Cai W, Chakraborty S, Huang W, Guo X, He R, Xue Z, Fennel K, Howden S and Tian H 2018 Satellite estimation of coastal  $p\text{CO}_2$  and air-sea flux of carbon dioxide in the northern Gulf of Mexico *Remote Sens. Environ.* **207** 71–83
- [425] Ouyang Z, Shao C, Chu H, Becker R, Bridgeman T, Stepien C A, John R and Chen J 2017 The effect of algal blooms on carbon emissions in western Lake Erie: an integration of remote sensing and eddy covariance measurements *Remote Sens.* **9** 44
- [426] Kutser T, Verpoorter C, Paavel B and Tranvik L J 2015 Estimating lake carbon fractions from remote sensing data *Remote Sens. Environ.* **157** 138–46
- [427] Battin T J, Luysaert S, Kaplan L A, Aufdenkampe A K, Richter A and Tranvik L J 2009 The boundless carbon cycle *Nat. Geosci.* **2** 598–600
- [428] Aufdenkampe A K, Mayorga E, Raymond P A, Melack J M, Doney S C, Alin S R, Aalto R E and Yoo K 2011 Riverine coupling of biogeochemical cycles between land, oceans, and atmosphere *Front. Ecol. Environ.* **9** 53–60
- [429] Wehrli B 2013 Conduits of the carbon cycle *Nature* **503** 346–7
- [430] Raymond P A, Hartmann J, Lauerwald R, Sobek S, McDonald C, Hoover M, Butman D, Striegl R, Mayorga E and Humborg C 2013 Global carbon dioxide emissions from inland waters *Nature* **503** 355–9
- [431] Sawakuchi H O et al 2017 Carbon dioxide emissions along the lower Amazon River *Front. Mar. Sci.* **4** 76
- [432] Tranvik L J, Cole J J and Prairie Y T 2018 The study of carbon in inland waters—from isolated ecosystems to players in the global carbon cycle *Limnol. Oceanogr. Lett.* **3** 41–48
- [433] Drake T W, Raymond P A and Spencer R G 2018 Terrestrial carbon inputs to inland waters: a current synthesis of estimates and uncertainty *Limnol. Oceanogr. Lett.* **3** 132–42
- [434] Vachon D, Sponseller R A and Karlsson J 2021 Integrating carbon emission, accumulation and transport in inland waters to understand their role in the global carbon cycle *Glob. Change Biol.* **27** 719–27
- [435] USGCRP 2018 *Second State of the Carbon Cycle Report (SOCCR2): A Sustained Assessment Report* ed N Cavallaro, G Shrestha, R Birdsey, M A Mayes, R G Najjar, S C Reed, P Romero-Lankao and Z Zhu (Washington, DC: U.S. Global Change Research Program) (available at: <https://carbon2018.globalchange.gov/>)
- [436] Stets E G and Striegl R G 2012 Carbon export by rivers draining the conterminous United States *Inland Waters* **2** 177–84
- [437] Meybeck M 1982 Carbon, nitrogen, and phosphorus transport by world rivers *Am. J. Sci.* **282** 401–50
- [438] Meybeck M and Ragu A 2012 *GEMS-GLORI World River Discharge Database* (Paris: Laboratoire de Géologie Appliquée, Université Pierre et Marie Curie)
- [439] Li M, Peng C, Wang M, Xue W, Zhang K, Wang K, Shi G and Zhu Q 2017 The carbon flux of global rivers: a re-evaluation of amount and spatial patterns *Ecol. Indic.* **80** 40–51
- [440] Karaska M A, Huguenin R L, Beacham J L, Wang M, Jensen J R and Kaufmann R S 2004 AVIRIS measurements of chlorophyll, suspended minerals, dissolved organic carbon, and turbidity in the Neuse River, North Carolina *Photogramm. Eng. Remote Sens.* **70** 125–33
- [441] Herrault P, Gandois L, Gascoïn S, Tananaev N, Le Dantec T and Teisserenc R 2016 Using high spatio-temporal optical remote sensing to monitor dissolved organic carbon in the Arctic river Yenisei *Remote Sens.* **8** 803
- [442] Chen J, Zhu W, Tian Y Q and Yu Q 2020 Monitoring dissolved organic carbon by combining Landsat-8 and Sentinel-2 satellites: case study in Saginaw River estuary, Lake Huron *Sci. Total Environ.* **718** 137374
- [443] Liu B, D'Sa E J and Joshi I 2019a Multi-decadal trends and influences on dissolved organic carbon distribution in the Barataria Basin, Louisiana from *in-situ* and Landsat/MODIS observations *Remote Sens. Environ.* **228** 183–202
- [444] Liu D, Pan D, Bai Y, He X, Wang D, Wei J and Zhang L 2015 Remote sensing observation of particulate organic carbon in the Pearl River Estuary *Remote Sens.* **7** 8683–704
- [445] Del Castillo C E and Miller R L 2008 On the use of ocean color remote sensing to measure the transport of dissolved organic carbon by the Mississippi River Plume *Remote Sens. Environ.* **112** 836–44
- [446] Olmanson L G, Brezonik P L, Finlay J C and Bauer M E 2016 Comparison of Landsat 8 and Landsat 7 for regional measurements of CDOM and water clarity in lakes *Remote Sens. Environ.* **185** 119–28
- [447] Massicotte P, Asmala E, Stedmon C and Markager S 2017 Global distribution of dissolved organic matter along the aquatic continuum: across rivers, lakes and oceans *Sci. Total Environ.* **609** 180–91
- [448] ChunHock S, Cherukuru N, Mujahid A, Martin P, Sanwani N, Warneke T, Rixen T, Notholt J and Müller M 2020 A new remote sensing method to estimate river to ocean DOC flux in Peatland dominated Sarawak Coastal Regions, Borneo *Remote Sens.* **12** 3380
- [449] Liu D, Bai Y, He X, Pan D, Chen C A, Li T, Xu Y, Gong C and Zhang L 2019 Satellite-derived particulate organic carbon flux in the Changjiang River through different stages of the Three Gorges Dam *Remote Sens. Environ.* **223** 154–65
- [450] Griffin C G, Frey K E, Rogan J and Holmes R M 2011 Spatial and interannual variability of dissolved organic matter in the Kolyma River, East Siberia, observed using satellite imagery *J. Geophys. Res. Biogeosci.* **116** G03018



- [451] Larson M D, Simic Milas A, Vincent R K and Evans J E 2018 Multi-depth suspended sediment estimation using high-resolution remote-sensing UAV in Maumee River, Ohio *Int. J. Remote Sens.* **39** 5472–89
- [452] Su J, Dai M, He B, Wang L, Gan J, Guo X, Zhao H and Yu F 2017 Tracing the origin of the oxygen-consuming organic matter in the hypoxic zone in a large eutrophic estuary: the lower reach of the Pearl River Estuary, China *Biogeosciences* **14** 4085–99
- [453] Richey J E, Melack J M, Aufdenkampe A K, Ballester V M and Hess L L 2002 Outgassing from Amazonian rivers and wetlands as a large tropical source of atmospheric CO<sub>2</sub> *Nature* **416** 617–20
- [454] Johnson M S, Lehmann J, Riha S J, Krusche A V, Richey J E, Ometto J P H and Couto E G 2008 CO<sub>2</sub> efflux from Amazonian headwater streams represents a significant fate for deep soil respiration *Geophys. Res. Lett.* **35** L17401
- [455] Maria de Fátima F L, Ballester M V R, Krusche A V, Salimon C, Montebelo L A, Alin S R, Victoria R L and Richey J E 2008 Estimating the surface area of small rivers in the southwestern Amazon and their role in CO<sub>2</sub> outgassing *Earth Interact.* **12** 1–16
- [456] Maria de Fátima F L, Krusche A V, Richey J E, Ballester M V and Victória R L 2013 Spatial and temporal variability of pCO<sub>2</sub> and CO<sub>2</sub> efflux in seven Amazonian Rivers *Biogeochemistry* **116** 241–59
- [457] Butman D and Raymond P A 2011 Significant efflux of carbon dioxide from streams and rivers in the United States *Nat. Geosci.* **4** 839–42
- [458] Buto S G and Anderson R D 2020 NHDPlus high resolution (NHDPlus HR)—a hydrography framework for the Nation (No. 2020–3033) *US Geological Survey*
- [459] Cole J J and Caraco N F 2001 Carbon in catchments: connecting terrestrial carbon losses with aquatic metabolism *Mar. Freshw. Res.* **52** 101–10
- [460] Battin T J, Kaplan L A, Findlay S, Hopkinson C S, Marti E, Packman A I, Newbold J D and Sabater F 2008 Biophysical controls on organic carbon fluxes in fluvial networks *Nat. Geosci.* **1** 95–100
- [461] Schiller D V, Marcé R, Obrador B, Gómez-Gener L, Casas-Ruiz J P, Acuña V and Koschorreck M 2014 Carbon dioxide emissions from dry watercourses *Inland Waters* **4** 377–82
- [462] Marcé R, Obrador B, Gómez-Gener L, Catalán N, Koschorreck M, Arce M I, Singer G and von Schiller D 2019 Emissions from dry inland waters are a blind spot in the global carbon cycle *Earth Sci. Rev.* **188** 240–8
- [463] Keller P S, Catalán N, von Schiller D, Grossart H, Koschorreck M, Obrador B, Frassl M A, Karakaya N, Barros N and Howitt J A 2020 Global CO<sub>2</sub> emissions from dry inland waters share common drivers across ecosystems *Nat. Commun.* **11** 1–8
- [464] Downing J and Duarte C M 2009 Lakes (formation, diversity, distribution): abundance and size distribution of lakes, ponds and impoundments *Encyclopedia of Inland Waters* (Amsterdam: Elsevier) editor-in-chief: GE Likens pp 469–78
- [465] USGS 2021 U.S. geological survey national elevation dataset (NED) (available at: [www.sciencebase.gov/catalog/item/4f4e48b1e4b07f02db530759](http://www.sciencebase.gov/catalog/item/4f4e48b1e4b07f02db530759)) (Accessed 22 March 2021)
- [466] Lang M, McDonough O, McCarty G, Oesterling R and Wilen B 2012 Enhanced detection of wetland-stream connectivity using LiDAR *Wetlands* **32** 461–73
- [467] Priestnall G and Aplin P 2006 Cover: spatial and temporal remote sensing requirements for river monitoring *Int. J. Remote Sens.* **27** 2111–20
- [468] Langat P K, Kumar L and Koech R 2019 Monitoring river channel dynamics using remote sensing and GIS techniques *Geomorphology* **325** 92–102
- [469] Legleiter C J and Harrison L R 2019 Remote sensing of river bathymetry: evaluating a range of sensors, platforms, and algorithms on the upper Sacramento River, California, USA *Water Resour. Res.* **55** 2142–69
- [470] Bizzi S, Demarchi L, Grabowski R C, Weissteiner C J and Van de Bund W 2016 The use of remote sensing to characterise hydromorphological properties of European rivers *Aquat. Sci.* **78** 57–70
- [471] Tomsett C and Leyland J 2019 Remote sensing of river corridors: a review of current trends and future directions *River Res. Appl.* **35** 779–803
- [472] Gleason C, Garambois P and Durand M 2017 Tracking river flows from space *EOS Earth and Space Science News* vol 98
- [473] Frasson R, Durand M, Callahan P, Turk J, Pottier C, Biancamaria S, Williams B and Wei R 2018 River vector product status *3rd Science Team Meeting* (Montreal: SWOT)
- [474] Stuurman C and Pottier C 2020 Level 2 KaRIn high rate river single pass vector product surface water and ocean topography (SWOT) project, SWOT product description (California Institute of Technology) (available at: [https://podaac-tools.jpl.nasa.gov/drive/files/misc/web/misc/swot\\_mission\\_docs/pdd/D-56413\\_SWOT\\_Product\\_Description\\_L2\\_HR\\_RiverSP\\_20200825a.pdf](https://podaac-tools.jpl.nasa.gov/drive/files/misc/web/misc/swot_mission_docs/pdd/D-56413_SWOT_Product_Description_L2_HR_RiverSP_20200825a.pdf))
- [475] Stallard R F 1998 Terrestrial sedimentation and the carbon cycle: coupling weathering and erosion to carbon burial *Glob. Biogeochem. Cycles* **12** 231–57
- [476] Qi J, Du X, Zhang X, Lee S, Wu Y, Deng J, Moglen G E, Sadeghi A M and McCarty G W 2020a Modeling riverine dissolved and particulate organic carbon fluxes from two small watersheds in the northeastern United States *Environ. Model. Softw.* **124** 104601
- [477] Qi J, Zhang X, Lee S, Wu Y, Moglen G E and McCarty G W 2020b Modeling sediment diagenesis processes on riverbed to better quantify aquatic carbon fluxes and stocks in a small watershed of the Mid-Atlantic region *Carbon Balance Manage.* **15** 1–14
- [478] Allen G H and Pavelsky T M 2018 Global extent of rivers and streams *Science* **361** 585–8
- [479] Rödenbeck C, Bakker D C, Gruber N, Iida Y, Jacobson A R, Jones S, Landschützer P, Metz N, Nakaoka S and Olsen A 2015 Data-based estimates of the ocean carbon sink variability—first results of the surface ocean pCO<sub>2</sub> mapping intercomparison (SOCOM) *Biogeosciences* **12** 7251–78
- [480] Buitenhuis E T, Hashioka T and Quéré C L 2013 Combined constraints on global ocean primary production using observations and models *Glob. Biogeochem. Cycles* **27** 847–58
- [481] Ott L E, Pawson S, Collatz G J, Gregg W W, Menemenlis D, Brix H, Rousseaux C S, Bowman K W, Liu J and Eldering A 2015 Assessing the magnitude of CO<sub>2</sub> flux uncertainty in atmospheric CO<sub>2</sub> records using products from NASA's carbon monitoring flux pilot project *J. Geophys. Res. Atmos.* **120** 734–65
- [482] Berthet S, Séférian R, Bricaud C, Chevallier M, Voldoire A and Ethé C 2019 Evaluation of an online grid-coarsening algorithm in a global eddy-admitting ocean biogeochemical model *J. Adv. Model. Earth Syst.* **11** 1759–83
- [483] Fay A R and McKinley G A 2014 Global open-ocean biomes: mean and temporal variability *Earth Syst. Sci. Data* **6** 273–84
- [484] DeVries T, Le Quéré C, Andrews O, Berthet S, Hauck J, Ilyina T, Landschützer P, Lenton A, Lima I D and Nowicki M 2019 Decadal trends in the ocean carbon sink *Proc. Natl Acad. Sci.* **116** 11646–51
- [485] McKinley G A, Pilcher D J, Fay A R, Lindsay K, Long M C and Lovenduski N S 2016 Timescales for detection of trends in the ocean carbon sink *Nature* **530** 469–72
- [486] Liao E, Resplandy L, Liu J and Bowman K W 2020 Amplification of the ocean carbon sink during El Niños: role of Poleward Ekman transport and influence on atmospheric CO<sub>2</sub> *Glob. Biogeochem. Cycles* **34** e2020GB006574

- [487] Rödenbeck C, Keeling R F, Bakker D C, Metz N, Olsen A, Sabine C and Heimann M 2013 Global surface-ocean pCO<sub>2</sub> and sea-air CO<sub>2</sub> flux variability from an observation-driven ocean mixed-layer scheme *Ocean Sci.* **9** 193–216
- [488] Landschützer P, Gruber N, Bakker D C E and Schuster U 2014 Recent variability of the global ocean carbon sink *Glob. Biogeochem. Cycles* **28** 927–49
- [489] Landschützer P, Gruber N and Bakker D C E 2016 Decadal variations and trends of the global ocean carbon sink *Glob. Biogeochem. Cycles* **30** 1396–417
- [490] Watson A J, Schuster U, Shutler J D, Holding T, Ashton I G, Landschützer P, Woolf D K and Goddijn-Murphy L 2020 Revised estimates of ocean-atmosphere CO<sub>2</sub> flux are consistent with ocean carbon inventory *Nat. Commun.* **11** 1–6
- [491] Gruber N et al 2019 The oceanic sink for anthropogenic CO<sub>2</sub> from 1994 to 2007 *Science* **363** 1193
- [492] Wang J S, Kawa S R, Collatz G J, Sasakawa M, Gatti L V, Machida T, Liu Y and Manyin M E 2018 A global synthesis inversion analysis of recent variability in CO<sub>2</sub> fluxes using GOSAT and *in situ* observations *Atmos. Chem. Phys.* **18** 11097–124
- [493] Waga H, Hirawake T, Fujiwara A, Grebmeier J M and Saitoh S 2019 Impact of spatiotemporal variability in phytoplankton size structure on benthic macrofaunal distribution in the Pacific Arctic *Deep Sea Res. II: Top. Stud. Oceanogr.* **162** 114–26
- [494] Corliss B H, Brown C W, Sun X and Showers W J 2009 Deep-sea benthic diversity linked to seasonality of pelagic productivity *Deep Sea Res. I: Oceanogr. Res. Pap.* **56** 835–41
- [495] Biggs D C, Hu C and Müller-Karger F E 2008 Remotely sensed sea-surface chlorophyll and POC flux at Deep Gulf of Mexico Benthos sampling stations *Deep Sea Res. II: Top. Stud. Oceanogr.* **55** 2555–62
- [496] Dierssen H M, Zimmerman R C, Drake L A and Burdige D J 2009 Potential export of unattached benthic macroalgae to the deep sea through wind-driven Langmuir circulation *Geophys. Res. Lett.* **36** L04602
- [497] Field C B, Behrenfeld M J, Randerson J T and Falkowski P 1998 Primary production of the biosphere: integrating terrestrial and oceanic components *Science* **281** 237–40
- [498] Boyd P W, Claustre H, Levy M, Siegel D A and Weber T 2019 Multi-faceted particle pumps drive carbon sequestration in the ocean *Nature* **568** 327–35
- [499] Bopp L, Monfray P, Aumont O, Dufresne J, Le Treut H, Madec G, Terray L and Orr J C 2001 Potential impact of climate change on marine export production *Glob. Biogeochem. Cycles* **15** 81–99
- [500] Eppley R W and Peterson B J 1979 Particulate organic matter flux and planktonic new production in the deep ocean *Nature* **282** 677–80
- [501] Eppley R W and Renger E H 1988 Nanomolar increase in surface layer nitrate concentration following a small wind event *Deep Sea Res. A* **35** 1119–25
- [502] Carr M, Friedrichs M A, Schmeltz M, Aita M N, Antoine D, Arrigo K R, Asanuma I, Aumont O, Barber R and Behrenfeld M 2006 A comparison of global estimates of marine primary production from ocean color *Deep Sea Res. II* **53** 741–70
- [503] Regaudie-de-gioux A, Huete-Ortega M, Sobrino C, López-Sandoval D C, González N, Fernández-Carrera A, Vidal M, Marañón E, Cermeño P and Latasa M 2019 Multi-model remote sensing assessment of primary production in the subtropical gyres *J. Mar. Syst.* **196** 97–106
- [504] Saba V S, Friedrichs M A, Antoine D, Armstrong R A, Asanuma I, Behrenfeld M J, Ciotti A M, Dowell M, Hoepffner N and Hyde K 2011 An evaluation of ocean color model estimates of marine primary productivity in coastal and pelagic regions across the globe *Biogeosciences* **8** 489–503
- [505] Silsbe G M, Behrenfeld M J, Halsey K H, Milligan A J and Westberry T K 2016 The CAFE model: a net production model for global ocean phytoplankton *Glob. Biogeochem. Cycles* **30** 1756–77
- [506] Boyd P W and Trull T W 2007 Understanding the export of biogenic particles in oceanic waters: is there consensus? *Prog. Oceanogr.* **72** 276–312
- [507] Henson S A, Sanders R, Madsen E, Morris P J, Le Moigne F and Quartly G D 2011 A reduced estimate of the strength of the ocean's biological carbon pump *Geophys. Res. Lett.* **38** L04606
- [508] Siegel D A, Buesseler K O, Doney S C, Saille S F, Behrenfeld M J and Boyd P W 2014 Global assessment of ocean carbon export by combining satellite observations and food-web models *Glob. Biogeochem. Cycles* **28** 181–96
- [509] Eppley R W, Stewart E, Abbott M R and Heyman U 1985 Estimating ocean primary production from satellite chlorophyll. Introduction to regional differences and statistics for the Southern California Bight *J. Plankton Res.* **7** 57–70
- [510] Behrenfeld M J and Falkowski P G 1997 A consumer's guide to phytoplankton primary productivity models *Limnol. Oceanogr.* **42** 1479–91
- [511] Platt T, Sathyendranath S and Ravindran P 1990 Primary production by phytoplankton: analytic solutions for daily rates per unit area of water surface *Proc. R. Soc. B* **241** 101–11
- [512] Lee Y J et al 2015 An assessment of phytoplankton primary productivity in the Arctic Ocean from satellite ocean color/*in situ* chlorophyll-a based models *J. Geophys. Res. Oceans* **120** 6508–41
- [513] Arrigo K R, Robinson D H, Worthen D L, Schieber B and Lizotte M P 1998 Bio-optical properties of the southwestern Ross Sea *J. Geophys. Res. Oceans* **103** 21683–95
- [514] Arrigo K R, van Dijken G L and Bushinsky S 2008 Primary production in the Southern Ocean, 1997–2006 *J. Geophys. Res. Oceans* **113** C08004
- [515] Behrenfeld M J and Falkowski P G 1997 Photosynthetic rates derived from satellite-based chlorophyll concentration *Limnol. Oceanogr.* **42** 1–20
- [516] Campbell J, Antoine D, Armstrong R, Arrigo K, Balch W, Barber R, Behrenfeld M, Bidigare R, Bishop J and Carr M 2002 Comparison of algorithms for estimating ocean primary production from surface chlorophyll, temperature, and irradiance *Glob. Biogeochem. Cycles* **16** 9–15
- [517] Longhurst A, Sathyendranath S, Platt T and Caverhill C 1995 An estimate of global primary production in the ocean from satellite radiometer data *J. Plankton Res.* **17** 1245–71
- [518] Platt T and Sathyendranath S 1988 Oceanic primary production: estimation by remote sensing at local and regional scales *Science* **241** 1613–20
- [519] Ryther J H and Yentsch C S 1957 The estimation of phytoplankton production in the ocean from chlorophyll and light data 1 *Limnol. Oceanogr.* **2** 281–6
- [520] Behrenfeld M J, Boss E, Siegel D A and Shea D M 2005 Carbon-based ocean productivity and phytoplankton physiology from space *Glob. Biogeochem. Cycles* **19** GB1006
- [521] Stramski D, Boss E, Bogucki D and Voss K J 2004 The role of seawater constituents in light backscattering in the ocean *Prog. Oceanogr.* **61** 27–56
- [522] Stramski D, Reynolds R A, Babin M, Kaczmarek S, Lewis M R, Röttgers R, Sciandra A, Stramska M, Twardowski M S and Franz B A 2008 Relationships between the surface concentration of particulate organic carbon and optical properties in the eastern South Pacific and eastern Atlantic Oceans *Biogeosciences* **5** 171–201
- [523] Zhang X, Lewis M and Johnson B 1998 Influence of bubbles on scattering of light in the ocean *Appl. Opt.* **37** 6525–36
- [524] Morel A and Bricaud A 1981 Theoretical results concerning light absorption in a discrete medium, and application to specific absorption of phytoplankton *Deep Sea Res. A* **28** 1375–93



- [525] Antoine D and Morel A 1996 Oceanic primary production: 1. Adaptation of a spectral light-photosynthesis model in view of application to satellite chlorophyll observations *Glob. Biogeochem. Cycles* **10** 43–55
- [526] Hirawake T, Takao S, Horimoto N, Ishimaru T, Yamaguchi Y and Fukuchi M 2011 A phytoplankton absorption-based primary productivity model for remote sensing in the Southern Ocean *Polar Biol.* **34** 291–302
- [527] Kiefer D A and Mitchell B G 1983 A Simple, Steady-State Description of Phytoplankton Growth Based on Absorption Cross-Section and Quantum Efficiency *Limnol. Oceanogr.* **28** 770–6
- [528] Lee Z P, Carder K L, Peacock T G, Davis C O and Mueller J L 1996 Method to derive ocean absorption coefficients from remote-sensing reflectance *Appl. Opt.* **35** 453–62
- [529] Ma S, Tao Z, Yang X, Yu Y, Zhou X, Ma W and Li Z 2014 Estimation of marine primary productivity from satellite-derived phytoplankton absorption data *IEEE J. Sel. Top. Appl. Earth Obs. Remote Sens.* **7** 3084–92
- [530] Marra J 1993 Proportionality between *in situ* carbon assimilation and bio-optical measures of primary production in the Gulf of Maine in summer *Limnol. Oceanogr.* **38** 232–8
- [531] Marra J, Ho C and Trees C 2003 An alternative algorithm for the calculation of primary productivity from remote sensing data *Lamont Doherty Earth Observatory Technical Report (LDEO-2003-1)*
- [532] Smyth T J, Tilstone G H and Groom S B 2005 Integration of radiative transfer into satellite models of ocean primary production *J. Geophys. Res. Oceans* **110** C10014
- [533] Zoffoli M L, Lee Z and Marra J F 2018 Regionalization and dynamic parameterization of quantum yield of photosynthesis to improve the ocean primary production estimates from remote sensing *Front. Mar. Sci.* **5** 446
- [534] Marra J, Trees C C, Bidigare R R and Barber R T 2000 Pigment absorption and quantum yields in the Arabian Sea *Deep Sea Res. II* **47** 1279–99
- [535] Ostrowska M, Woźniak B and Dera J 2012 Modelled quantum yields and energy efficiency of fluorescence, photosynthesis and heat production by phytoplankton in the World Ocean *Oceanologia* **54** 565–610
- [536] Sorensen J C and Siegel D A 2001 Variability of the effective quantum yield for carbon assimilation in the Sargasso Sea *Deep Sea Res. II* **48** 2005–35
- [537] Iluz D and Dubinsky Z 2013 Quantum yields in aquatic photosynthesis *Photosynthesis* (Rijeka: Intech) pp 135–58
- [538] DeVries T and Weber T 2017 The export and fate of organic matter in the ocean: new constraints from combining satellite and oceanographic tracer observations *Glob. Biogeochem. Cycles* **31** 535–55
- [539] Arteaga L, Haëntjens N, Boss E, Johnson K S and Sarmiento J L 2018 Assessment of export efficiency equations in the southern ocean applied to satellite-based net primary production *J. Geophys. Res. Oceans* **123** 2945–64
- [540] Goes J I, Do R Gomes H, Limsakul A, Balch W M and Saino T 2001 El Niño related interannual variations in biological production in the North Pacific as evidenced by satellite and ship data *Prog. Oceanogr.* **49** 211–25
- [541] Goes J I, Saino T, Oaku H, Ishizaka J, Wong C S and Nojiri Y 2000 Basin scale estimates of sea surface nitrate and new production from remotely sensed sea surface temperature and chlorophyll *Geophys. Res. Lett.* **27** 1263–6
- [542] Siegel D A, Buesseler K O, Behrenfeld M J, Benitez-Nelson C R, Boss E, Brzezinski M A, Burd A, Carlson C A, D'Asaro E A and Doney S C 2016 Prediction of the export and fate of global ocean net primary production: the EXPORTS science plan *Front. Mar. Sci.* **3** 22
- [543] Matsuoka A, Hooker S B, Bricaud A, Gentili B and Babin M 2013 Estimating absorption coefficients of colored dissolved organic matter (CDOM) using a semi-analytical algorithm for southern Beaufort Sea waters: application to deriving concentrations of dissolved organic carbon from space *Biogeosciences* **10** 917–27
- [544] Le C, Zhou X, Hu C, Lee Z, Li L and Stramski D 2018 A color-index-based empirical algorithm for determining particulate organic carbon concentration in the ocean from satellite observations *J. Geophys. Res. Oceans* **123** 7407–19
- [545] Balch W M, Gordon H R, Bowler B C, Drapeau D T and Booth E S 2005 Calcium carbonate measurements in the surface global ocean based on moderate-resolution imaging spectroradiometer data *J. Geophys. Res. Oceans* **110** C07001
- [546] Mitchell C, Hu C, Bowler B, Drapeau D and Balch W M 2017 Estimating particulate inorganic carbon concentrations of the global ocean from ocean color measurements using a reflectance difference approach *J. Geophys. Res. Oceans* **122** 8707–20
- [547] Evers-King H, Martinez-Vicente V, Brewin R J, Dall'Olmo G, Hickman A E, Jackson T, Kostadinov T S, Krasemann H, Loisel H and Röttgers R 2017 Validation and intercomparison of ocean color algorithms for estimating particulate organic carbon in the oceans *Front. Mar. Sci.* **4** 251
- [548] Behrenfeld M J, Hu Y, Hostetler C A, Dall'Olmo G, Rodier S D, Hair J W and Trepte C R 2013 Space-based lidar measurements of global ocean carbon stocks *Geophys. Res. Lett.* **40** 4355–60
- [549] Balch W M, Bowler B C, Drapeau D T, Lubelczyk L C and Lyczkowski E 2018 Vertical distributions of coccolithophores, PIC, POC, biogenic Silica, and chlorophyll a throughout the global ocean *Glob. Biogeochem. Cycles* **32** 2–17
- [550] Hedges J I and Keil R G 1995 Sedimentary organic matter preservation: an assessment and speculative synthesis *Mar. Chem.* **49** 81–115
- [551] Dunne J, Sarmiento J and Gnanadesikan A 2007 A synthesis of global particle export from the surface ocean and cycling *Glob. Biogeochem. Cycles* **21** GB4006
- [552] DeVries B, Huang C, Lang M W, Jones J W, Huang W, Creed I F and Carroll M L 2017 Automated quantification of surface water inundation in wetlands using optical satellite imagery *Remote Sens.* **9** 807
- [553] Moore J K, Doney S C, Glover D M and Fung I Y 2002 Iron cycling and nutrient-limitation patterns in surface waters of the World Ocean *Deep Sea Res. II* **49** 463–507
- [554] Muller-Karger F E, Varela R, Thunell R, Luerssen R, Hu C and Walsh J J 2005 The importance of continental margins in the global carbon cycle *Geophys. Res. Lett.* **32** L01602
- [555] Jahnke R A 2010 *Global synthesis Carbon and Nutrient Fluxes in Continental Margins* ed K K Liu, L Atkinson, R Quinones and L Talaue-mcmanus (Berlin: Springer) pp 597–615
- [556] Cai W 2011 Estuarine and coastal ocean carbon paradox: CO<sub>2</sub> sinks or sites of terrestrial carbon incineration? *Annu. Rev. Mar. Sci.* **3** 123–45
- [557] Bourgeois T, Orr J C, Resplandy L, Terhaar J, Ethé C, Gehlen M and Bopp L 2016 Coastal-ocean uptake of anthropogenic carbon *Biogeosciences* **13** 4167–85
- [558] Gattuso J, Frankignoulle M and Wollast R 1998 Carbon and carbonate metabolism in coastal aquatic ecosystems *Annu. Rev. Ecol. Syst.* **29** 405–34
- [559] Hopkins J and Balch W M 2018 A new approach to estimating coccolithophore calcification rates from space *J. Geophys. Res. Biogeosci.* **123** 1447–59
- [560] Gordon H R, Boynton G C, Balch W M, Groom S B, Harbour D S and Smyth T J 2001 Retrieval of coccolithophore calcite concentration from SeaWiFS imagery *Geophys. Res. Lett.* **28** 1587–90
- [561] Benway H M et al 2016 A science plan for carbon cycle research in North American coastal waters *Report of the Coastal Carbon Synthesis (CCARS) Community Workshop (19–21 August 2014)* ed Ocean Carbon and Biogeochemistry Program and North American Carbon Program (Woods Hole, MA) p 84

- [562] Fennel K, Alin S, Barbero L, Evans W, Bourgeois T, Cooley S, Dunne J, Feely R A, Hernandez-Ayon J M and Hu X 2019 Carbon cycling in the North American coastal ocean: a synthesis *Biogeosciences* **16** 1281–304
- [563] Signorini S R, Mannino A, Najjar J, Raymond G, Friedrichs M A M, Cai W, Salisbury J, Wang Z A, Thomas H and Shadwick E 2013 Surface ocean pCO<sub>2</sub>(2) seasonality and sea-air CO<sub>2</sub> flux estimates for the North American east coast *J. Geophys. Res. Oceans* **118** 5439–60
- [564] Najjar R G et al 2018 Carbon budget of tidal wetlands, estuaries, and shelf waters of eastern North America *Glob. Biogeochem. Cycles* **32** 389–416
- [565] Bélanger S, Babin M and Tremblay J 2013 Increasing cloudiness in Arctic damps the increase in phytoplankton primary production due to sea ice receding *Biogeosciences* **10** 4087–101
- [566] Huot Y, Babin M and Bruyant F 2013 Photosynthetic parameters in the Beaufort Sea in relation to the phytoplankton community structure *Biogeosciences* **10** 3445–54
- [567] Liu M, Tian H, Yang Q, Yang J, Song X, Lohrenz S E and Cai W 2013 Long-term trends in evapotranspiration and runoff over the drainage basins of the Gulf of Mexico during 1901–2008 *Water Resour. Res.* **49** 1988–2012
- [568] Lohrenz S E, Cai W, Chakraborty S, Gundersen K and Murrell M C 2014 Nutrient and carbon dynamics in a large river-dominated coastal ecosystem: the Mississippi-Atchafalaya River system *Biogeochemical Dynamics at Major River-Coastal Interfaces: Linkages with Global Change* (New York: Cambridge University Press) pp 448–72
- [569] Ren W, Tian H, Tao B, Yang J, Pan S, Cai W, Lohrenz S E, He R and Hopkinson C S 2015 Large increase in dissolved inorganic carbon flux from the Mississippi River to Gulf of Mexico due to climatic and anthropogenic changes over the 21st century *J. Geophys. Res. Biogeosci.* **120** 724–36
- [570] Ren W, Tian H, Cai W, Lohrenz S E, Hopkinson C S, Huang W, Yang J, Tao B, Pan S and He R 2016 Century-long increasing trend and variability of dissolved organic carbon export from the Mississippi River basin driven by natural and anthropogenic forcing *Glob. Biogeochem. Cycles* **30** 1288–99
- [571] Tao B, Tian H, Ren W, Yang J, Yang Q, He R, Cai W and Lohrenz S 2014 Increasing Mississippi river discharge throughout the 21st century influenced by changes in climate, land use, and atmospheric CO<sub>2</sub> *Geophys. Res. Lett.* **41** 4978–86
- [572] Tian H, Ren W, Yang J, Tao B, Cai W, Lohrenz S E, Hopkinson C S, Liu M, Yang Q and Lu C 2015 Climate extremes dominating seasonal and interannual variations in carbon export from the Mississippi River Basin *Glob. Biogeochem. Cycles* **29** 1333–47
- [573] Tian H, Yang Q, Najjar R G, Ren W, Friedrichs M A, Hopkinson C S and Pan S 2015 Anthropogenic and climatic influences on carbon fluxes from eastern North America to the Atlantic Ocean: a process-based modeling study *J. Geophys. Res. Biogeosci.* **120** 757–72
- [574] Xue Z, He R, Fennel K, Cai W, Lohrenz S and Hopkinson C 2013 Modeling ocean circulation and biogeochemical variability in the Gulf of Mexico *Biogeosciences* **10** 7219–34
- [575] Signorini S R et al 2019 Estuarine dissolved organic carbon flux from space: with application to Chesapeake and Delaware Bays *J. Geophys. Res. Oceans* **124** 3755–78
- [576] Shanmugam P, Varunan T, Jaiganesh S N N, Sahay A and Chauhan P 2016 Optical assessment of colored dissolved organic matter and its related parameters in dynamic coastal water systems *Estuar. Coast. Shelf Sci.* **175** 126–45
- [577] Mannino A, Russ M E and Hooker S B 2008 Algorithm development and validation for satellite-derived distributions of DOC and CDOM in the US Middle Atlantic Bight *J. Geophys. Res. Oceans* **113** C07051
- [578] Balch W, Huntington T, Aiken G, Drapeau D, Bowler B, Lubelczyk L and Butler K 2016 Toward a quantitative and empirical dissolved organic carbon budget for the Gulf of Maine, a semienclosed shelf sea *Glob. Biogeochem. Cycles* **30** 268–92
- [579] Vantrepotte V, Danhiez F, Loisel H, Ouillon S, Mériaux X, Cauvin A and Dessailly D 2015 CDOM-DOC relationship in contrasted coastal waters: implication for DOC retrieval from ocean color remote sensing observation *Opt. Express* **23** 33–54
- [580] Cai W J, Chen C A and Borges A 2013 Carbon dioxide dynamics and fluxes in coastal waters influenced by river plumes *Biogeochemical Dynamics at Major River-Coastal Interfaces* ed T S Bianchi, M A Allison and W J Cai (Cambridge: Cambridge University Press) pp 155–73
- [581] Guo X, Cai W, Huang W, Wang Y, Chen F, Murrell M C, Lohrenz S E, Jiang L, Dai M and Hartmann J 2012 Carbon dynamics and community production in the Mississippi River plume *Limnol. Oceanogr.* **57** 1–17
- [582] Huang W, Cai W, Wang Y, Lohrenz S E and Murrell M C 2015a The carbon dioxide system on the Mississippi River-dominated continental shelf in the northern Gulf of Mexico: 1. Distribution and air-sea CO<sub>2</sub> flux *J. Geophys. Res. Oceans* **120** 1429–45
- [583] Huang W, Cai W, Wang Y, Hu X, Chen B, Lohrenz S E, Chakraborty S, He R, Brandes J and Hopkinson C S 2015b The response of inorganic carbon distributions and dynamics to upwelling-favorable winds on the northern Gulf of Mexico during summer *Cont. Shelf Res.* **111** 211–22
- [584] Huang W, Cai W, Castelar R M, Wang Y and Lohrenz S E 2013 Effects of a wind-driven cross-shelf large river plume on biological production and CO<sub>2</sub> uptake on the Gulf of Mexico during spring *Limnol. Oceanogr.* **58** 1727–35
- [585] Xue Z, He R, Fennel K, Cai W, Lohrenz S, Huang W and Tian H 2014 Modeling pCO<sub>2</sub> variability in the Gulf of Mexico *Biogeosci. Discuss.* **11** 12673–95
- [586] Chakraborty S and Lohrenz S E 2015 Phytoplankton community structure in the river-influenced continental margin of the northern Gulf of Mexico *Mar. Ecol. Prog. Ser.* **521** 31–47
- [587] Chakraborty S, Lohrenz S E and Gundersen K 2017 Photophysiological and light absorption properties of phytoplankton communities in the river-dominated margin of the northern Gulf of Mexico *J. Geophys. Res. Oceans* **122** 4922–38
- [588] Wang Z A, Wanninkhof R, Cai W, Byrne R H, Hu X, Peng T and Huang W 2013 The marine inorganic carbon system along the Gulf of Mexico and Atlantic coasts of the United States: insights from a transregional coastal carbon study *Limnol. Oceanogr.* **58** 325–42
- [589] O'Mara N A and Dunne J P 2019 Hot spots of carbon and alkalinity cycling in the coastal oceans *Sci. Rep.* **9** 1–8
- [590] Dale A W, Graco M and Wallmann K 2017 Strong and dynamic benthic-pelagic coupling and feedbacks in a coastal upwelling system (Peruvian shelf) *Front. Mar. Sci.* **4** 29
- [591] Theodor M, Schmiedl G, Jorissen F and Mackensen A 2016 Stable carbon isotope gradients in benthic foraminifera as proxy for organic carbon fluxes in the Mediterranean Sea *Biogeosciences* **13** 6385–404
- [592] Sanchez-Vidal A, Pasqual C, Kerhervé P, Calafat A, Heussner S, Palanques A, Durrieu de Madron X, Canals M and Puig P 2008 Impact of dense shelf water cascading on the transfer of organic matter to the deep western Mediterranean basin *Geophys. Res. Lett.* **35** L05605
- [593] Kwon E Y, DeVries T, Galbraith E, Hwang J, Kim G and Timmermann A 2020 Stable carbon isotopes suggest large terrestrial carbon inputs to the global ocean *Glob. Biogeochem. Cycles* **35** e2020GB006684
- [594] UNFCCC 1997 United Nations framework convention on climate change *Kyoto Protocol (Kyoto)* vol 19 p 497
- [595] Hiraishi T, Krug T, Tanabe K, Srivastava N, Baasansuren J, Fukuda M and Troxler T G 2014 2013 Supplement to the 2006 IPCC Guidelines for National Greenhouse Gas Inventories: Wetlands (Switzerland: IPCC)

- [596] Rehdanz K, Tol R S and Wetzal P 2006 Ocean carbon sinks and international climate policy *Energy Policy* **34** 3516–26
- [597] IPCC 2019 *IPCC Special Report on the Ocean and Cryosphere in a Changing Climate* ed H O Pörtner, D C Roberts, V Masson-Delmotte, P Zhai, M Tignor, E Poloczanska, K Mintenbeck, A Alegría, M Nicolai, A Okem, J Petzold, B Rama and N M Weyer
- [598] UNFCCC 2015 1/CP. 21, adoption of the Paris agreement *Report of the Conference of the Parties on Its Twenty-First Session, Held in Paris*
- [599] Zeng Y, Friess D A, Sarira T V, Siman K and Koh L P 2021 Global potential and limits of mangrove blue carbon for climate change mitigation *Curr. Biol.* **31** 1737–1743.e3
- [600] Pindilli E, Sleeter R and Hogan D 2018 Estimating the societal benefits of carbon dioxide sequestration through peatland restoration *Ecol. Econ.* **154** 145–55
- [601] Chimner R A, Cooper D J, Wurster F C and Rochefort L 2017 An overview of peatland restoration in North America: where are we after 25 years? *Restor. Ecol.* **25** 283–92
- [602] Halabisky M, Moskal L M and Hall S A 2011 Object-based classification of semi-arid wetlands *J. Appl. Remote Sens.* **5** 053511
- [603] Kennedy R E, Yang Z, Gorelick N, Braaten J, Cavalcante L, Cohen W B and Healey S 2018 Implementation of the LandTrendr algorithm on google earth engine *Remote Sens.* **10** 691
- [604] Sharma S, MacKenzie R A, Tieng T, Soben K, Tulyasuwan N, Resanond A, Blate G and Litton C M 2020 The impacts of degradation, deforestation and restoration on mangrove ecosystem carbon stocks across Cambodia *Sci. Total Environ.* **706** 135416
- [605] Chmura G L 2013 What do we need to assess the sustainability of the tidal salt marsh carbon sink? *Ocean Coast. Manage.* **83** 25–31
- [606] Krishna K V, Shanmugam P and Nagamani P V 2020 A multiparametric nonlinear regression approach for the estimation of global surface ocean  $p\text{CO}_2$  using satellite oceanographic data *IEEE J. Sel. Top. Appl. Earth Obs. Remote Sens.* **13** 6220–35
- [607] Sasmito S D, Taillardat P, Clendenning J N, Cameron C, Friess D A, Murdiyarso D and Hutley L B 2019 Effect of land-use and land-cover change on mangrove blue carbon: a systematic review *Glob. Change Biol.* **25** 4291–302
- [608] Lagomasino D, Fatoyinbo L, Castaneda E, Cook B, Montesano P, Neigh C, Lawrence C, Ott L, Chavez S and Morton D 2021. Storm surge and ponding explain mangrove dieback in southwest Florida following Hurricane Irma *Nat. Commun.* **12** 4003
- [609] Krauss K W and Osland M J 2020 Tropical cyclones and the organization of mangrove forests: a review *Ann. Bot.* **125** 213–34
- [610] Osland M J *et al* 2020b Rapid peat development beneath created, maturing mangrove forests: ecosystem changes across a 25-yr chronosequence *Ecol. Appl.* **30** e02085
- [611] Shutler J D, Wanninkhof R, Nightingale P D, Woolf D K, Bakker D C, Watson A, Ashton I, Holding T, Chapron B and Quilfen Y 2020 Satellites will address critical science priorities for quantifying ocean carbon *Front. Ecol. Environ.* **18** 27–35